J. Phys. G: Nucl. Part. Phys. **34** (2007) R459–R528 doi:10.1088/0954-3899/34/12/R02

TOPICAL REVIEW

The Lorentz integral transform (LIT) method and its applications to perturbation-induced reactions

V D Efros[1], W Leidemann[2], G Orlandini[2] and N Barnea[3,4]

[1] Russian Research Centre 'Kurchatov Institute', Kurchatov Square, 1, 123182 Moscow, Russia
[2] Dipartimento di Fisica, Università di Trento and Istituto Nazionale di Fisica Nucleare, Gruppo Collegato di Trento, I-38100 Trento, Italy
[3] The Racah Institute of Physics, The Hebrew University, 91904 Jerusalem, Israel
[4] Institute for Nuclear Theory, University of Washington, Seattle, WA 98195, USA

E-mail: orlandin@science.unitn.it

Received 15 August 2007
Published 25 October 2007
Online at stacks.iop.org/JPhysG/34/R459

Abstract

The LIT method has allowed *ab initio* calculations of electroweak cross sections in light nuclear systems. This review presents a description of the method from both a general and a more technical point of view, as well as a summary of the results obtained by its application. The remarkable features of the LIT approach, which make it particularly efficient in dealing with a general reaction involving continuum states, are underlined. Emphasis is given on the results obtained for electroweak cross sections of few-nucleon systems. Their implications for the present understanding of microscopic nuclear dynamics are discussed.

Contents

1. Introduction

1.1. Preliminary remarks

A very challenging problem in quantum mechanics is the *ab initio* calculation of the cross section for a perturbation-induced reaction involving a many-body system. With *ab initio* we intend a calculation that requires a Hamiltonian $\hat{H}$ and the kinematic conditions of the reaction as only inputs, and treats all degrees of freedom of the many-body system explicitly (microscopic approach). In general, if the reaction implies a state belonging to the continuum spectrum of $\hat{H}$, the challenge may become enormous since one has to deal with a many-body scattering problem, which may lack a viable solution already for a very small number of constituents in the system. One is then forced to introduce various approximations that are either based on rather general physical considerations or need to be validated by experiment. This situation, however, is particularly unsatisfactory in cases where experiments cannot be performed, like e.g. for some nuclear reactions of astrophysical relevance, or where the object under investigation is just the main input of the calculation, i.e. the potential $\hat{V}$ in the Hamiltonian. This situation is typical for nuclear physics as well as for any 'non-fundamental' theory, where one would like to test the reliability of the 'effective' degrees of freedom in the

Hamiltonian and of the interaction $\hat{V}$. In this case, the comparison between theoretical results and experimental data is expected to give that information, but such a comparison risks to be inconclusive if the quality of the approximation is not under control. In both cases described above an accurate *ab initio* calculation may be demanded.

The difficulty in calculating a many-body cross section involving continuum states can be understood if one considers that at a given energy the wavefunction of the system may have many different components (channels) corresponding to all its partitions into fragments of various sizes. Already in a rather small system of four constituents the two-, the three- and the four-body break-up channels contribute at energies beyond the so-called four-body break-up threshold. In configuration space the task consists in finding the solution of the four-body Schrödinger equation with the proper boundary conditions. It is just the implementation of the boundary conditions for a continuum wavefunction which constitutes the main obstacle to the practical solution of the problem. In fact, the necessary matching of the wavefunction to the oscillating asymptotic behaviour (sometimes even difficult to be defined unambiguously) is not feasible in practice. In momentum space the situation is as complicated. The proper extension of the Lippmann–Schwinger equation to a many-body system has been formulated long ago with the Faddeev–Yakubowski equations [1, 2]. However, because of the involved analytical structure of their kernels and the number of equations itself, it would be very hard to solve the problem directly with their help, at energies above the four-fragment break-up threshold, even for a number of constituents as small as four. The great merit of the LIT method is that it allows us to avoid all the complications of a continuum calculation, reducing the difficulties to those encountered in a typical bound-state problem, where the boundary conditions are well defined and much easier to implement.

1.2. Some historical notes

The LIT method [3] is the natural extension of an original idea [4] to calculate reaction cross sections with the help of integral transforms. This kind of approach is rather 'unconventional'. It starts from the consideration that the amount of information contained in the wavefunction is redundant with respect to the transition matrix elements needed in the cross section. Therefore, one can avoid the difficult task of solving the Schrödinger equation. Instead one can concentrate directly on the matrix elements. With the help of theorems based on the closure property of the Hamiltonian eigenstates, it is proved that these matrix elements (or some combinations of them) can be obtained by a calculation of an integral transform with a suitable kernel, and its subsequent inversion. The main point is that for some kernels the calculation of the transform requires the solution of a Schrödinger-like equation with a source, and that its solutions have asymptotic conditions similar to a bound state. In this sense one can say that the integral transform method reduces the *continuum* problem to a much less problematic *bound-state-like* problem.

The form of the kernel in the integral transform is crucial. The reason is that in order to get the quantities of interest the transform needs to be inverted. Since it is normally calculated numerically it is affected by inaccuracies, and inverting an inaccurate transform is somewhat problematic. Actually, when the inaccuracies in the input transform tend to decrease, and a proper regularization is used in the course of inversion, the final result approaches the true one for various kernels [5]. However, the quality of the result of the inversion may vary substantially according to the form of the kernels, even for inaccuracies of similar size in the transforms. In particular, when, for a specific kernel, the accuracy of the transform is insufficient, the result may be corrupted with oscillations superimposing the true solution.

In [4], the Stieltjes kernel was proposed and its reliability was tested and discussed in simple model studies. Later, in a test of the method on a realistic electromagnetic cross section, calculated also in the conventional way for the deuteron [6], it has been found that the use of the Stieltjes kernel is not satisfactory, since it leads to quite inaccurate results. The problem with the Stieltjes kernel can be understood if one notices that its form is not qualitatively different from that of the Laplace kernel. In fact it is well known that the problem of the inversion of a Laplace transform is extremely ill posed when the input is numerically noisy and incomplete [7]. Nevertheless the use of Laplace transforms is common in various fields of physics, from condensed matter to lattice QCD, and elaborated algorithms (e.g. the maximum entropy method [8]) are sometimes employed for its inversion.

The problems encountered in inverting the Stieltjes as well as the Laplace transform has led to the conclusion that, differently from those two cases, the 'best' kernel should be of a finite range. Its extension should be, roughly speaking, about the range of the quantity to be obtained as the result of the inversion. This allows us to eliminate extraneous low-frequency oscillations in the inversion results, even at a moderate accuracy of the input integral transform, while high-frequency oscillations are excluded by a regularization (see section 3.5). At the same time, of course, the transform has to be calculable in practice. In [3], it has been found that the Lorentzian kernel satisfies both requisites and the analogous test, as had been performed in [6] for the Stieltjes kernel, has led to very accurate results.

The present work constitutes the first comprehensive review article of the LIT method. Only short summaries of this approach have been published in [9, 10]. Overviews of the LIT method and of its applications have been presented at various conferences [11, 12]

1.3. Descriptive plan of the review

In section 2 it is shown that the integral transform method in general, and the LIT in particular, can be formulated for any perturbation-induced reaction, of inclusive (section 2.1) as well exclusive (section 2.2) character, involving a general system of N interacting particles. There it becomes evident that another remarkable feature of the method is that the calculation of an inclusive cross section turns out to be simpler than the calculation of any single exclusive cross section. Among the exclusive reactions we focus in particular on the two-fragment case (section 2.2.1), since up to now the LIT applications to exclusive reactions have been limited to this kind of reactions. The application of the LIT method to the case of charge fragments requires some clarification, therefore we discuss it in section 2.2.2. The application of the LIT method to other reactions like for example those which are not induced by perturbation (strong reactions) is discussed in section 2.3.

Once the general idea of the method is outlined, in section 3 we turn to its practical implementation. In order to apply the method in an efficient way it is necessary to understand better the role of the parameters of the Lorentzian kernels. This is illustrated in sections 3.2 and 3.3, after having defined a few key quantities in section 3.1. Some particular cases, e.g. energy-dependent transition operators, are discussed in 3.4. The inversion of the transform is discussed in section 3.5, while in sections 3.6 and 3.7 a more technical description on the practical implementation of the LIT method is given.

In section 4 the LIT approach is compared to other methods that exhibit some similarities.

As already stated above, in all cases the core of the LIT approach resides in a non-homogeneous Schrödinger-like equation, whose solution has asymptotic conditions similar to a bound state, and therefore can be solved with a bound-state technique. In section 5 we describe one of such techniques that has been successfully applied to study nuclear, atomic

and molecular few-body systems [13–18]. It belongs to the class of methods that make use of expansions on complete sets. In this specific case the basis set is given by hyperspherical harmonics (HH) functions. The approach is called the HH method and comes in two variations, which differ essentially only by the way the convergence to the exact solution is 'accelerated'. The first one (known as CHH) makes use of a *correlation* function, which *correlates* the pure HH basis in order to reflect the characteristics of the potential. In the second one (known as EIHH) an effective interaction is introduced, which is built from the bare potential by means of a similarity transformation. Details on CHH and EIHH are given in appendices A and B. The results presented in section 8 have been obtained using both approaches.

In section 6 the formalism of the electroweak perturbation-induced reactions, discussed in section 8, are described in greater detail.

Section 7 contains four numerical tests of the LIT method. In sections 7.1 and 7.2 two interesting test cases for the reliability of the inversion procedure, as well as of the whole LIT approach, are presented. In particular in section 7.2 the comparison between a response obtained via the LIT method and the corresponding LCZR of section 4.4 is discussed. In section 7.3 a test on the inversion algorithm is performed on ^{4}He and finally, in section 7.4 a comparison between the eigenvalue method described in section 3.6 and the use of the Lanczos algorithm to calculate the LIT (section 3.7) is presented.

Section 8 presents a selection of the results of the various LIT applications. Up to now the method has been tested and largely applied to reactions induced by a perturbation (the electroweak probe) on a strong interacting system (the nucleus). There is a reason for this choice, which we explain in the following.

In section 9 a brief summary of the review is given.

As already pointed out above, the strength of an *ab initio* method like the LIT resides in allowing to study the effective degrees of freedom in the Hamiltonian and the reliability of the potential $\hat{V}$. Nowadays this is a much debated topics in nuclear physics and the LIT method represents a unique tool to clarify some important issues. In particular it can address the question of the nature of the nuclear force. Questions like whether the force is exclusively of two-body nature or three- or more-body forces are required to describe the nuclear phenomenology can be addressed also in reactions with more than three nucleons. At the same time one is able to discriminate among potentials derived within purely phenomenological or semi-phenomenological (boson exchange) or effective field theory approaches. But more than that and differently from the purely strong reactions, electroweak reactions with nuclei can provide additional information on the relevant degrees of freedom in nuclear physics. In fact the real or virtual photons, as well as neutrinos, probe not only the explicit degrees of freedom in the Hamiltonian (protons and neutrons), but also the implicit ones that generate the exchange (charge or weak) currents. In the examples reported here particular emphasis on these aspects is given.

2. The LIT method: general theory

2.1. Inclusive processes

In inclusive processes the quantities of interest have the following structure:

$$r(E) = \sum\!\!\!\!\!\!\int \mathrm{d}\gamma \langle Q|\Psi_\gamma\rangle\langle\Psi_\gamma|Q'\rangle\delta(E_\gamma - E), \tag{2.1}$$

where $|\Psi_\gamma\rangle$ are solutions to the dynamic equation

$$(\hat{H} - E_\gamma)|\Psi_\gamma\rangle = 0, \tag{2.2}$$

and $\hat{H}$ is the Hamiltonian of the system. The set $|\Psi_\gamma\rangle$ is assumed to be complete and orthonormal,

$$\sum\!\!\!\!\!\!\int d\gamma |\Psi_\gamma\rangle\langle\Psi_\gamma| = 1. \tag{2.3}$$

The integration and summation here and in (2.1) go over all discrete states and continuum spectrum states in the set. We suppose that the norms $\langle Q|Q\rangle$ and $\langle Q'|Q'\rangle$ are finite.

In the case of perturbation-induced reactions one has $|Q\rangle = \hat{O}|\Psi_0\rangle$, $|Q'\rangle = \hat{O}'|\Psi_0\rangle$, where $|\Psi_0\rangle$ is the initial state in a reaction (generally the ground state of the system undergoing the perturbation), and $\hat{O}$, $\hat{O}'$ are transition operators. Then one has

$$r(E) = \sum\!\!\!\!\!\!\int d\gamma \langle\Psi_0|\hat{O}^\dagger|\Psi_\gamma\rangle\langle\Psi_\gamma|\hat{O}'|\Psi_0\rangle\delta(E_\gamma - E). \tag{2.4}$$

Here $|\Psi_\gamma\rangle$ is a set of final states. If $\hat{O} = \hat{O}'$, quantity (2.4) may represent a response function or, in general, a contribution to the response of the system to a perturbative probe transferring energy E to it.

When the energy E and the number of particles in a system increase the direct calculation of the quantity $r(E)$ becomes prohibitive (only in case that E becomes larger than the interaction energy, perturbation theory can be used). The difficulty is related to the fact that in these cases a great number of continuum spectrum states $|\Psi_\gamma\rangle$ contribute to $r(E)$ and the structure of these states is very complicated.

The approach to overcome this difficulty that is presented here can be considered as a generalization of the sum rule approach, since the use of the closure property of the Hamiltonian eigenstates plays a fundamental role. Consider for example a simple sum rule for quantity (2.4), based on the closure property (2.3) i.e.

$$\sum\!\!\!\!\!\!\int r(E)\,dE = \langle Q|Q'\rangle. \tag{2.5}$$

The calculation of this quantity is much easier than a direct calculation of $r(E)$ itself, since it requires the knowledge of $|Q\rangle$ and $|Q'\rangle$ only. This can be obtained with bound-state methods since we have supposed that $|Q\rangle$ and $|Q'\rangle$ have finite norms. However, this sum rule contains only a limited information on $r(E)$. In order to get much more information about it we consider instead an integral transform

$$\Phi(\sigma) = \sum\!\!\!\!\!\!\int K(\sigma, E)r(E)\,dE, \tag{2.6}$$

with a smooth kernel K (specified below). This yields

$$\begin{aligned}\Phi(\sigma) &= \sum\!\!\!\!\!\!\int d\gamma \langle Q|\Psi_\gamma\rangle K(\sigma, E_\gamma)\langle\Psi_\gamma|Q'\rangle \\ &= \sum\!\!\!\!\!\!\int d\gamma \langle Q|\hat{K}(\sigma, \hat{H})|\Psi_\gamma\rangle\langle\Psi_\gamma|Q'\rangle.\end{aligned} \tag{2.7}$$

Using the closure property (2.3) one obtains

$$\Phi(\sigma) = \langle Q|\hat{K}(\sigma, \hat{H})|Q'\rangle. \tag{2.8}$$

Therefore equation (2.8) may be viewed as a generalized sum rule depending on a continuous parameter σ. With a proper choice of the kernel K the right-hand side of (2.8) may be calculated using *bound-state*-type methods. Once $\Phi(\sigma)$ is available, (2.6) may be solved to obtain $r(E)$ via an inversion of the transform.

Our choice of the kernel $K(\sigma, E)$ is such that both the calculation of $\Phi(\sigma)$ and the inversion of (2.6) are feasible. We choose [3]

$$K(\sigma, E) = \frac{1}{(E - \sigma^*)(E - \sigma)}. \tag{2.9}$$

Note that the energy parameters σ that we consider are complex. For convenience we define them as

$$\sigma = E_0 + \sigma_R + \mathrm{i}\sigma_I, \tag{2.10}$$

where E_0 is the ground-state energy and $\sigma_I \neq 0$, so that $K(\sigma, E)$ is actually a Lorentzian function centred on $E_0 + \sigma_R$, having σ_I as a halfwidth

$$K(\sigma_R, \sigma_I, E) = \frac{1}{(E - E_0 - \sigma_R)^2 + \sigma_I^2}. \tag{2.11}$$

Then the integral transform (2.6) becomes

$$L(\sigma_R, \sigma_I) = \sum\!\!\!\!\!\!\int \mathrm{d}E \frac{r(E)}{(E - E_0 - \sigma_R)^2 + \sigma_I^2}. \tag{2.12}$$

Here and in the following the integral transform $\Phi(\sigma)$ with a Lorentz kernel is denoted by $L(\sigma_R, \sigma_I)$. Using definition (2.4) it is easy to show that quantity (2.12) may be represented as

$$L(\sigma_R, \sigma_I) = \langle \tilde{\Psi} | \tilde{\Psi}' \rangle, \tag{2.13}$$

where the 'LIT functions' $\tilde{\Psi}$ and $\tilde{\Psi}'$ are given by

$$|\tilde{\Psi}\rangle = (\hat{H} - E_0 - \sigma_R - \mathrm{i}\sigma_I)^{-1} \hat{O} |\Psi_0\rangle, \tag{2.14}$$

$$|\tilde{\Psi}'\rangle = (\hat{H} - E_0 - \sigma_R - \mathrm{i}\sigma_I)^{-1} \hat{O}' |\Psi_0\rangle. \tag{2.15}$$

These functions are solutions to the inhomogeneous equations

$$(\hat{H} - E_0 - \sigma_R - \mathrm{i}\sigma_I)|\tilde{\Psi}\rangle = \hat{O}|\Psi_0\rangle, \tag{2.16}$$

$$(\hat{H} - E_0 - \sigma_R - \mathrm{i}\sigma_I)|\tilde{\Psi}'\rangle = \hat{O}'|\Psi_0\rangle. \tag{2.17}$$

Let us suppose that $\hat{O}' = \hat{O}$ ($\hat{O} = \hat{O}'$). In this case $L(\sigma)$ equals to $\langle \tilde{\Psi} | \tilde{\Psi} \rangle$ ($\langle \tilde{\Psi}' | \tilde{\Psi}' \rangle$). Since for $\sigma_I \neq 0$ the integral in (2.12) does exist, the norm of $|\tilde{\Psi}\rangle$ ($|\tilde{\Psi}'\rangle$) is finite. This implies that $|\tilde{\Psi}\rangle$ and $|\tilde{\Psi}'\rangle$ are *localized* functions. Consequently, (2.16) and (2.17) can be solved with bound-state-type methods. Similar to the problem of calculating a bound state it is sufficient to impose the only condition that the solutions of (2.16) and (2.17) are localized. This means that in contrast to continuum spectrum problems, in order to construct a solution, it is not necessary here to reproduce a complicated large distance asymptotic behaviour in the coordinate representation or singularity structure in the momentum representation. This is a very substantial simplification[5].

Obviously, localized solutions to (2.16) and (2.17) are unique. Once $L(\sigma)$ is calculated, $r(E)$ is obtained by inversion of the integral transform with a Lorentzian kernel (2.12) (Lorentz integral transform). The inversion of the LIT will be discussed in section 3.5.

Before ending this section we should mention that if the Hamiltonian is rotationally invariant it is useful to expand the states $\hat{O}|\Psi_0\rangle$ and $\hat{O}'|\Psi_0\rangle$ over states possessing given values J and M of the angular momentum and its projection. Then the whole calculation may be done in separate subspaces of states belonging to given J and M. Furthermore, the calculations are M independent. An explicit example is discussed in section 6.1.2.

[5] In the case of Faddeev–Yakubowsky equations one also needs not impose boundary conditions to get a solution. However, this is achieved due to an involved structure of these equations that seriously complicates calculations already for $A = 4$. In contrast, we use a simpler Schrödinger operator.

2.2. *Exclusive processes*

Here we illustrate the LIT method for perturbation-induced exclusive processes. Some comments on non-perturbative processes will be listed as well, at the end of this section.

The relevant matrix element that one has to calculate in the case of an exclusive perturbation-induced reaction is

$$M_{fi}(E) = \langle \Psi_f^-(E)|\hat{O}|\Psi_0\rangle, \tag{2.18}$$

where $\hat{O}$ is a perturbation operator that causes the transition, $|\Psi_0\rangle$ is again the localized initial state, while $|\Psi_f^-(E)\rangle$ represents the continuum final state with energy E. The calculation proceeds as follows [4]. We set [19]

$$|\Psi_f^-(E)\rangle = \mathcal{A}|\phi_f(E)\rangle + (E - \hat{H} - \mathrm{i}\eta)^{-1}|\bar{\phi}_f(E)\rangle, \tag{2.19}$$

where $\mathcal{A}|\phi_f(E)\rangle$ is the 'channel' function, $\mathcal{A}$ being the antisymmetrizer[6]. In general this will be the properly antisymmetrized product of fragment bound states times their *free* relative motion sub-states of given momenta (we temporarily neglect the long-range Coulomb interaction between fragments in the final state; the Coulomb case is discussed in section 2.2.2). To deal with states of well-defined rotational quantum numbers one can write $\mathcal{A}|\phi_f(E)\rangle$ as properly antisymmetrized product of fragment states and free relative motion sub-states of given orbital angular momentum quantum numbers, coupled to proper total angular momentum. The states $|\bar{\phi}_f(E)\rangle$ in (2.19) are

$$|\bar{\phi}_f\rangle \equiv \mathcal{A}\hat{V}_f|\phi_f\rangle = (\hat{H} - E)\mathcal{A}|\phi_f\rangle, \tag{2.20}$$

where $\hat{V}_f$ is the interaction between particles belonging to different fragments in the non-antisymmetrized state $|\phi_f\rangle$

Using (2.19), we rewrite the reaction amplitude (2.18) as

$$M_{fi}(E) = \langle \mathcal{A}\phi_f(E)|\hat{O}|\Psi_0\rangle + \langle \bar{\phi}_f(E)|(E - \hat{H} + \mathrm{i}\eta)^{-1}\hat{O}|\Psi_0\rangle. \tag{2.21}$$

The first term in (2.21) is called the Born term and can be computed directly. The second term takes into account the final-state interaction and represents the difficult part of the problem. However, if we represent it as a sum over the discrete spectrum E_n and integral over the continuous energies E', i.e. in the form

$$\langle \bar{\phi}_f(E)|(E - \hat{H} + \mathrm{i}\eta)^{-1}\hat{O}|\Psi_0\rangle = \sum_n (E - E_n)^{-1} F_{fi}(E, E_n) + \int_{E_{\mathrm{th}}}^{\infty} (E - E' + \mathrm{i}\eta)^{-1} F_{fi}(E, E')\,\mathrm{d}E', \tag{2.22}$$

where the form factor F_{fi} is defined as

$$F_{fi}(E, E') = \sum\!\!\!\!\!\!\int \mathrm{d}\gamma \langle \bar{\phi}_f(E)|\Psi_\gamma\rangle\langle\Psi_\gamma|\hat{O}|\Psi_0\rangle\delta(E_\gamma - E'), \tag{2.23}$$

we realize that (2.23) has the same formal structure as (2.1), with $E \to E'$. Therefore the form factor (2.23) can be calculated at a given E value as a solution to the equation

$$\Phi_{fi}(E, \sigma) = \sum\!\!\!\!\!\!\int K(\sigma, E')F_{fi}(E, E')\,\mathrm{d}E'. \tag{2.24}$$

This equation is similar to (2.6). Therefore $F_{fi}(E, E')$ can be obtained calculating first $\Phi_{fi}(E, \sigma)$ from (2.8) and then inverting the transform.

[6] Note that here any expression containing $x \pm \mathrm{i}\eta$ is understood to be evaluated at $\eta > 0$ with the limit $\eta \to 0$ then taken.

Also in this case we adopt the Lorentz kernel. However, it is useful to express it as

$$K(\sigma, E') = \frac{1}{2i\sigma_I}\left(\frac{1}{E'-\sigma} - \frac{1}{E'-\sigma^*}\right), \tag{2.25}$$

where $\sigma = \sigma_R + i\sigma_I$. Then [20]:

$$L_{fi}(E,\sigma) = (2i\sigma_I)^{-1}\langle\bar{\phi}_f(E)(|\tilde{\Psi}_1\rangle - |\tilde{\Psi}_2\rangle), \tag{2.26}$$

where

$$|\tilde{\Psi}_1\rangle = (\hat{H} - \sigma_R - i\sigma_I)^{-1}\hat{O}|\Psi_0\rangle, \tag{2.27}$$

$$|\tilde{\Psi}_2\rangle = (\hat{H} - \sigma_R + i\sigma_I)^{-1}\hat{O}|\Psi_0\rangle. \tag{2.28}$$

Therefore $|\tilde{\Psi}_1\rangle$ and $|\tilde{\Psi}_2\rangle$ are the solutions of the two inhomogeneous equations

$$(\hat{H} - \sigma_R - i\sigma_I)|\tilde{\Psi}_1\rangle = \hat{O}|\Psi_0\rangle, \tag{2.29}$$

$$(\hat{H} - \sigma_R + i\sigma_I)|\tilde{\Psi}_2\rangle = \hat{O}|\Psi_0\rangle. \tag{2.30}$$

Equation (2.26) is convenient for several reasons. The solution of (2.29) or (2.30) involves only σ and is independent of the energy E. In other words, to obtain $M_{fi}(E)$ one needs to solve these equations for a set of σ values irrespective to E. In fact only one of the equations is to be solved since $|\tilde{\Psi}_1\rangle$ and $|\tilde{\Psi}_2\rangle$ are related to each other in a simple way. Furthermore, the dynamic calculation to be performed is independent of the final-state channel f.

Inserting $|\tilde{\Psi}_1\rangle$ and $|\tilde{\Psi}_2\rangle$ into (2.26) one obtains $L_{fi}(E,\sigma)$. Then the Lorentz transform (2.26) is inverted, i.e. the integral equation (2.24) is solved for $F_{fi}(E,E')$, and the singular integral in (2.22) is calculated as

$$\int_{E_{\rm th}}^{\infty}(E - E' + i\eta)^{-1}F_{fi}(E,E')\,dE' = -i\pi F_{fi}(E,E) + P\int_{E_{\rm th}}^{\infty}(E-E')^{-1}F_{fi}(E,E')\,dE'. \tag{2.31}$$

After having calculated the non-trivial term $\langle\bar{\phi}_f(E)|(E - \hat{H} + i\eta)^{-1}\hat{O}|\Psi_0\rangle$ from (2.22) it is added in (2.21) to the Born term to obtain the matrix element $M_{fi}(E)$.[7]

2.2.1. Two-fragment break-up reactions. In case of two-body break-up reactions the calculation can also proceed in a different way. In fact this alternative method has been used in the various exclusive LIT applications discussed in section 8.

The procedure is the same as described by (2.18)–(2.24), but the Lorentz kernel is taken in the form (2.9) instead of (2.25). Then one has

$$L_{fi}(E,\sigma) = \langle\tilde{\Psi}_a|\tilde{\Psi}_b\rangle, \tag{2.32}$$

with

$$|\tilde{\Psi}_a\rangle = (\hat{H} - \sigma)^{-1}\hat{O}|\Psi_0\rangle, \tag{2.33}$$

$$|\tilde{\Psi}_b\rangle = (\hat{H} - \sigma)^{-1}|\bar{\phi}_f\rangle. \tag{2.34}$$

Obviously $\tilde{\Psi}_{a,b}$ are the solutions of the two inhomogeneous equations

$$(\hat{H} - \sigma_R - i\sigma_I)|\tilde{\Psi}_a\rangle = \hat{O}|\Psi_0\rangle, \tag{2.35}$$

$$(\hat{H} - \sigma_R - i\sigma_I)|\tilde{\Psi}_b\rangle = |\bar{\phi}_f\rangle. \tag{2.36}$$

In [21], the general and the two-fragment break-up methods have been used for calculating the $d(e,e'p)n$ cross section. There were only small differences in the results (about 1%).

[7] It is convenient to calculate the principal value integral entering here as a sum of ordinary integrals, $P\int_{E_{\rm th}}^{\infty}\frac{f(E')}{E-E'}\,dE' = \int_{E_{\rm th}}^{E-\Delta}\frac{f(E')}{E-E'}\,dE' - \int_{E-\Delta}^{E+\Delta}\frac{f(E')-f(E)}{E'-E}\,dE' + \int_{E+\Delta}^{\infty}\frac{f(E')}{E-E'}\,dE'$, where Δ is arbitrary, provided that $E_{\rm th} < E - \Delta$.

2.2.2. Case of fragments interacting via Coulomb potential. In order to take into account the long-range Coulomb interaction between the fragments one may proceed as follows.

Let us denote with $\hat{U}_f^C$ the average Coulomb potential between fragments, i.e. the Coulomb potential between the charges of the fragments concentrated in their centres of mass. Let $\mathcal{A}|\varphi_f^{(-)}\rangle$ be the continuum state given by the properly antisymmetrized product of the bound states of fragments times the 'plane-plus-ingoing wave' sub-state $|\psi^-\rangle$ of their relative motion in this average Coulomb potential. The latter is the wavefunction satisfying

$$\big(\hat{T}_{\rm rel} + \hat{U}_f^C - E\big)|\psi^-\rangle = 0, \tag{2.37}$$

where $\hat{T}_{\rm rel}$ is the kinetic energy of this relative motion. ($\mathcal{A}|\varphi_f^{(-)}\rangle$ may as well be the corresponding angular-momentum coupled state of this type.) In analogy with (2.20), let us denote with $|\bar{\varphi}_f^{(-)}\rangle$ the properly antisymmetrized state

$$|\bar{\varphi}_f^{(-)}\rangle \equiv \mathcal{A}\big(\hat{V}_f - \hat{U}_f^C\big)|\varphi_f^{(-)}\rangle = (\hat{H} - E)\mathcal{A}|\varphi_f^{(-)}\rangle. \tag{2.38}$$

Then one may write (see equation (108) in chapter 5 of [19])

$$|\Psi_f^-(E)\rangle = \mathcal{A}|\varphi_f^{(-)}(E)\rangle + (E - \hat{H} - {\rm i}\eta)^{-1}|\bar{\varphi}_f^{(-)}(E)\rangle. \tag{2.39}$$

Because of this relationship one may use the same procedure as in section 2.2 or 2.2.1 with the replacements $|\phi_f\rangle \to |\varphi_f^{(-)}\rangle$ and $|\bar{\phi}_f\rangle \to |\bar{\varphi}_f^{(-)}\rangle$. However, one has to consider that, different from the case with no Coulomb interaction, the corresponding sub-states $|\psi^-\rangle$ are no longer plane waves. This problem is easily overcome when the Coulomb interaction acts only between one pair of fragments since in this case $|\psi^-\rangle$ is known exactly.

2.3. Comments on the application of the method to other kinds of processes

With the integral transform approach one can also obtain the amplitudes of non-perturbative reactions of the general type, without calculating continuum states. In the non-perturbative case the procedure is rather similar to that described above for perturbation-induced transitions [4]. In fact in this case one has to calculate a matrix element like in (2.18), where, however, $\hat{O}|\Psi_0\rangle$ is replaced by $|\bar{\phi}_i(E)\rangle$, i.e. the initial state of the reaction, defined in a similar way as the state $|\bar{\phi}_f(E)\rangle$ in (2.20). The state $|\bar{\phi}_i(E)\rangle$ normally corresponds to two colliding fragments. The key point is therefore again to calculate the form factor of (2.23) type with the above-mentioned replacement. The transformation with the Lorentz kernel may be employed to calculate this form factor. No such calculations have yet been performed. Since in this case the source term $|\bar{\phi}_i(E)\rangle$ in the equations corresponding to (2.27) and (2.28) depends on E, the corresponding dynamic calculation has to be done separately for each E value.

Semi-inclusive processes, like e.g. $(e, e'N)$ reactions, are sometimes discussed in the framework of the so-called spectral function approximation [22]. Although the corresponding cross section is not an inclusive one, but only semi-inclusive, it may be calculated with the procedure of the type presented in section 2.1. The calculation of the spectral function in the A-particle case is reduced to the corresponding calculation of a quantity of (2.1) type in the $(A-1)$-particle subsystem, with the state $|Q\rangle$ depending on the momentum of the knocked-out nucleon [23].

A non-perturbative amplitude of inelastic scattering of a fast projectile on a target in the framework of the Glauber approximation [24] is of the form $\langle\Psi_f|Q\rangle$, where $|\Psi_f\rangle$ is the continuum final state of the target and $|Q\rangle$ includes its initial state and the profile function playing the role of the transition operator. This amplitude has the same structure as the perturbative amplitude of (2.18) and therefore can be calculated in a similar way. No such calculations are known.

3. The LIT method: practical implementation

3.1. Discrete and continuum spectra

Separating in $r(E)$, defined in (2.1), the discrete and continuum spectrum contributions, one may write

$$L(\sigma_R, \sigma_I) = \sum_n \frac{r_n}{(\sigma_R - e_n)^2 + \sigma_I^2} + \int_{e_{\rm th}}^{\infty} \mathrm{d}e \frac{r(e)}{(\sigma_R - e)^2 + \sigma_I^2} \equiv L_D(\sigma_R, \sigma_I) + L_C(\sigma_R, \sigma_I), \tag{3.1}$$

where we have introduced the excitation energy $e = E - E_0$. In particular, e_n are the discrete excitation energies $e_n = E_n - E_0$ and r_n represent the corresponding contributions to the function r:

$$r_n = \langle Q|\Psi_n\rangle\langle\Psi_n|Q'\rangle. \tag{3.2}$$

The second term in (3.1) is related to the continuum part of the spectrum with $e_{\rm th}$ representing the continuum threshold energy ($e_n < e_{\rm th}$) and

$$r(e) = \int_{e_{\rm th}+E_0}^{\infty} \mathrm{d}E_\gamma \langle Q|\Psi_\gamma\rangle\langle\Psi_\gamma|Q'\rangle\delta(E_\gamma - E). \tag{3.3}$$

The aim of the LIT method is to obtain both r_n and $r(e)$ solving (3.1) with $L(\sigma_R, \sigma_I)$ as an input. It is expedient to use L calculated at a fixed σ_I in a range of σ_R values. One may also use $\sigma_I = \sigma_I(\sigma_R)$. The first task is to get $L_D(\sigma_R, \sigma_I)$ i.e. the discrete contributions to (3.1). One way to get the contributions from the discrete levels is to calculate these levels explicitly to obtain $|\Psi_n\rangle$ and e_n and evaluate directly the overlaps (3.2) and their contributions to the response function. Alternatively one can extract these contributions by calculating the transform $L = \langle\tilde{\Psi}|\tilde{\Psi}'\rangle$ at a very small σ_I value for a range of σ_R values between zero and $e_{\rm th}$. For fixed σ_I, in the vicinity of a level e_n, the transform L is dominated by the corresponding single term

$$L_D(\sigma_R, \sigma_I) \simeq \frac{r_n}{(\sigma_R - e_n)^2 + \sigma_I^2}. \tag{3.4}$$

This σ_R dependence allows extracting e_n and r_n. The procedure is convenient when one deals with few well-separated levels. The accuracy in determining e_n and r_n may affect the continuous contribution $r(e)$ to be obtained subsequently.

After calculating $L(\sigma_R, \sigma_I)$ from (2.13) and subtracting the discrete contributions from it, the following integral equation of the first kind with the Lorentz kernel is to be solved to obtain $r(e)$:

$$L_C(\sigma_R, \sigma_I) = \int_{e_{\rm th}}^{\infty} \mathrm{d}e \frac{r(e)}{(\sigma_R - e)^2 + \sigma_I^2}. \tag{3.5}$$

To simplify the notation in the following we will omit the σ_I dependence and use $L(\sigma_R)$ to indicate its continuum part only, i.e. $L_C(\sigma_R)$, unless specified explicitly.

3.2. Role of the width of the Lorentzian kernel

Let us comment on the choice of the σ_I value. The resulting response $r(e)$ from an 'exact' calculation of L and subsequent inversion should be independent of this choice. However, the rate of convergence in the calculation may depend on σ_I. Let us show that the value of σ_I determines the relative error in $r(e)$ manifesting in components with high frequencies. The LITs of such high-frequency components become very small because of the averaging out in

the integral. Denoting with $r_\nu \exp(\mathrm{i}\nu e)$ the component of $r(e)$ with frequency ν and with L_ν its transform, one can show that if $|\nu|\sigma_I$ is less or about unity one has $(\sigma_I/\pi)|L_\nu| \simeq |r_\nu|$, while if $|\nu|\sigma_I \gg 1$ one has

$$\frac{\sigma_I}{\pi}|L_\nu| \simeq \frac{1}{\pi|\nu|\sigma_I}\frac{1}{1+(\sigma_R-e)^2/\sigma_I^2}|r_\nu|. \tag{3.6}$$

When one solves (3.5) numerically one may adopt that the errors δL in the transform and δr in the response are related to each other in accordance with

$$\delta L(\sigma_R) = \int_{e_{\mathrm{th}}}^{\infty} \mathrm{d}e \frac{\delta r(e)}{(\sigma_R-e)^2+\sigma_I^2}. \tag{3.7}$$

Let us denote the component of δL by δL_ν that corresponds to the component $\delta r_\nu \exp(\mathrm{i}\nu e)$ of δr. Furthermore, let us use the notation δL_0, L_0, δr_0 and r_0 for the components δL_ν, L_ν, δr_ν and r_ν with a low frequency. When $|\nu|\sigma_I \gg 1$, $|L_\nu|$ substantially decreases according to (3.6) and it may occur that $|\delta L_\nu/\delta L_0| \gg |L_\nu/L_0|$. This gives $|\delta r_\nu/r_\nu| \gg |\delta r_0/r_0|$. Therefore it is desirable that for all the frequencies ν substantial to reproduce the main structure of $r(e)$ the quantity $|\nu|\sigma_I$ would not be large. To this aim, in order to solve the integral equation (3.5) a regularization is applied, which suppresses high frequencies (see section 3.5). When the mentioned condition is fulfilled, this ensures approximate stability of $r(e)$ thus obtained and its closeness to the true solution.

From the above point of view smaller σ_I values are preferable. On the other hand, when σ_I decreases one approaches the scattering regime in (2.16) and (2.17), which makes it harder to obtain L with bound-state-type methods. For example, suppose that those equations are solved in a subspace of localized functions of dimension N (see section 3.6). If we denote $e_n^N = E_n^N - E_0^N$, where E_n^N are the eigenvalues of the Hamiltonian matrix in this subspace then the approximate total transform L_N (including both discrete and continuum contributions) has the structure

$$L_N = \sum_{n=1}^{N} \frac{\gamma_n^N}{\left(\sigma_R - e_n^N\right)^2 + \sigma_I^2}. \tag{3.8}$$

Here the terms with lower e_n^N values represent the discrete contributions in (3.1) while other terms correspond to a discretization of the continuum. When N increases the density of the latter type e_n^N values increases as well, providing a considerable number of them within a range $\sigma_R - \sigma_I \leqslant e_n^N \leqslant \sigma_R + \sigma_I$. When this occurs, overlaps of peaks from separate contributions to (3.8) lead to a smooth L_N approaching the true L as N tends to infinity. However, the smaller is σ_I, the higher should be the N value to represent the true L with a given accuracy. Therefore performing a calculation with too small a value of σ_I is not expedient.

3.3. Role of the centroid of the Lorentzian kernel

Let us comment on the range of σ_R values for which (3.5) is to be solved. If one adopts that the spectrum $r(e)$ to be obtained extends over the range $e_{\mathrm{th}} \leqslant e \leqslant e_{\max}$ then it is reasonable to employ $L(\sigma_R)$ approximately in the range $e_{\mathrm{th}} - \sigma_I \leqslant \sigma_R \leqslant e_{\max} + \sigma_I$. At such conditions complete information on $r(e)$ contained in $L(\sigma_R)$ is used.

Suppose that $r(e')$ does not change considerably in the range $e - \sigma_I \leqslant e' \leqslant e + \sigma_I$ and that the r values in this range are not much smaller than the values beyond this range. Then performing the integration in (3.5) one may approximately take r out of the integral at the point $e = \sigma_R$. If $e > e_{\mathrm{th}} + \sigma_I$ this gives

$$r(e) \simeq \frac{\sigma_I}{\pi} L(e). \tag{3.9}$$

Thus the input transform itself looks similar to the output response.

At large $|\sigma_R|$, the asymptotics

$$L(\sigma_R) \simeq \sigma_R^{-2} \iint r(e)\,\mathrm{d}e = \sigma_R^{-2}\langle Q|Q'\rangle \tag{3.10}$$

can be used to calculate the input transform (see the sum rule (2.5)). However, one may prove that the asymptotics (3.10) is valid when and only when $e^2 r(e)$ tends to zero as e tends to infinity. Moreover, one can note that at large $|\sigma_R|$ the regime (3.10) occurs when $\sigma_R^{-2}\langle Q|Q'\rangle$ is much higher than $\pi r(\sigma_R)/\sigma_I$, while the regime (3.9) takes place in the opposite case.

3.4. Remarks on particular cases

Equation (2.4) corresponds to a non-relativistic calculation. It is implied that the centre-of-mass subspace is separated out and states entering the response are defined in the relative motion subspace. The operators $\hat{O}$ and $\hat{O}'$ are 'internal' operators acting in the latter subspace. The corresponding matrix elements are taken between internal initial and final states with given momenta, with the momentum conservation delta function omitted. The energy E pertains to the relative motion subspace. In some cases, in order to take into account relativistic corrections one needs to consider responses defined in such a way, but with the energy conservation delta function that corresponds to relativistic kinematics. Up to some factors such responses may be expressed in the same form as the non-relativistic responses (2.4) so that the present considerations are applicable (see [25]).

Performing closure to get (2.8) we have assumed that the transition operators $\hat{O}$ and $\hat{O}'$ do not include dependence on the final-state energy E_γ. But in some cases, like e.g. in the electrodisintegration problem (see section 6.1.1) these operators are of the form $\sum_\alpha G_\alpha \hat{O}_\alpha$, where G_α are form factors that depend on E_γ. In that case the response functions in the cross section may be written as

$$R = \sum_\alpha G_\alpha^2 r_{\alpha\alpha} + \sum_{\alpha<\beta} G_\alpha G_\beta (r_{\alpha\beta} + r^*_{\alpha\beta}), \tag{3.11}$$

where $r_{\alpha\alpha}$ are functions of the form (2.4) with $\hat{O} = \hat{O}' = \hat{O}_\alpha$, and $r_{\alpha\beta}$ are again functions of that form with $\hat{O} = \hat{O}_\alpha$, $\hat{O}' = \hat{O}_\beta$. All the $r_{\alpha\beta}$ are independent of E_γ and are calculated as described above. Extra factors depending on E_γ may also arise when the continuity equation is used to express some parts of the electric multipole operators of the current in terms of the density multipole operators [26]. In this case one may act in the same way.

The operators $\hat{O}$ and $\hat{O}'$ may include a more complicated dependence on E_γ. Then one may proceed as follows [27]. One replaces the operators $\hat{O}(E_\gamma)$ and $\hat{O}'(E_\gamma)$ with those $\hat{O}(\bar{E})$ and $\hat{O}'(\bar{E})$ depending on a fixed energy $\bar{E}$ rather than E_γ. The response $r(E)$ is replaced with the arising subsidiary response $r'(E, \bar{E})$, and the latter is calculated as described above. If $r(E)$ in some E range is of interest then $r'(E, \bar{E})$ is to be found for a set of $\bar{E}$ values lying in the same range. After that $r(E)$ can be obtained via interpolation as $r'(E, \bar{E} = E)$.

3.5. Inversion of the LIT

As already pointed out, the main advantage of the LIT method to study reactions is that one avoids to solve the many-body scattering problem. One solves instead, with bound-state methods, equations of the form (2.16). The knowledge of those solutions leads to the LIT of the function r of interest. A crucial part of the method is then the inversion of this integral transform. In section 3.1 we have seen how to obtain the discrete contributions to r, so one is left with the most challenging part represented by the solution of (3.5). The inversion of this integral transform has to be made with care, since it is unstable with respect to high-frequency

oscillations as explained in section 3.2. In this sense the LIT inversion problem belongs to the class of so-called ill-posed problems.

In [5], the mathematical aspects of such problems are studied. It is also described how solutions of ill-posed problems can be obtained adopting a regularization scheme. Therefore, following [5] we have implemented a specific regularization in inverting the Lorentz transforms obtained in all the calculations reported in this review. This has led to very safe inversion results. Alternative inversion methods are discussed in [28]. They can be advantageous in case of response functions with more complex structures. Up to now, however, such complex structures have not been encountered in actual LIT applications, since the various considered $r(e)$ have normally (i) a rather simple structure, where essentially only a single peak of $r(e)$ has to be resolved, or (ii) a more complicated structure, which however can be subdivided into a sum of simply structured responses, where the various LITs can be inverted separately. The second case (ii) has already been encountered in [3] and is also discussed in section 6.1.2.

The present 'standard' LIT inversion method consists in the following ansatz for the response function

$$r(e') = \sum_{n=1}^{N_{\max}} c_n \chi_n(e', \alpha_i), \tag{3.12}$$

with $e' = e - e_{\text{th}}$, where e_{th} is the threshold energy for the break-up into the continuum. The χ_n are given functions with nonlinear parameters α_i. A basis set frequently used for LIT inversions is

$$\chi_n(\epsilon, \alpha_i) = \epsilon^{\alpha_1} \exp\left(-\frac{\alpha_2 \epsilon}{n}\right). \tag{3.13}$$

In addition also possible information on narrow levels could be incorporated easily into the set χ_n. Substituting such an expansion into the right-hand side of (3.5) (here too we omit to write the σ_I dependence) one obtains

$$L(\sigma_R) = \sum_{n=1}^{N_{\max}} c_n \tilde{\chi}_n(\sigma_R, \alpha_i), \tag{3.14}$$

where

$$\tilde{\chi}_n(\sigma_R, \alpha_i) = \int_0^\infty \mathrm{d}e' \frac{\chi_n(e', \alpha_i)}{(e' - \sigma_R)^2 + \sigma_I^2}. \tag{3.15}$$

For given α_i, the linear parameters c_n are determined from a least-square best fit of $L(\sigma_R)$ of equation (3.14) to the calculated $L(\sigma_R)$ of equation (2.13) for a number of σ_R points much larger than $N_{\max}$.

If one uses the basis set (3.13), in performing the least-square fit of $L(\sigma_R)$ one should vary the nonlinear parameter α_2 over a rather large range. If no Coulomb interaction acts between fragments, with the proper α_1 the factor ϵ^{α_1} in (3.13) reproduces the energy dependence at threshold of a response function, or a form factor. This correct α_1 value can be obtained from the case when the short-range interaction between fragments is absent. Therefore, to have good quality results in the threshold region one may adopt this α_1 value. In the usual case when the lowest open channel is that of two charged fragments the factor ϵ^{α_1} in (3.13) may also be replaced by the corresponding Gamow factor to take into account the Coulomb interaction. Alternatively, one may include the parameter α_1 in the least-square fit. However, it should be noted that the least-square procedure may not be sensitive enough to a contribution from the threshold region to ensure the proper behaviour.

For every value of $N_{\max}$ the overall best fit is selected and then the procedure is repeated for $N'_{\max} = N_{\max} + 1$ till a stability of the inverted response is obtained and taken as inversion

result. A further increase of $N_{\max}$ will eventually reach a point, where the inversion becomes unstable leading typically to random oscillations. The reason is that $L(\sigma_R)$ of equation (3.14) is not determined precisely enough so that a randomly oscillating $r(e)$ leads to a better fit than the true response. If the accuracy in the determination of $L(\sigma_R)$ from the dynamic equation is increased then one may include more basis functions in the expansion (3.14).

It is evident that the number of functions $N_{\max}$ plays the role of a regularization parameter and has to be chosen within the above-mentioned stability region. Normally, such a stability region is reached without greater problems. However, in principle it can happen that one does not find a stable result. In such cases one can either try to improve the precision of the calculated $L(\sigma_R)$ or use different basis sets, or enlarge the flexibility of the basis set (3.13) by taking e.g. $\{\chi^{\beta}(e, \alpha_i), \beta_{\min} \leqslant \beta \leqslant \beta_{\max}\}$,

$$\chi_1^{\beta}(e, \alpha_i) = e^{\alpha_1} \exp(-\alpha_2 e), \qquad \chi_n^{\beta}(e, \alpha_i) = e^{\alpha_1} \exp\left(-\frac{\alpha_2 e}{n\beta}\right), \quad n \geqslant 2, \tag{3.16}$$

with suitable values for $\beta_{\min}$ and $\beta_{\max}$.

In case that the inversion leads to a response that exhibits an unexpected structure it is useful to decrease the parameter σ_I in order to have a better resolution in the transform.

We mention that, according to what is said above, any basis set may be used only up to a certain value of $N_{\max}$. Information which can be parametrized only via χ_n with $n > N_{\max}$ is lost anyway. Therefore it is important to work with a basis set, where a relatively small $N_{\max}$ leads to a high-quality estimate of $r(e)$. Varying the nonlinear parameters α_i of χ_n (and also β in case of χ_n^{β}) is equivalent to using many different basis sets. Usually it is no problem to find a proper set.

The reliability of the inversion method outlined above has already been proved for various cases [3, 21, 29]. A discussion about two additional interesting cases can be found in section 7.

3.6. Calculation of the LIT via the eigenvalue method

As we have seen in section 2, the LIT method can be used to reformulate a scattering problem as a Schrödinger-like equation with source terms which depend on the kind of reaction under consideration. These equations, which we will call the 'LIT equations' are essentially the same for any reaction, differing by the source term, i.e. by their right-hand side (see (2.16), (2.17) and (2.36)). In all cases the asymptotic boundary conditions are bound-state like. Consequently the solutions of these equations can be found with similar methods as for the bound-state wavefunctions. Therefore the problem is much simpler than solving the Schrödinger equation for the continuum spectrum. Quantum mechanical bound-state problems may be solved in various ways. One can search for a direct solution of the dynamic equations (differential, integro-differential or integral) either in the coordinate or momentum representation. Alternatively, one can employ expansions over some basis set of localized functions. These expansion methods become more and more advantageous than the above-mentioned ones as the number of particles increases. Methods of all these types may be employed to calculate the localized LIT functions as well. In the following we discuss in greater detail the expansion methods to find the LIT functions. This is done both for the just-mentioned reason and because they have been used for the vast majority of the LIT applications. (For a solution of the three-body LIT equation with the direct Faddeev-type approach see [30].)

The truncation of the basis set converts the bound-state Schrödinger equation into a matrix eigenvalue problem and the LIT equations into a set of linear equations. These equations can be solved with various iteration methods and also Gauss-type non-iteration ones. Such strategies

have the drawback that one should solve these equations many times, as many as the number of σ_R values that one needs for a proper inversion of the transform. In this section and in the following one we present two better strategies for calculating $L(\sigma)$. The first strategy, which we call the eigenvalue method and which we discuss here, involves the full diagonalization of the Hamiltonian matrix and expresses the LIT through its eigenvalues. This method is instructive from a theoretical point of view.

Regardless of the reaction under consideration and the process that one wants to study, the LIT method requires the calculation of the overlap (see (2.13)–(2.15), or (2.26)–(2.28), or (2.32)–(2.34))

$$\begin{aligned} L(\sigma_R, \sigma_I) &= \langle \tilde{\Psi} | \tilde{\Psi}' \rangle \\ &= \langle Q | \frac{1}{(\hat{H} - E_0 - \sigma_R + \mathrm{i}\sigma_I)} \frac{1}{(\hat{H} - E_0 - \sigma_R - \mathrm{i}\sigma_I)} | Q' \rangle, \end{aligned} \tag{3.17}$$

where $|Q'\rangle$ and $|Q\rangle$ contain the information about the kind of reaction one is considering. Seeking $|\tilde{\Psi}\rangle$ and $|\tilde{\Psi}'\rangle$ as expansions over N localized basis states, it is convenient to choose as basis states N linear combinations of states that diagonalize the Hamiltonian matrix. We denote these combinations $|\varphi_\nu^N\rangle$ and the eigenvalues ϵ_ν^N. The index N is to remind that they both depend on N. If the continuum starts at $E = E_{\mathrm{th}}$ then at sufficiently high N the states $|\varphi_N\rangle$ having $\epsilon_\nu^N < E_{\mathrm{th}}$ will represent approximately the bound states. The other states will gradually fill in the continuum as N increases. The expansions of our localized LIT functions read as

$$|\tilde{\Psi}\rangle = \sum_\nu^N \frac{\langle \varphi_\nu^N | Q \rangle}{\epsilon_\nu^N - E_0 - \sigma_R - \mathrm{i}\sigma_I} |\varphi_\nu^N\rangle, \tag{3.18}$$

$$|\tilde{\Psi}'\rangle = \sum_\nu \frac{\langle \varphi_\nu^N | Q' \rangle}{\epsilon_\nu^N - E_0 - \sigma_R - \mathrm{i}\sigma_I} |\varphi_\nu^N\rangle. \tag{3.19}$$

Substituting (3.18) and (3.19) into (3.17) yields the following expression for the LIT,

$$L(\sigma_R, \sigma_I) = \sum_\nu \frac{\langle Q | \varphi_\nu^N \rangle \langle \varphi_\nu^N | Q' \rangle}{\left(\epsilon_\nu^N - E_0 - \sigma_R\right)^2 + \sigma_I^2}, \tag{3.20}$$

and for $|Q'\rangle = |Q\rangle$

$$L(\sigma_R, \sigma_I) = \sum_\nu \frac{\left|\langle \varphi_\nu^N | Q \rangle\right|^2}{\left(\epsilon_\nu^N - E_0 - \sigma_R\right)^2 + \sigma_I^2}. \tag{3.21}$$

From (3.20) and (3.21) it is clear that $L(\sigma_R, \sigma_I)$ is a sum of Lorentzians. The inversion of the LIT contributions from the states with $\epsilon_\nu^N < E_{\mathrm{th}}$ gives the discrete part of a response function (see also section 3.1), whereas the inversion of the rest gives its continuum part. The spacing between the corresponding eigenvalues with $\epsilon_\nu^N > E_{\mathrm{th}}$ depends on N and in a given energy region the density of these eigenvalues increases with N. (Since the extension of the basis states grows with N, this resembles the increase of the density of states in a box, when its size increases.) For the reliability of the inversion procedure one needs to reach the regime when one has a sufficient number of levels ϵ_ν^N within the σ_I extensions of the Lorentzians, as will be illustrated in section 7.3.

3.7. Calculation of the LIT via the Lanczos algorithm

In this section a second strategy to obtain the LIT is described. This utilizes the Lanczos algorithm [31, 32] to express the LIT as a continuous fraction. It turns out that for obtaining

an accurate LIT only a relatively small number of Lanczos steps are needed. As the number of particles in the system under consideration increases the number of basis states grows up very rapidly and the Lanczos approach seems at present the only viable method to calculate the LIT.

The motivation to use the Lanczos approach comes from the observation that from the computational point of view the calculation of the LIT is much more complicated and demanding than finding the ground-state wavefunction of an A-particle system. In fact, to obtain the ground-state wavefunction one needs only to find the lowest eigenvector of the Hamiltonian matrix. In contrast, as it is clear from (3.20) and (3.21), the complete spectra of $\hat{H}$ over a wide energy range should be known to calculate the LIT. Therefore it is no surprise that the computational time and the memory needed to calculate $L(\sigma)$ have been the limiting factors in extending the LIT method for systems with more than four particles. It turns out that these obstacles can be overcome if the LIT method is reformulated using the Lanczos algorithm. Following reference [33], in this section it is shown how this can be done.

To this end we assume that the source states $|Q\rangle$ and $|Q'\rangle$ are real and rewrite the LIT in the following form:

$$L(\sigma) = -\frac{1}{\sigma_I}\mathrm{Im}\left\{\langle Q|\frac{1}{\sigma_R + \mathrm{i}\sigma_I + E_0 - \hat{H}}|Q'\rangle\right\}. \tag{3.22}$$

A similar relation connects the response function $r(e)$ to the Green's function

$$r(e) = -\frac{1}{\pi}\mathrm{Im}\left\{\lim_{\eta\to 0} G(e + \mathrm{i}\eta + E_0)\right\}; \qquad G(z) = \langle Q|\frac{1}{z - \hat{H}}|Q'\rangle, \tag{3.23}$$

provided that $z = e + \mathrm{i}\eta$ is replaced by $\sigma_R + \mathrm{i}\sigma_I$. This is not surprising since the properly normalized Lorentzian kernel is one of the representations of the δ-function and $\sigma_I/\pi L(\sigma_R) \to r(\sigma_R)$ for $\sigma_I \to 0$. In condensed matter calculations [34–36] the Lanczos algorithm has been applied to the calculation of the Green function with a small value of η, and its imaginary part has been interpreted as $r(e)$ directly. This can be done if the spectrum is discrete (or discretized) and η is sufficiently small. In our case we have a genuine continuum problem and we want to avoid any discretization, therefore we calculate $L(\sigma_R)$ in the same way, i.e. with finite σ_I using the Lanczos algorithm, but then we antitransform $L(\sigma_R)$ in order to obtain $r(e)$.

This section is divided into two parts. First we discuss the application of the Lanczos method for a symmetric LIT, i.e. for the $|Q'\rangle = |Q\rangle$ case. This case is somewhat simpler than the general case discussed in the second part and can be used as a starting point for it.

3.7.1. The Lanczos algorithm. The Lanczos algorithm [31, 32] is a technique to solve large, sparse, Hermitian eigenvalue problems. The method involves partial *tridiagonalizations* of the matrix $\hat{H}$ without generating, however, intermediate full submatrices. Equally important is that the extreme eigenvalues of $\hat{H}$ tend to emerge long before the tridiagonalization is complete. In order to apply the Lanczos algorithm for calculating the ground-state energy of an Hamiltonian matrix $\hat{H}$ one begins by choosing a starter vector $|\phi_0\rangle$ (also called the Lanczos *pivot*), which must have a non-zero overlap with the ground state $|\psi_0\rangle$. One then proceeds building the Lanczos orthonormal basis $\{|\phi_i\rangle, i = 0, \ldots, n-1\}$ by applying the Lanczos algorithm recursively

$$|w_{i+1}\rangle = \hat{H}|\phi_i\rangle - a_i|\phi_i\rangle - b_i|\phi_{i-1}\rangle, \tag{3.24}$$

where the Lanczos coefficients a_i and b_i are defined as

$$a_i = \langle\phi_i|\hat{H}|\phi_i\rangle; \qquad b_i = \| |w_i\rangle \|; \qquad b_0 = 0;, \tag{3.25}$$

and

$$|\phi_i\rangle = \frac{|w_i\rangle}{b_i}; \qquad |\phi_{-1}\rangle = 0; \qquad \langle\phi_i|\phi_j\rangle = \delta_{ij}. \tag{3.26}$$

If one applies M Lanczos steps to an $M \times M$ matrix, then the original matrix is reduced into a tridiagonal form. As mentioned above, the power of the Lanczos algorithm lays in the fact that even after $m \ll M$ steps the eigenvalues of the $m \times m$ tridiagonal Lanczos matrix are good approximations of the extreme eigenvalues of $\hat{H}$. These eigenvalues converge rapidly with increasing number of Lanczos steps. Working with finite precision, it is necessary to recall that at each step there are round-off errors so that after a certain number of steps the Lanczos vectors loose their orthogonality. In order to obtain accurate results this loss has to remain small, otherwise one has to apply an additional re-orthogonalization procedure.

3.7.2. The symmetric case $|Q'\rangle = |Q\rangle$. The application of the Lanczos algorithm to the symmetric LIT,

$$L(\sigma) = -\frac{1}{\sigma_I}\mathrm{Im}\left\{\langle Q|\frac{1}{\sigma_R + \mathrm{i}\sigma_I + E_0 - \hat{H}}|Q\rangle\right\}, \tag{3.27}$$

starts by choosing the normalized source vector

$$|\phi_0\rangle = \frac{|Q\rangle}{\sqrt{\langle Q|Q\rangle}}, \tag{3.28}$$

as the *pivot* for the Lanczos basis and setting $z = E_0 + \sigma_R + \mathrm{i}\sigma_I$. With the help of these definitions one can rewrite $L(\sigma)$ as

$$L(\sigma) = -\frac{1}{\sigma_I}\langle Q|Q\rangle\mathrm{Im}\left\{\langle\phi_0|\frac{1}{z - \hat{H}}|\phi_0\rangle\right\}. \tag{3.29}$$

Therefore the LIT depends on the matrix element

$$x_{00} = \langle\phi_0|\frac{1}{z - \hat{H}}|\phi_0\rangle\,. \tag{3.30}$$

This matrix element can be calculated applying Cramer's rule to the solution of the linear system [34, 37]

$$\sum_n (z - \hat{H})_{mn} x_{n0} = \delta_{m0}, \tag{3.31}$$

(where $x_{n0} = \langle\phi_n|\frac{1}{z-\hat{H}}|\phi_0\rangle$) which arises from the identity

$$(z - \hat{H})(z - \hat{H})^{-1} = I, \tag{3.32}$$

on the Lanczos basis $\{|\phi_i\rangle; i = 0, \ldots, n-1\}$. Using Cramer's rule one gets

$$x_{00} = \frac{\det(M_{00})}{\det(z - \hat{H})}, \tag{3.33}$$

where

$$M_{00} = \begin{pmatrix} 1 & -b_1 & 0 & \cdots \\ 0 & z - a_1 & -b_2 & \cdots \\ 0 & -b_2 & z - a_2 & \cdots \\ \vdots & \vdots & \vdots & \ddots \end{pmatrix}, \tag{3.34}$$

and the a_n and b_n are the Lanczos coefficients. Defining D_i as the matrix obtained by removing the first i rows and i columns from $(z - \hat{H})$, one sees that $D_0 = (z - \hat{H})$,

$$\det(M_{00}) = \det(D_1) \tag{3.35}$$

and

$$\det(D_0) = (z - a_0)\det(D_1) - b_1^2 \det(D_2). \tag{3.36}$$

Thus one has

$$x_{00} = \frac{1}{z - a_0 - b_1^2 \frac{\det(D_2)}{\det(D_1)}}. \tag{3.37}$$

The recurrence relation (3.36), is valid for any submatrix D_i. Substituting the appropriate expression for $\det(D_1)$ one gets

$$x_{00} = \frac{1}{z - a_0 - \frac{b_1^2}{z - a_1 - b_2^2 \frac{\det(D_3)}{\det(D_2)}}}. \tag{3.38}$$

In this way one is able to write x_{00} as a continued fraction containing the Lanczos coefficients a_i and b_i,

$$x_{00} = \frac{1}{z - a_0 - \frac{b_1^2}{z - a_1 - \frac{b_2^2}{z - a_2 - b_3^2 \ldots}}}, \tag{3.39}$$

and thus also the LIT becomes a function of the Lanczos coefficients

$$L(\sigma) = -\frac{1}{\sigma_I} \mathrm{Im} \left\{ \frac{\langle Q|Q\rangle}{z - a_0 - \frac{b_1^2}{z - a_1 - \frac{b_2^2}{z - a_2 - b_3^2 \ldots}}} \right\}. \tag{3.40}$$

This result illustrates how, using the Lanczos method, $L(\sigma)$ is determined without solving the LIT equations, i.e. without inverting or diagonalizing the Hamiltonian matrix.

3.7.3. The general case. Now we turn to the application of the Lanczos method to the general LIT case, i.e. when $|Q\rangle \neq |Q'\rangle$. One can reformulate the problem in two different ways.

Reformulation 1. The LIT

$$L(\sigma) = -\frac{1}{\sigma_I} \mathrm{Im} \left\{ \langle Q| \frac{1}{z - \hat{H}} |Q'\rangle \right\} \tag{3.41}$$

is rewritten as a sum of four symmetric terms through the relation

$$\begin{aligned} \langle Q| \frac{1}{z - \hat{H}} |Q'\rangle = {} & \frac{1}{4}(\langle Q| + \langle Q'|) \frac{1}{z - \hat{H}} (|Q\rangle + |Q'\rangle) - \frac{1}{4}(\langle Q| - \langle Q'|) \frac{1}{z - \hat{H}} (|Q\rangle - |Q'\rangle) \\ & - \frac{\mathrm{i}}{4}(\langle Q| + \mathrm{i}\langle Q'|) \frac{1}{z - \hat{H}} (|Q\rangle + \mathrm{i}|Q'\rangle) + \frac{\mathrm{i}}{4}(\langle Q| - \mathrm{i}\langle Q'|) \frac{1}{z - \hat{H}} (|Q\rangle - \mathrm{i}|Q'\rangle). \end{aligned} \tag{3.42}$$

In this form one can apply the results of the previous section.

Reformulation 2. Although quite elegant the previous reformulation requires four separate LIT calculations. In [33], a powerful alternative reformulation has been derived, which allows the calculation of all the non-diagonal LITs, just with one set of Lanczos coefficients. Writing the LIT in the form (see (2.25))

$$L(z) = -\frac{1}{2\mathrm{i}\sigma_I} \langle Q| \left(\frac{1}{z - \hat{H}} - \frac{1}{z^* - \hat{H}} \right) |Q'\rangle, \tag{3.43}$$

choosing as previously the *pivot* (3.28) and assuming that after n steps the Lanczos vectors approximately form a complete basis, i.e. $\sum_{i=0}^{n-1} |\phi_i\rangle\langle\phi_i| \simeq 1$, one gets

$$L(\sigma) = \frac{\mathrm{i}}{2\sigma_I} \sum_{i=0}^{n-1} \langle Q|\phi_i\rangle \left[\langle \phi_i | \frac{1}{z - \hat{H}} |Q'\rangle - \langle \phi_i | \frac{1}{z^* - \hat{H}} |Q'\rangle \right]$$
$$= -\frac{\sqrt{\langle Q'|Q'\rangle}}{\sigma_I} \sum_{i=0}^{n-1} \langle Q|\phi_i\rangle \mathrm{Im}\{x_{i0}\}, \tag{3.44}$$

where the *pivot* $|\phi_0\rangle$ is defined as in (3.28) with $|Q\rangle \to |Q'\rangle$ and the matrix elements

$$x_{i0} = \langle \phi_i | \frac{1}{z - \hat{H}} |\phi_0\rangle, \tag{3.45}$$

can be written as continued fractions of the Lanczos coefficients in a similar way as in (3.39). One can note that $\mathrm{Im}\{x_{i0}\} = \mathrm{Im}\{x_{0i}\}$, therefore in the following we describe a simple algorithm for a recursive calculation of all the x_{0i} starting from x_{00}. Equation (3.31) can be generalized to

$$\sum_n (z - \hat{H})_{mn} x_{ni} = \delta_{mi}. \tag{3.46}$$

From this one can obtain all the x_{0i} matrix elements for $n = 0$ and $m = i$. The matrix element x_{01} is obtained solving the linear system

$$\begin{pmatrix} z - a_0 & -b_1 & 0 & \cdots \\ -b_1 & z - a_1 & -b_2 & \cdots \\ 0 & -b_2 & z - a_2 & \cdots \\ \vdots & \vdots & \vdots & \ddots \end{pmatrix} \begin{pmatrix} x_{01} \\ x_{11} \\ x_{21} \\ \vdots \end{pmatrix} = \begin{pmatrix} 0 \\ 1 \\ 0 \\ \vdots \end{pmatrix}. \tag{3.47}$$

Using Cramer's rule one has

$$x_{01} = \frac{\det(M_{01})}{\det(z - \hat{H})}, \tag{3.48}$$

where M_{01} has the following form

$$M_{01} = \begin{pmatrix} 0 & -b_1 & 0 & \cdots \\ 1 & z - a_1 & -b_2 & \cdots \\ 0 & -b_2 & z - a_2 & \cdots \\ \vdots & \vdots & \vdots & \ddots \end{pmatrix}. \tag{3.49}$$

Since

$$\det(M_{01}) = b_1 \det(D_2); \tag{3.50}$$
$$\det(z - \hat{H}) = (z - a_0)\det(D_1) - b_1^2 \det(D_2), \tag{3.51}$$

one has

$$x_{01} = \frac{b_1 \det(D_2)}{(z - a_0)\det(D_1) - b_1^2 \det(D_2)}. \tag{3.52}$$

In section 3.7.2 it has been shown that for evaluating x_{00}, one has to rewrite it in terms of the ratio between $\det(D_2)$ and $\det(D_1)$. In an analogous way, x_{01} must be written in terms of the ratio $\frac{\det(D_3)}{\det(D_2)}$. To this aim it is useful to rearrange the denominator of (3.52) in such a way that

the ratio between $\det(D_3)$ and $\det(D_2)$ appears in the formula. This is achieved by using the following equation:

$$\det(D_1) = (z - a_1)\det(D_2) - b_2^2 \det(D_3). \tag{3.53}$$

In fact one has

$$\begin{aligned} x_{01} &= \frac{b_1}{(z-a_0)(z-a_1) - b_1^2 - (z-a_0)b_2^2 \frac{\det(D_3)}{\det D_2}} \\ &= \frac{1}{(z-a_0)\frac{(z-a_1)}{b_1} - b_1 - \frac{z-a_0}{b_1} \cfrac{b_2^2}{z-a_2 - \cfrac{b_3^2}{z-a_3 - \cfrac{b_4^2}{z-a_4 - b_5^2 \cdots}}}}. \end{aligned} \tag{3.54}$$

Proceeding in an analogous way and using in addition the relation

$$\det(D_2) = (z - a_2)\det(D_3) - b_3^2 \det(D_4), \tag{3.55}$$

one obtains

$$\begin{aligned} x_{02} = \frac{b_1 b_2 \det(D_3)}{(z-a_0)\det(D_1) - b_1^2 \det(D_2)} &= \left[\frac{(z-a_2)}{b_2} \left(\frac{(z-a_1)(z-a_0)}{b_1} - b_1 \right) - \frac{(z-a_0)}{b_1} b_2 \right. \\ &\quad \left. - \frac{1}{b_2} \left(\frac{(z-a_1)(z-a_0)}{b_1} - b_1 \right) b_3^2 \frac{\det(D_4)}{\det(D_3)} \right]^{-1} \\ &= \left[\frac{(z-a_2)}{b_2} \left(\frac{(z-a_1)(z-a_0)}{b_1} - b_1 \right) - \frac{(z-a_0)}{b_1} b_2 \right. \\ &\quad \left. - \frac{1}{b_2} \left(\frac{(z-a_1)(z-a_0)}{b_1} - b_1 \right) \cfrac{b_3^2}{z-a_3 - \cfrac{b_4^2}{z-a_4 - \cfrac{b_5^2}{z-a_5 - b_6^2 \cdots}}} \right]^{-1}. \end{aligned} \tag{3.56}$$

At this point it is clear that defining

$$g(\nu) = -\cfrac{b_\nu^2}{z - a_\nu - \cfrac{b_{\nu+1}^2}{z-a_{\nu+1} - \cfrac{b_{\nu+2}^2}{z-a_{\nu+2} - \cfrac{b_{\nu+3}^2}{\cdots}}}}, \tag{3.57}$$

one has

$$x_{00} = \frac{1}{z - a_0 + g(1)}; \qquad x_{01} = \frac{1}{(z-a_1)\lambda_{00} - b_1 + \lambda_{00} g(2)}, \tag{3.58}$$

where $\lambda_{00} = z - a_0/b_1$ is obtained from x_{00}. Now a new parameter

$$\lambda_{01} = \frac{(z-a_1)\lambda_{00} - b_1}{b_2} \tag{3.59}$$

can be obtained from x_{01}, leading to the evaluation of

$$x_{02} = \frac{1}{(z-a_2)\lambda_{01} - b_2\lambda_{00} + \lambda_{01} g(3)}, \tag{3.60}$$

which generates the parameter λ_{02}

$$\lambda_{02} = \frac{(z-a_2)\lambda_{01} - b_2\lambda_{00}}{b_3} \tag{3.61}$$

and so on. Therefore one has

$$x_{0i} = \frac{1}{(z - a_i)\lambda_{0i-1} - b_i\lambda_{0i-2} + \lambda_{0i-1}g(\mathrm{i}+1)}, \tag{3.62}$$

with

$$\lambda_{0i} = \frac{(z - a_i)\lambda_{0i-1} - b_i\lambda_{0i-2}}{b_{i+1}}, \tag{3.63}$$

where $\lambda_{0-1} = 1$.

4. Comments on related approaches

4.1. Integral transform methods with other kernels

A microscopic study of few-body responses with the integral transform approach has been suggested in [4, 38]. In [38], the Stieltjes kernel

$$K(\sigma, E) = \frac{1}{E + \sigma} \tag{4.1}$$

has been employed to this purpose. The values of σ are real here and $-\sigma$ does not belong to the spectrum. The corresponding transform

$$\Phi(\sigma) = \langle\Psi_0|\hat{O}^\dagger(\hat{H} + \sigma)^{-1}\hat{O}|\Psi_0\rangle \tag{4.2}$$

can be obtained with standard bound-state-type methods. The inversion has not been considered. Instead it has been suggested to compare $\Phi(\sigma)$ with the corresponding transform of the experimental $r(E)$. Such a procedure is inferior to the direct comparison between the experimental and theoretical $r(E)$. In fact, when one passes from responses to transforms interesting physical effects, that can be visible only in certain limited ranges of E, can be obscured in the transform. In fact, they can be spread out on a larger σ_R range by the integral with such a kernel. Moreover, experimental data in the whole range of E are required to perform the comparison and they may be missing. Sometimes the lack of data is compensated by theoretical results obtained within some model assumption. However, it may be difficult then to judge how appropriate these assumptions are, given the above-mentioned spreading of that information by the integral.

Besides the Stieltjes kernel, also the kernel

$$K(\sigma, E) = \frac{1}{(E + \sigma)^2} \tag{4.3}$$

has been considered in [4]. In addition it has been shown how to calculate with this approach not only exclusive perturbation-induced reactions, but also general strong interaction-induced reactions. The necessity of an inversion of the transforms, in order to compare directly the responses with the experimental data, has also been underlined, since it is a necessary element for such applications. To this aim accurate inversions of the transforms with the kernels (4.1) and (4.3) have been performed in some model problems. However, it has been realized that a considerably higher accuracy in the input transforms than in the output responses was required. This is just the important difference with the case of the Lorentz kernel.

In [6], the realistic problem of the deuteron electrodisintegration has been addressed using the Stieltjes kernel (4.1). Transforms (4.2) have been calculated using standard routines for solving ordinary differential equations. It has been found that these transforms do not ensure sufficiently stable inversion. The conclusion is that the Lorentz transform is preferable even if the calculation of the Stieltjes transform may be somewhat easier.

The Laplace kernel

$$K(\sigma, E) = \exp(-E/\sigma) \tag{4.4}$$

leads to transform (2.8)

$$\Phi(\sigma) = \langle Q|\exp(-\hat{H}/\sigma)|Q'\rangle \tag{4.5}$$

of $r(E)$ defined in (2.1). Monte Carlo techniques for calculating quantities of the form (4.5) have been studied starting from [39] in connection with the determination of thermodynamic Green functions[8].

The problem of the inversion of the Monte Carlo Laplace transforms of temperature-dependent condensed matter response functions has been addressed in [42, 43]. The input transforms can be obtained with only a limited accuracy and the inversion is problematic. In [44], transform (4.5) of a few-body (α-particle) response has been calculated using a known Green function Monte Carlo-type technique. In [44], an attempt has been made to perform a comparison with experiment at the response level, inverting the Laplace transform of the response. However, information sufficient to judge on the quality of the inversion is not listed there. In subsequent papers the authors shifted to comparisons between theory and experiment at the level of the Laplace transform. In [45], the Laplace transforms (4.5) of electrodisintegration responses of a number of nuclei have been compared with the transforms (2.6) with the kernel (4.4) of experimental data.

4.2. The method of moments

The method of moments (MM) has been used to calculate responses in atomic physics (see e.g. [46, 47]). As an input one uses the moments

$$M_n = \int\!\!\!\!\!\!\int (E + \bar{E})^{-n} r(E)\,\mathrm{d}E. \tag{4.6}$$

They are calculated with the help of closure as explained in section 2.1. The procedure is a recursive one. Comparing the MM with the LIT approach one finds a few similarities and one noticeable difference. The former consist in that also (4.6) can be considered as a kind of mapping depending on two parameters: in the LIT case σ_R and σ_I, in the MM case n and $\bar{E}$. Moreover, in both cases one of them is kept constant (σ_I or $\bar{E}$) and varies the other one (σ_R or n). In this way one deals essentially with a mapping of E into σ_R or n. The important difference consists in the fact that the continuous variable E is mapped in our case to a parameter which can be varied continuously (σ_R) while in the MM case n can only be discrete.

While positive results have been obtained with the MM approach, it has some limitations. The response is reconstructed from the moments using the classical machinery. First of all one has to be sure that all used moments exist. Then the machinery is rather complicated and it includes solving nonlinear problems. Another shortcoming is related to the loss of accuracy in higher moments because of the necessity to calculate them recursively, while a rather high accuracy in its moments is required to reconstruct the detailed behaviour of $r(E)$.

Another interesting approach to calculate electron scattering response functions has been proposed in [48]. There a few 'cumulant expansions' have been suggested, that could restrict the number of moments necessary for reconstructing the energy spectrum. To our knowledge such an approach has not been investigated further.

[8] In [40], the authors refer to [41] inappropriately in relation to the present approach. Indeed, in [41] methods to calculate any many-body quantities like (4.5) are not discussed. This paper is devoted exclusively to a procedure for reconstructing the Fourier or Laplace transform of the thermodynamic Green functions from some discrete Fourier coefficients. This procedure is based on the periodicity-in-time boundary condition of the thermodynamic Green functions at finite temperatures (the period is $(kT)^{-1}$) and has no relevance to the present zero temperature problems.

4.3. Response function from LIT in the zero-width limit

Using in (2.1) the Lorentzian representation of the delta function

$$\delta(E_\gamma - E) = \frac{1}{\pi}\lim_{\eta\to\infty}\mathrm{Im}\frac{1}{E_\gamma - E - \mathrm{i}\eta} = \lim_{\eta\to\infty}\frac{\eta}{\pi}\frac{1}{(E_\gamma - E)^2 + \eta^2}, \tag{4.7}$$

one realizes that $r(E)$ may be calculated as follows:

$$r(E) = \lim_{\sigma_I\to 0} r_{\sigma_I}(E), \qquad r_{\sigma_I}(E) = \frac{\sigma_I}{\pi}\left\langle\tilde{\Psi}_{\sigma_I}\middle|\tilde{\Psi}'_{\sigma_I}\right\rangle, \tag{4.8}$$

where

$$\left|\tilde{\Psi}_{\sigma_I}\right\rangle = (\hat{H} - E - \mathrm{i}\sigma_I)^{-1}|Q\rangle, \tag{4.9}$$

$$\left|\tilde{\Psi}'_{\sigma_I}\right\rangle = (\hat{H} - E - \mathrm{i}\sigma_I)^{-1}|Q'\rangle. \tag{4.10}$$

Therefore $r_{\sigma_I}(E) \equiv (\sigma_I/\pi)L(E, \sigma_I)$.

However, unfortunately the limit $\sigma_I = 0$ cannot be realized in a simple way via an extrapolation of the σ_I-dependent LIT. If, for example, the calculation of $r_{\sigma_I}(E)$ is performed solving (4.9) and (4.10) in a subspace of localized functions of a fixed dimension N for many σ_I, then the extrapolation of its results to $\sigma_I = 0$ would give a model response of the form

$$r(E) = \sum_{n=1}^{N} r_n \delta(E_n - E). \tag{4.11}$$

This limiting response in a given finite subspace is quite different from the smooth true response that corresponds to transitions to continuum.

As already discussed in section 3.2 the smaller is σ_I the more difficult is to obtain $\left|\tilde{\Psi}_{\sigma_I}\right\rangle$ and $\left|\tilde{\Psi}'_{\sigma_I}\right\rangle$ and hence the response $r_{\sigma_I}(E)$, with the help of 'simple' bound-state-type methods. Therefore we believe that this way of proceeding is more troublesome than the LIT method, which relies on the inversion of the transform. The latter gives an opportunity to perform a dynamic calculation with a higher σ_I value, which is certainly an easier task.

In [49], a procedure has been given to calculate the $A = 3$ response functions in the framework of the Faddeev description of dynamics. The equation of (4.9) form at $\sigma_I \to 0$ has been transformed to inhomogeneous integral equations of Faddeev type. Different from the case of σ_I finite, the solutions of such equations are not localized. No inversion is required here. As a result the summation over contributions to a response from separate final states has been performed in a closed form, i.e. using the closure property, like in the LIT case.

Here we should also mention calculations, made in the same spirit for $A = 2 - 4$, of the non-Born part of the T-matrix at complex energy with subsequent analytic continuation [50, 51].

4.4. Methods with Hamiltonian matrix diagonalization

The response $r(E)$ may also be obtained in the following way [20] (compare also section 3.6). Consider a complete set of localized functions, and let $|\varphi_\nu^N\rangle$ and ϵ_ν^N be eigenstates and eigenvalues of the Hamiltonian matrix in a subspace that spans the first N states in the set. Then from (2.7) one gets

$$\Phi_N(\sigma) = \sum_{\nu}^{N}\left\langle Q\middle|\varphi_\nu^N\right\rangle K\left(\sigma, \epsilon_\nu^N\right)\left\langle\varphi_\nu^N\middle|Q'\right\rangle. \tag{4.12}$$

It is easy to show that if either $\langle Q|Q\rangle$ or $\langle Q'|Q'\rangle$ is finite and the kernel is uniformly bounded ($K(\sigma, E) < C$) then $\Phi_N \to \Phi(\sigma)$ uniformly in σ as $N \to \infty$.

While the transform Φ_N tends to the true transform Φ when N increases, the corresponding $r_N(E)$ are quite different from each other at any N. While the real $r(E)$ is continuous and smooth, the r_N corresponding to (4.12) consists of transitions to quasi-levels (the same states as in (3.18)–(3.21)),

$$r_N(E) = \sum_{\nu}^{N} \langle Q|\varphi_\nu^N\rangle\langle\varphi_\nu^N|Q'\rangle\delta(\epsilon_\nu^N - E). \tag{4.13}$$

The transition amplitudes entering r_N are rather chaotic, and as $N \to \infty$ the r_N do not tend to any limit in the normal sense.

To get a reasonable approximation to the true $r(E)$ from the approximate transform (4.12) one should solve

$$\Phi_N(\sigma) = \int\!\!\!\!\!\!\int K(\sigma, E) r(E)\, \mathrm{d}E, \tag{4.14}$$

imposing a regularization condition. This ensures a smooth output. In this way one comes to a continuous smooth response $r_N^s(E)$ that does tend to $r(E)$ as $N \to \infty$. When N increases the difference between the response $r_N^s(E)$ and the response (4.13) consists in components with higher and higher frequencies.

In accordance with the discussion above it is expedient to apply this procedure with 'smoothing-type' kernels, like the Lorentz kernel (2.11) or the Gaussian kernel $K(\sigma_R, \sigma_I, E) = \exp\left[-(E-\sigma_R)^2/\sigma_I^2\right]$ (for analogy with the Lorentz case the centroid and width of the Gaussian are indicated by σ_R and σ_I, respectively). One may expect that $\Phi_N(\sigma)$ reaches stability at N values that provide sufficiently many levels ϵ_ν^N in an energy range corresponding to the widths of the kernels.

In some shell model studies (see e.g. [52]) the following procedure to calculate response functions has been adopted. The Hamiltonian has been diagonalized in a large model space with the Lanczos algorithm and the model response (4.13) has been obtained. Then this model response has been smoothed using the Lorentz or the Gaussian leading to the so-called *Lanczos response* (LCZR) smoothed function, and the result of (4.12) form has been taken as the final response. However, such a quantity can reproduce the true response only up to the width of a smoothing function. On the other hand, the smaller is this width the larger dimension N of the model space is required to ensure convergence with respect to N of such a smoothed response.

In the light of our experience with the LIT method we recommend a better procedure: not to adopt quantity (4.12) as the final response $r(E)$ but to extract the latter as a regularized solution to (4.14). This would allow using the 'smoothing functions', or kernels, with larger widths and, correspondingly, employing shell model spaces of lower dimensions N. Different from the above procedure, the resolution of the spectrum obtained in this way is better than the width of a smoothing function. This occurs because of the improvement in the results when one passes from a transform to a response.

A numerical example which shows the comparison between the LCZR and that obtained by inversion of the LIT is given in section 7.2.

5. Solution of the relevant equations: the hyperspherical harmonics approach

In section 2 it has been explained that the LIT method demands a good bound-state resolution technique that allows an accurate solution, not only for the ground-state wavefunction of the target system, but also for the LIT functions (see (2.16), (2.17) and (2.30)). As was already

stated in section 3.6, methods of expansion over basis sets turn out to be advantageous with increasing number of particles. In this section we shortly summarize one of them, namely the hyperspherical harmonics expansion method, since it has been used in most of the applications presented in this review (for LIT application to the no core shell model (NCSM) approach see [53]).

We first introduce the hyperspherical formalism and define the HH basis on which the expansions are made. The two practical ways to accelerate the convergence rate of the HH expansion are described in appendices A and B. In particular, in appendix A we describe the correlated HH expansion method (CHH), and in appendix B the method which makes use of an effective interaction defined in a subspace of the HH basis (EIHH). Most of the results presented in this review have been obtained using one or the other of these two approaches.

In the HH formalism, which has been successfully applied to study nuclear, atomic and molecular few-body systems [13–18], the Jacobi coordinates are replaced by a single length coordinate, the hyperradius, and a set of $(3A-4)$ hyperangles. The HH are the A-body generalization of the two-body spherical harmonics, and likewise depend only on the hyperangular (angular) coordinates in the hyperspherical (spherical) decomposition of the A-body (two-body) system. In general, the wavefunction can be expanded in a series consisting of products of HH basis functions and hyperradial basis functions. This decomposition makes the HH expansion rather flexible in describing the A-body wavefunction and allows an accurate description of the wavefunctions at large distances.

5.1. The hyperspherical coordinates

To introduce the hyperspherical coordinates we start from the set composed by the centre of mass coordinate $\boldsymbol{R} = \frac{1}{A}\sum_{i=1}^{A} \boldsymbol{r}_i$ and the normalized reversed order $(A-1)$ Jacobi coordinates (A represents the total number of particles)

$$\begin{aligned}
\boldsymbol{\eta}_1 &= \sqrt{\frac{A-1}{A}}\left[\boldsymbol{r}_1 - \frac{1}{A-1}(\boldsymbol{r}_2+\boldsymbol{r}_3+\cdots+\boldsymbol{r}_A)\right]\\
\boldsymbol{\eta}_2 &= \sqrt{\frac{A-2}{A-1}}\left[\boldsymbol{r}_2 - \frac{1}{A-2}(\boldsymbol{r}_3+\boldsymbol{r}_4+\cdots+\boldsymbol{r}_A)\right]\\
&\cdots\\
\boldsymbol{\eta}_{A-1} &= \sqrt{\frac{1}{2}}(\boldsymbol{r}_{A-1}-\boldsymbol{r}_A),
\end{aligned} \tag{5.1}$$

which describe the positions of the j th particle relative to the centre of mass of particles $j+1$ to A. Each Jacobi coordinate $\boldsymbol{\eta}_j$ consists of a radial coordinate η_j and a pair of angular coordinates $\hat{\boldsymbol{\eta}}_j \equiv (\theta_j, \phi_j)$.

The $(A-1)$ Jacobi coordinates are then transformed into the hyperangular coordinates $\alpha_2, \ldots, \alpha_{A-1}$ through the relations

$$\sin\alpha_n = \eta_n/\rho_n, \tag{5.2}$$

where

$$\rho_n^2 = \rho_{n-1}^2 + \eta_n^2 = \sum_{j=1}^{n}\eta_j^2, \tag{5.3}$$

with $\rho_0^2 = 0$. For $n = A-1$ one has

$$\rho^2 \equiv \rho_{A-1}^2 = \frac{1}{A}\sum_{i<j}^{A}(\boldsymbol{r}_i-\boldsymbol{r}_j)^2. \tag{5.4}$$

From this relation it is evident that the hyperradial coordinate ρ is symmetric with respect to permutations of the single particle coordinates. After the transformation described above the $3(A-1)$ internal coordinates for the A-particle system consist of one hyperradial coordinate $\rho \equiv \rho_{A-1}$, and $(3A-4)$ hyperangular coordinates $\hat{\Omega} \equiv \{\hat{\eta}_1, \hat{\eta}_2, \ldots, \hat{\eta}_{A-1}, \alpha_2, \alpha_3, \ldots, \alpha_{A-1}\}$.

By using hyperspherical coordinates one can write the Laplace operator for n Jacobi coordinates ($n = 1, \ldots, N$), as a sum of two terms

$$\Delta_n = \frac{1}{\rho_n^{3n-1}} \frac{\partial}{\partial \rho_n} \rho_n^{3n-1} \frac{\partial}{\partial \rho_n} - \frac{1}{\rho_n^2} \hat{K}_n^2. \tag{5.5}$$

The hyperspherical, or grand angular momentum operator $\hat{K}_n^2$ of the n Jacobi coordinates can be expressed in terms of $\hat{K}_{n-1}^2$ and $\hat{\ell}_n^2$ as follows [54]

$$\hat{K}_n^2 = -\frac{\partial^2}{\partial \alpha_n^2} + \frac{3n-6-(3n-2)\cos(2\alpha_n)}{\sin(2\alpha_n)} \frac{\partial}{\partial \alpha_n} + \frac{1}{\cos^2 \alpha_n} \hat{K}_{n-1}^2 + \frac{1}{\sin^2 \alpha_n} \hat{\ell}_n^2, \tag{5.6}$$

where we define $\hat{K}_1^2 \equiv \hat{\ell}_1^2$. The angular momentum operator associated with these n coordinates is $\hat{\boldsymbol{L}}_n = \hat{\boldsymbol{L}}_{n-1} + \hat{\boldsymbol{\ell}}_n$ ($\hat{\boldsymbol{L}}_0 = 0$). The operators $\hat{K}_n^2$, $\hat{\ell}_n^2$, $\hat{K}_{n-1}^2$, $\hat{L}_n^2$ and $\hat{L}_n^z$ commute with each other.

5.2. *The hyperspherical harmonics basis*

The hyperspherical harmonics functions $\mathcal{Y}_{[K_n]}$ are the eigenfunctions of the hyperangular operator (5.6). The explicit expression for the HH functions of the first n Jacobi coordinates is given by [55]

$$\begin{aligned}\mathcal{Y}_{[K_n]} = &\left[\sum_{m_1,\ldots,m_n} \langle \ell_1 m_1 \ell_2 m_2 | L_2 M_2 \rangle \langle L_2 M_2 \ell_3 m_3 | L_3 M_3 \rangle \right. \\ &\left. \times \ldots \times \langle L_{n-1} M_{n-1} \ell_n m_n | L_n M_n \rangle \prod_{j=1}^{n} Y_{\ell_j, m_j}(\hat{\eta}_j) \right] \\ &\times \left[\prod_{j=2}^{n} \mathcal{N}_{\mu_j}^{\ell_j + \frac{1}{2}, K_{j-1} + \frac{3j-5}{2}} (\sin \alpha_j)^{\ell_j} (\cos \alpha_j)^{K_{j-1}} \; P_{\mu_j}^{(\ell_j + \frac{1}{2}, K_{j-1} + \frac{3j-5}{2})} (\cos(2\alpha_j)) \right],\end{aligned} \tag{5.7}$$

where $Y_{\ell,m}$ are the spherical harmonics functions, $P_\mu^{(a,b)}$ are the Jacobi polynomials [56] and $\mathcal{N}_\mu^{a,b}$ are normalization constants given by [54]:

$$\mathcal{N}_\mu^{a,b} = \left[\frac{2(2\mu + a + b + 1)\mu! \Gamma(\mu + a + b + 1)}{\Gamma(\mu + a + 1)\Gamma(\mu + b + 1)} \right]^{\frac{1}{2}}. \tag{5.8}$$

The symbol $[K_n]$ stands for the set of quantum numbers $\ell_1, \ldots, \ell_n, L_2, \ldots, L_n, \mu_2, \ldots, \mu_n$ and M_n. The quantum numbers K_j are given by

$$K_j = 2\mu_j + K_{j-1} + \ell_j; \qquad \mu_1 \equiv 0, \tag{5.9}$$

and the μ_j are non-negative integers. By construction, $\rho_n^{K_n} \mathcal{Y}_{[K_n]}$ is a harmonic polynomial of degree K_n. The HH function $\mathcal{Y}_{[K_n]}$ is an eigenfunction of $\hat{K}_n^2$ with eigenvalues $K_n(K_n+3n-2)$.

In view of equations (5.3) and (5.4) it is evident that the harmonic oscillator (HO) Hamiltonian may be written in the form

$$\frac{\hbar\omega}{2}\sum_{j=1}^{N}\left(-\Delta_{\bar{\eta}_j}+\bar{\eta}_j^2\right)\equiv\frac{\hbar\omega}{2}(-\Delta_{A-1}+\bar{\rho}^2)$$
$$=\frac{\hbar\omega}{2}\left(-\frac{\partial^2}{\partial\bar{\rho}^2}-\frac{3N-1}{\bar{\rho}}\frac{\partial}{\partial\bar{\rho}}+\frac{\hat{K}^2}{\bar{\rho}^2}+\bar{\rho}^2\right), \tag{5.10}$$

where $\bar{\eta}_j=\boldsymbol{\eta}_j/r_0$, $\bar{\rho}=\rho/r_0$ where $r_0=(\hbar/(m\omega))^{1/2}$ is the oscillator length. It has the eigenvectors

$$\Psi_{\rm HO}=R_{n_\rho}(\rho)\mathcal{Y}_{[K]} \tag{5.11}$$

with eigenvalues

$$E_n=\hbar\omega\left(\frac{3(A-1)}{2}+n\right)=\hbar\omega\left(\frac{3(A-1)}{2}+2n_\rho+K\right). \tag{5.12}$$

Therefore the HH K-quantum number can be associated with the quanta of excitations of the HO wavefunction, assuming no hyperradial excitation.

When applying the HH method to the solution of the A-body problem one is facing two problems

(i) in general the HH basis states possess no special symmetry under particle permutations. For the three- and four-body problem, this is a minor problem since a direct (anti) symmetrization of the wavefunction is still feasible. For larger systems, direct symmetrization becomes impractical and there is a need for a more sophisticated symmetrization method [57–59];

(ii) for strongly repulsive potentials the convergence rate of the HH basis turns out to be rather slow, therefore two methods have been suggested in order to 'accelerate' it. The first one (CHH) makes use of *correlation* functions, which *correlate* the pure HH basis in order to reflect the characteristics of the potential. In the second one (EIHH) the convergence is accelerated by an effective interaction, built from the bare potential by means of a similarity transformation. The description of these two methods can be found in appendices A and B.

6. Applications

The LIT method has been applied to various perturbation-induced reactions with nuclei. For the strong interacting nucleons the perturbation is represented by the electroweak probe (photons, electrons, neutrinos) and the cross sections contain the responses of the systems to the perturbation. In this section the formalisms for such reactions are outlined, putting in evidence how the cross sections are related to the response functions, which can be calculated with the LIT method. It is also discussed which are the relevant operators $\hat{O}$ and $\hat{O}'$ to be used for each reaction.

6.1. Electromagnetic reactions

The principal aim in studying of electromagnetic interactions with nuclei is to investigate the nuclear dynamics and to clarify the role of effective nuclear and subnuclear degrees of freedom. These are traditionally described by nucleons, mesons, and isobars and lead to two- and three-nucleon forces. In principle the effective degrees of freedom and the corresponding forces should be related to the more fundamental quark–gluon dynamics of QCD.

A great part of our present knowledge about the internal structure of nuclei has been obtained from electromagnetic reactions. The electromagnetic interaction has various

advantages. It is a fundamental theory and it is weak enough, so that in most cases lowest order perturbation theory is sufficient, allowing a simple interpretation of cross sections and other observables in terms of charge and current density matrix elements.

In particular the study of the photoabsorption spectra has proved to be fundamental for the comprehension of the dynamics of a quantum system. Photoabsorption experiments on nuclear targets have been performed extensively since the dawn of nuclear physics until the beginning of the eighties. Later, however, this activity has slowed down somewhat. One of the possible reasons for this may have been the lack of theoretical progress, which made the comparison theory–experiment rather inconclusive. In relation to this, it is interesting to quote here a sentence from [60] that expresses this concern. The title of the paper is '*photodisintegration of* ^{3}H *and* ^{3}He'. In the conclusions the authors write: 'more theoretical work will be needed before the experimental results for the photodisintegration of three-body nuclei can test quantitatively the charge symmetry of the nuclear interaction. The present theoretical models are still rudimentary in that they do not include simultaneously a consistent treatment of the final-state interactions . . . ,' and a list follows of other shortcomings in the calculations available at that time. The authors conclude that '*as a consequence of these problems the agreement between experimental and theoretical results is, in the mean, not notably good.*' The progress achieved in recent years in the theory of few-body systems, and in particular the possibility opened by the LIT method of performing consistent treatments of initial and final states, also for systems with $A > 3$, has allowed a sort of revival of the field, with particular emphasis on the lightest nuclei, and has stimulated new experimental investigations with modern techniques. In particular, both inclusive and exclusive cross sections have been addressed.

The information about nuclear dynamics that one can get from electron scattering reactions is complementary to that obtained by real photons and much richer. The reason is that, while the energy of the photon fixes the momentum transferred to the target, an electron can transfer energy and momentum independently. This allows us to study the dynamics of the system at different wavelengths via the elastic or inelastic form factors (also called electron scattering response functions) that appear in the cross section. In about fifty years of experimental activity in electron scattering a wealth of data on targets all over the nuclear table has been collected at low as well as intermediate and high energies and momenta. Various laboratories are still active in this field, both in the United States (Jefferson Laboratory) and in Europe (Mainz, Bonn, Darmstadt). In Darmstadt a collider of electrons and beams of nuclei far from stability is planned. Considering both present and planned activities of these laboratories one can note that they are concentrating on 'light' targets. A special role play the few-body systems ^{2}H and ^{3}He, since they also serve as effective neutron targets.

6.1.1. Electron scattering reactions. In the one-photon-exchange approximation the inclusive electron scattering cross section can be written as [61]

$$\frac{\mathrm{d}^2\sigma}{\mathrm{d}\Omega \mathrm{d}\omega} = \sigma_M \left[\frac{q_\mu^4}{q^4} R_L(q,\omega) + \left(\frac{q_\mu^2}{2q^2} + \tan^2 \frac{\theta}{2} \right) R_T(q,\omega) \right], \tag{6.1}$$

where σ_M is the Mott cross section, ω is the electron energy loss, q the magnitude of the momentum transferred by the electron, θ the electron scattering angle and $q_\mu^2 = q^2 - \omega^2$. The functions R_L and R_T are the electron scattering longitudinal and transverse response functions, respectively. The function R_L represents the response of the nucleus to the electron field via the nuclear charge and is given by

$$R_L(q,\omega) = \sum\!\!\!\!\!\!\int \mathrm{d}f \langle\Psi_0|\hat{\rho}^\dagger(\boldsymbol{q},\omega)|\Psi_f\rangle\langle\Psi_f|\hat{\rho}(\boldsymbol{q},\omega)|\Psi_0\rangle \times \delta\left(E_f - E_0 + \frac{q^2}{2M_T} - \omega\right), \quad (6.2)$$

where $\hat{\rho}(\boldsymbol{q},\omega)$ represents the charge density operator and M_T is the mass of the target nucleus.

The results presented in section 8 are obtained with the following charge density operator:

$$\hat{\rho}(\boldsymbol{q},\omega) = \sum_{j=1}^{A} \hat{\rho}_j^{nr}(\boldsymbol{q},\omega) + \hat{\rho}_j^{rc}(\boldsymbol{q},\omega), \quad (6.3)$$

where

$$\hat{\rho}_j^{nr}(\boldsymbol{q},\omega) = \hat{e}_j\, \mathrm{e}^{\mathrm{i}\boldsymbol{q}\cdot\boldsymbol{r}_j}, \quad (6.4)$$

$$\hat{\rho}_j^{rc}(\boldsymbol{q},\omega) = -\frac{q^2}{8m^2}\hat{e}_j\, \mathrm{e}^{\mathrm{i}\boldsymbol{q}\cdot\boldsymbol{r}_j} - \mathrm{i}\frac{\hat{e}_j - 2\hat{\mu}_j}{4m^2}\boldsymbol{\sigma}_j\cdot(\boldsymbol{q}\times\boldsymbol{p}_j)\,\mathrm{e}^{\mathrm{i}\boldsymbol{q}\cdot\boldsymbol{r}_j}, \quad (6.5)$$

$$\hat{e}_j = G_E^p\left(q_\mu^2\right)\frac{1+\boldsymbol{\tau}_j^3}{2} + G_E^n\left(q_\mu^2\right)\frac{1-\boldsymbol{\tau}_j^3}{2} \equiv \frac{1}{2}\left[G_E^S\left(q_\mu^2\right) + G_E^V\left(q_\mu^2\right)\boldsymbol{\tau}_j^3\right], \quad (6.6)$$

$$\hat{\mu}_j = G_M^p\left(q_\mu^2\right)\frac{1+\boldsymbol{\tau}_j^3}{2} + G_M^n\left(q_\mu^2\right)\frac{1-\boldsymbol{\tau}_j^3}{2} \equiv \frac{1}{2}\left[G_M^S\left(q_\mu^2\right) + G_M^V\left(q_\mu^2\right)\boldsymbol{\tau}_j^3\right]. \quad (6.7)$$

In (6.4)–(6.7) $\boldsymbol{r}$, $\boldsymbol{p}$, $\boldsymbol{\sigma}$, and $\boldsymbol{\tau}$ are the nucleon position, momentum, spin and isospin operators, respectively, m is the nucleon mass, $G_{E,M}^{p,n}$ are the proton/neutron Sachs form factors and $G_{E,M}^{S,V}$ are the isoscalar/isovector nucleon form factors. The two terms in (6.5) proportional to m^{-2} are the Darwin–Foldy (DF) and spin–orbit (SO) relativistic corrections to the main operator (6.4) (see e.g. [62, 63]). We refer to the main operator (6.4) as the non-relativistic one, although the dependence of the nucleon form factors on q_μ^2 does not allow a non-relativistic interpretation.

The operator $\hat{\rho}$ can also be conveniently rewritten in terms of the isoscalar and isovector charge nucleon form factors from (6.6),

$$\hat{\rho}(\boldsymbol{q},\omega) = G_E^S\left(q_\mu^2\right)\hat{\rho}_s(\boldsymbol{q}) + G_E^V\left(q_\mu^2\right)\hat{\rho}_v(\boldsymbol{q}). \quad (6.8)$$

As to the transverse response function, it represents the response of the nucleus to the electron field via the current density operator $\hat{\boldsymbol{j}}_T$ transverse with respect to $\hat{\boldsymbol{q}}$:

$$R_T(q,\omega) = \sum\!\!\!\!\!\!\int \mathrm{d}f \langle\Psi_0|\hat{\boldsymbol{j}}_T^\dagger(\boldsymbol{q},\omega)|\Psi_f\rangle\langle\Psi_f|\hat{\boldsymbol{j}}_T(\boldsymbol{q},\omega)|\Psi_0\rangle \times \delta\left(E_f - E_0 + \frac{q^2}{2M_T} - \omega\right). \quad (6.9)$$

The current density in (6.9) consists first of all of the transverse components of a convection and a spin current

$$\hat{\boldsymbol{j}}_{(1)}(\boldsymbol{q},\omega) = \hat{\boldsymbol{j}}_{(1)}^c(\boldsymbol{q},\omega) + \hat{\boldsymbol{j}}_{(1)}^s(\boldsymbol{q},\omega), \quad (6.10)$$

with

$$\hat{\boldsymbol{j}}_{(1)}^c(\boldsymbol{q},\omega) = \frac{1}{2m}\sum_j \hat{e}_j\{\boldsymbol{p}_j, \mathrm{e}^{\mathrm{i}\boldsymbol{q}\cdot\boldsymbol{r}_j}\}, \quad (6.11)$$

$$\hat{\boldsymbol{j}}_{(1)}^s(\boldsymbol{q},\omega) = \frac{1}{2m}\sum_j \hat{\mu}_j\boldsymbol{\sigma}_j\times\boldsymbol{q}\,\mathrm{e}^{\mathrm{i}\boldsymbol{q}\cdot\boldsymbol{r}_j}. \quad (6.12)$$

Index (1) indicates that the operator is one-body. In order to satisfy the continuity equation, however, the momentum and/or isospin-dependent n-body interaction $\hat{V}$ requires a n-body current density operator $\hat{\boldsymbol{j}}_{(n)}$. This is called the interaction (or meson exchange) current. As is

well known, the continuity equation is not sufficient to determine the n-body current uniquely. Therefore, in principle, one needs a dynamical model for the nuclear potential which reveals the underlying interaction mechanism. Such a model can be supplied by the meson exchange picture of the nucleon–nucleon (NN) interaction. Even for a phenomenological potential a consistent two-body current can often be constructed [64–66].

If one wants to apply the LIT method to the calculation of the electron scattering response functions $R_{L,T}$ one has to deal with an 'unpleasant' feature of the operators. In fact they depend on energy via the nucleon form factors. In section 3.4 it has been shown that the operators can be put in the form (3.11) and one can deal with the corresponding energy independent $r^{L,T}_{\alpha\beta}$.

6.1.2. Multipole expansions. In order to apply the LIT method it is useful first to put in evidence the rotational quantum numbers J and M in each $\alpha\beta$-component of the response functions

$$r^{L}_{\alpha\beta}(q,\omega) = \frac{1}{2J_0+1}\sum_{M_0,J,M}\!\!\!\!\!\!\int\!\!\!\!\!\!\int \mathrm{d}f\,\langle\Psi_0(J_0,M_0)|\hat{\rho}^{\dagger}_{\alpha}(\mathbf{q})|\Psi_f(J,M)\rangle \times\langle\Psi_f(J,M)|\hat{\rho}_{\beta}(\mathbf{q})|\Psi_0(J_0,M_0)\rangle\delta\left(E_f-E_0+\frac{q^2}{2M_T}-\omega\right), \tag{6.13}$$

$$r^{T}_{\alpha\beta}(q,\omega) = \frac{1}{2J_0+1}\sum_{M_0,J,M}\!\!\!\!\!\!\int\!\!\!\!\!\!\int \mathrm{d}f\,\langle\Psi_0(J_0,M_0)|\hat{\mathbf{j}}^{T\dagger}_{\alpha}(\mathbf{q})|\Psi_f(J,M)\rangle \times\langle\Psi_f(J,M)|\hat{\mathbf{j}}^{T}_{\beta}(\mathbf{q})|\Psi_0(J_0,M_0)\rangle\delta\left(E_f-E_0+\frac{q^2}{2M_T}-\omega\right), \tag{6.14}$$

where J_0 is the total angular momentum of the ground state. Here f labels asymptotic quantum numbers other than J, M. The labels α, β refer to the isoscalar and isovector parts of the operators (see discussion about (3.11)). Then one can expand the ω-independent parts of the charge and current density operators (to simplify the notation we now omit the subscripts 'α' and 'β') as

$$\hat{\rho}(\boldsymbol{q}) = 4\pi\sum_{jm}\mathrm{i}^{j}\hat{\rho}_{jm}(q)Y^{*}_{jm}(\hat{\mathbf{q}}), \tag{6.15}$$

$$\hat{\mathbf{j}}_T(\boldsymbol{q}) = 4\pi\sum_{\lambda=\mathrm{el,mag}}\sum_{jm} i^{j-\epsilon}\hat{T}^{\lambda}_{jm}(q)\mathbf{Y}^{\lambda *}_{jm}(\hat{\mathbf{q}}). \tag{6.16}$$

Here $\hat{\mathbf{q}} = q^{-1}\mathbf{q}$ and $\mathbf{Y}^{\lambda}_{jm}$ are electric and magnetic vector spherical harmonics [67]. The operators $\hat{\rho}_{jm}$ and $\hat{T}^{\lambda}_{jm}$ are irreducible tensors of rank j. In (6.16) we set $\epsilon = 0$ in the electric case and $\epsilon = 1$ in the magnetic case. With this choice the matrix elements of the $\hat{T}^{\lambda}_{jm}$ operators between the conventional angular momentum states are real. In Appendix C, it is shown that one can write

$$r^{L}(q,\omega) = \frac{4\pi}{2J_0+1}\sum_{Jj}(2J+1)[r^{L}(q,\omega)]^{j}_{J}, \tag{6.17}$$

$$r^{T}(q,\omega) = \frac{4\pi}{2J_0+1}\sum_{\lambda=\mathrm{el,mag}}\sum_{Jj}(2J+1)[r^{T}(q,\omega)]^{j\lambda}_{J}, \tag{6.18}$$

where the partial responses $(r^L)^j_J$ and $(r^T)^{j\lambda}_J$ correspond to transitions induced by the multipoles $\hat{\rho}_{jm}$ and $\hat{T}^{\lambda}_{jm}$ to states with a given J. There it is also shown that these partial responses do not depend on M and m.[9]

The LIT of (6.17) and (6.18) are

$$L^L(q,\sigma_R) = \frac{4\pi}{2J_0+1}\sum_{Jj}(2J+1)[L^L(q,\sigma_R)]^j_J, \tag{6.19}$$

$$L^T(q,\sigma_R) = \frac{4\pi}{2J_0+1}\sum_{\lambda=\mathrm{el,mag}}\sum_{Jj}(2J+1)[L^T(q,\sigma_R)]^{j\lambda}_J. \tag{6.20}$$

The partial transforms entering the right-hand sides of (6.19) and (6.20) are calculated in subspaces with given J, M and parity from dynamic equations with sources depending on J and j. The calculation is M independent. To obtain the responses (6.17) and (6.18) from these transforms the integral equations of the form (3.1) are to be solved. Alternatively, one may invert the single terms separately and then sum up the corresponding partial contributions to the responses.

6.1.3. Photoabsorption reactions. The inclusive photoabsorption cross section is given by the following expression:

$$\sigma_\gamma(\omega) = \tfrac{4}{3}\pi^2\alpha\omega R(\omega), \tag{6.21}$$

where α is the fine structure constant, ω represents the photon energy and $R(\omega)$ is the response of the nucleus to the photon perturbation in unretarded dipole approximation, defined as

$$R(\omega) = \sum\!\!\!\!\!\!\int \mathrm{d}f\,|\langle\Psi_f|\hat{\boldsymbol{D}}|\Psi_0\rangle|^2\delta(E_f-\omega-E_0). \tag{6.22}$$

Here $|\Psi_0\rangle$ and E_0 are the nuclear ground-state wavefunction and energy, $|\Psi_f\rangle$ and E_f denote eigenstates and eigenvalues of the nuclear Hamiltonian $\hat{H}$, and

$$\hat{\boldsymbol{D}} = \frac{1}{2}\sum_i^A \mathbf{r}_i\tau_i^3, \tag{6.23}$$

where A is the number of nucleons, τ_i^3 is the third component of the isospin operator and $\boldsymbol{r}_i$ the coordinate of the ith particle in the centre of mass frame.

As mentioned above, equations (6.22) and (6.23) represent the so-called unretarded dipole approximation to the total cross section. The approximations consist in the following: (i) neglect of target recoil; (ii) neglect of all electric multipoles E_j of order higher than $j = 1$; (iii) after application of charge conservation, known as 'Siegert's theorem', reduction to the first-order term in the Taylor expansion of the Bessel function of order $j = 1$ in $\hat{\rho}_{jm}(q)$ (see [61]); (iv) neglect of all magnetic multipoles M_j in the interaction between the photon and the nuclear currents. It is clear that approximations (i)–(iii) are justified for 'low'-energy photons. However, the limit of validity of approximation (iv) needs to be investigated, because it is relevant in relation to the problem of nuclear currents and of their consistency with the

[9] The following notation is often found in the literature and will also be used in section 6.2: the longitudinal multipoles of order j are indicated with C_j, the transverse electric with E_j and the transverse magnetic with M_j. As an example: $(r^L)^j_J \equiv r_{C_j}$, $(r^T)^{j\lambda}_J \equiv r_{E_j}$ if $\lambda = el$ and $(r^T)^{j\lambda}_J \equiv r_{M_j}$ if $\lambda = \mathrm{mag}$. Note that in neutrino scattering (section 6.2) also multipoles of longitudinal character appear in the response to the Z_0 field via the axial current density. This does not happen in electron scattering, since charge conservation can be applied and such multipoles can be rewritten in terms of the C_j.

potential, i.e. the problem, already mentioned in the introduction, of understanding the implicit degrees of freedom of nuclear dynamics. This can be understood considering the following: as already mentioned above in (iii) the dipole operator $\hat{\boldsymbol{D}}$ is the long wavelength limit of the $j = 1$ term in $\hat{\rho}_{jm}(q)$. The longitudinal C_1 operator (and not the transverse E_1 multipole operator) enters the cross section, because one has used charge conservation connecting the current density to the charge density, thus one works with the so-called Siegert's operator (Siegert theorem). Therefore, while $\hat{\boldsymbol{D}}$ is written in terms of single-nucleon coordinates, information on many-body currents is included. In fact for energies where approximations (ii) and (iii) are valid, the knowledge of the form of the potential is sufficient to include all consistent currents in the dipole cross section, without knowing their formal expressions. However, Siegert's theorem does not apply to magnetic multipoles therefore if (iv) is not valid one needs models for the many-body currents that can be tested in the comparison with experiments.

Of course, also the extension in energy of the validity of (ii) and (iii) has to be investigated. Some studies have been performed in the past on the two- and three-body systems [29, 68], but the situation for heavier nuclei is still unclear.

Regarding the exclusive reaction of a photon induced two-body break-up of the nucleus into a nucleon and a residual $(A-1)$ system, one can write the total exclusive cross section $\sigma_\gamma^{\rm TB}$, within approximations (i)–(iv) mentioned above, as

$$\sigma_\gamma^{\rm TB}(\omega) = \frac{4}{3}\pi^2\,\alpha\omega\,k\mu \sum_{M_N, M_{(A-1)}} \int {\rm d}\Omega_k |\langle \Psi^-_{N,(A-1)}(E_{N,(A-1)})|\hat{\boldsymbol{D}}|\Psi_0\rangle|^2, \quad (6.24)$$

where μ and k denote the reduced mass and the relative momentum of the fragments, respectively, M_N and $M_{(A-1)}$ denote the total angular momentum projections of the nucleon and the $(A-1)$ system, $\Psi^-_{N,(A-1)}$ is the final-state continuum wavefunction of the minus type pertaining to the N, $(A-1)$ channel [19] and $E_{N,(A-1)}$ is the energy of the final state

$$E_{N,(A-1)} = \omega + E_0 = \frac{k^2}{2\mu} + E_{(A-1)}, \quad (6.25)$$

with $E_{(A-1)}$ representing the ground-state energy of the fragment $(A-1)$.

It is evident that $R(\omega)$ in (6.22) has the form (2.4). Therefore in order to calculate it, one has to invert the LIT (2.13) obtained by solving (2.16) ($\hat{O} = \hat{O}' = \hat{\boldsymbol{D}}$). In the exclusive case the matrix element in (6.24) can be calculated using the LIT method explained in section 2.2, again with $\hat{O} = \hat{\boldsymbol{D}}$.

6.2. Neutrino reactions

The interest in inelastic neutrino reactions with nuclear targets stems from the role they play in major questions of contemporary physics. Such reactions are of central importance in various astrophysical phenomena, such as supernova explosions and the nucleosynthesis of the elements.

Core collapse supernovae are widely accepted to be a neutrino driven explosion of a massive star. When the iron core of a massive star becomes gravitationally unstable it collapses until short-range nuclear forces halt the collapse and drive an outgoing shock through the outer layers of the core and the inner envelope. However, the shock loses energy through dissociation of iron nuclei and neutrino radiation, and gradually stalls, it becomes an accretion shock. It is believed, but to date not proved, that the shock is then revived as neutrinos emitted from the collapsed core (the proto–neutron star) deposit energy in the collapsing layers to overcome the infall and eventually reverse the flow to an outgoing shock which explodes the star. In order to revive the shock, the neutrinos must deposit about 1% of their energy in the matter behind

the shock. The latter, which is assumed to be in thermodynamic equilibrium, is composed mainly of protons, neutrons, electrons, and light nuclei. In contrast to the fairly known cross sections of neutrinos with electrons and nucleons, the inelastic interaction of neutrinos with light nuclei such as ^{4}He,^{3} He or ^{3}H cannot be accurately measured, and one must rely on theoretical calculations in order to evaluate the cross sections.

The neutrinos migrating out of the proto–neutron star are in flavour equilibrium for most of their migration. The electron–neutrinos remain in equilibrium with matter for a longer period than their heavy-flavour counterparts, due to the larger cross sections for scattering of electrons and because of charge current reactions. Thus the heavy-flavour neutrinos decouple from deeper within the star, where temperatures are higher. Typical calculations yield temperatures of $\sim$10 MeV for μ- and τ-neutrinos [69], which is approximately twice the temperature of electron–neutrinos. Consequently, there is a considerable amount of $\nu_{\mu,\tau}$ with energies above 20 MeV that can dissociate the ^{4}He, not to mention other nuclei, through neutral current reaction.

The flux of neutrinos emitted in the collapse process is sufficiently large to initiate nucleosynthesis in the overlaying shells of heavy elements. Neutral reactions of alpha particle and neutrino in the inner helium shell are part of reaction sequences leading to the production of the rare $A = 7$ lithium and beryllium isotopes [70]. Thus, better understanding of the ν–α reaction can lead to better prediction for the abundances of these elements.

In the following we shall limit the discussion to neutral current neutrino–nuclei reactions. The extension to charged current reactions is straightforward, due to isospin symmetry.

In the limit of small momentum transfer (compared to the Z-boson rest mass) and using the multipole expansion (see section 6.1.2, including the footnote), the cross section can be written as [71]

$$\begin{aligned}\frac{\mathrm{d}\sigma}{\mathrm{d}k_f} = \frac{4G^2}{2J_0+1}k_f^2\int_0^\pi \sin\theta\,\mathrm{d}\theta\left\{\left(\sin^2\frac{\theta}{2}-\frac{q^\mu q_\mu}{2q^2}\cos^2\frac{\theta}{2}\right)\sum_{J,j\geqslant 1}\left[R^J_{Mj}(q,\omega)+R^J_{Ej}(q,\omega)\right]\right.\\ \mp\sin\frac{\theta}{2}\sqrt{\sin^2\frac{\theta}{2}-\frac{q^\mu q_\mu}{2q^2}\cos^2\frac{\theta}{2}}\sum_{J,j\geqslant 1}2R^J_{Ej,Mj}(q,\omega)\\ \left.+\cos^2\frac{\theta}{2}\sum_{J,j\geqslant 0}R^J_{Cj-\frac{\omega}{q}Lj}(q,\omega)\right\},\end{aligned} \tag{6.26}$$

where k_f is the final momentum of the neutrino and θ is the scattering angle. The rest of the notation is the same as for the electron scattering cross section (section 6.1.1). The minus sign $(-)$ in (6.26) stands for neutrino scattering and the plus (+) for antineutrino. The functions $R_{\hat{O},\hat{O}'}(q,\omega)$ are the response functions with respect to the multipole transition operators $\hat{O}$ and $\hat{O}'$ (when $\hat{O}=\hat{O}'$ we use the notation $R_{\hat{O}}=R_{\hat{O},\hat{O}}$). At the supernova energy regime the neutrinos carry few tens of MeV. Therefore, it is both useful and instructive to apply the long wavelength approximation and restrict the sum in (6.26) to the leading multipoles. In the limit $q\to 0$ they are the Gamow–Teller E_1^A, L_1^A and Fermi C_0^V operators which are q-independent and then the axial vector operators E_2^A, L_2^A, M_1^A, L_0^A and the vector C_1^V, E_1^V, L_1^V, which are linear in q . The main low-energy contribution usually comes from the Gamow–Teller and Fermi operators. However, for double closed shell nuclei such as the ^{4}He nucleus these operators are suppressed and the leading contribution is linear in q. The complete current is composed of one-body terms (the impulse approximation) and many-body terms. It turns out that in the long wavelength limit the leading axial two-body current contribute mainly to the Gamow–Teller term [72].

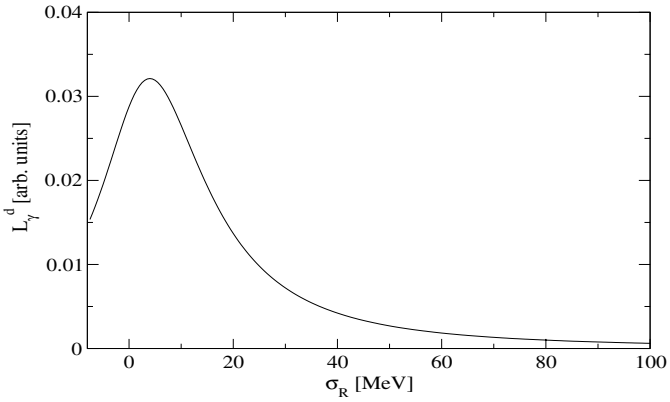

Figure 1. LIT of the deuteron photoabsorption cross section L_γ^d of (7.1) with $\sigma_I = 10$ MeV.

7. Numerical examples

In this section we perform various numerical tests, both internal to the LIT method itself, and regarding the comparison with other approaches. We take as test observable the total photoabsorption cross section in unretarded dipole approximation (see section 6.1.3) of ^{2}H and ^{4}He. In the first two sections two interesting test cases for the reliability of the inversion methods, as well as of the whole LIT approach, are presented. In section 7.2 we discuss the comparison between a response obtained via the LIT method and the corresponding LCZR of section 4.4). Finally, in section 7.4 we present a comparison between the eigenvalue method and the use of the Lanczos algorithm to calculate the LIT (see sections 3.6 and 3.7).

7.1. A test of the inversion algorithm on the deuteron

The deuteron total photoabsorption cross section is calculated in strict analogy to [6]. Following the notations there, one concentrates on the following LIT:

$$L_\gamma^d(\sigma_R, \sigma_I) = \frac{1}{3}\sum_{jl}(2j+1)\int_0^\infty \mathrm{d}r\,|\phi_{L=1,jl}(\sigma_R, \sigma_I, r)|^2. \tag{7.1}$$

Here only electric dipole transitions are taken into account ($L = 1$). Then one has to consider the following combinations for total angular momentum and angular momentum quantum numbers j and l of the outgoing neutron–proton (np) pair: $(j, l) = (0, 1), (1, 1), (2, 1), (2, 3)$. The inversion of L_γ^d leads to the unretarded dipole response function (6.22) and the corresponding cross section is given by (6.21). The complex $\phi_{L=1,jl}$ are obtained from the same radial differential equations as equations (27) and (28) of [6], but with a complex $\sigma = -\sigma_R + \mathrm{i}\sigma_I$ and taking for the excitation operator θ the dipole operator $\hat{\boldsymbol{D}}$ of (6.23). The radial differential equations can be solved in two different ways: (i) direct numerical solution, as normally done for a two-nucleon problem, and (ii) expansion of the solution in a complete set with a subsequent determination of the expansion coefficients. In this section we use method (i), while method (ii) is taken for the study in section 7.2.

In figure 1, we show L_γ^d calculated with the AV14 NN potential [73]. One sees that the transform is dominated by a low-energy peak and that further structures are not present. An inversion of L_γ^d with the basis set (3.13) leads to a rather slow convergence in $N_{\max}$ and thus

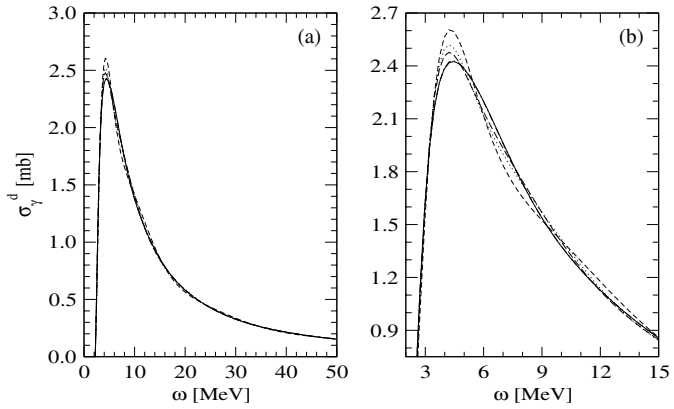

Figure 2. Total deuteron photoabsorption cross section up to 50 MeV (a) and 15 MeV (b) from inversion of L_γ^d with various $N_{\max}$-values (see (3.12): 10 (short dashed), 15 (dotted), 20 (long dashed), 25 (solid), 26 (dash-dotted).

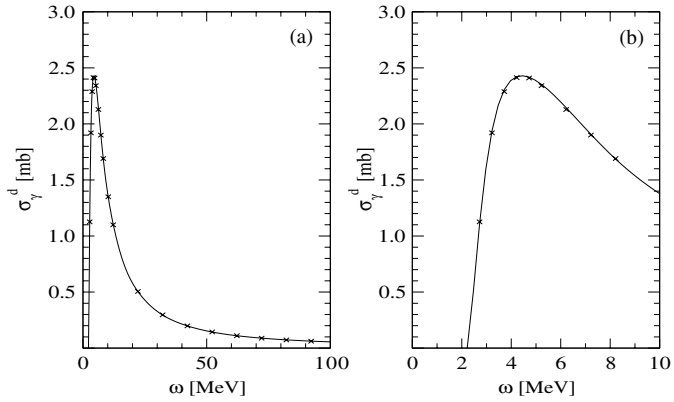

Figure 3. Total deuteron photoabsorption cross section up to 100 MeV (a) and 10 MeV (b): LIT result (solid) and from calculation with explicit *np* final-state wavefunction (x).

we use the enlarged set (3.16) with $\alpha_1 = 3/2$, $\beta_{\min} = 1$ and $\beta_{\max} = 2$. In the past we did not observe a similar slow convergence for other LIT applications. This is caused by the steep low-energy rise of the cross section combined with a rather narrow peak at only about 2 MeV above threshold. In figure 2, we illustrate the convergence pattern of the cross section as a function of $N_{\max}$. One sees that the peak height is steadily reduced with growing $N_{\max}$, while the cross section is quite stable at $E > 10$ MeV. The reduction of the peak height ends with $N_{\max} = 25$; $N_{\max} = 26$ leads to an almost identical result, and also for even higher $N_{\max}$ the decrease of the peak height does not continue further. Therefore we consider the inversion result with $N_{\max} = 25$ as the final result for the cross section.

As mentioned one can make a conventional calculation of the cross section by using the proper np scattering states. In figure 3, we show the result of such a calculation in comparison to that obtained via the LIT method, plotted in figure 2. One observes an excellent agreement between the two calculations, showing the high precision that can be obtained with the LIT method.

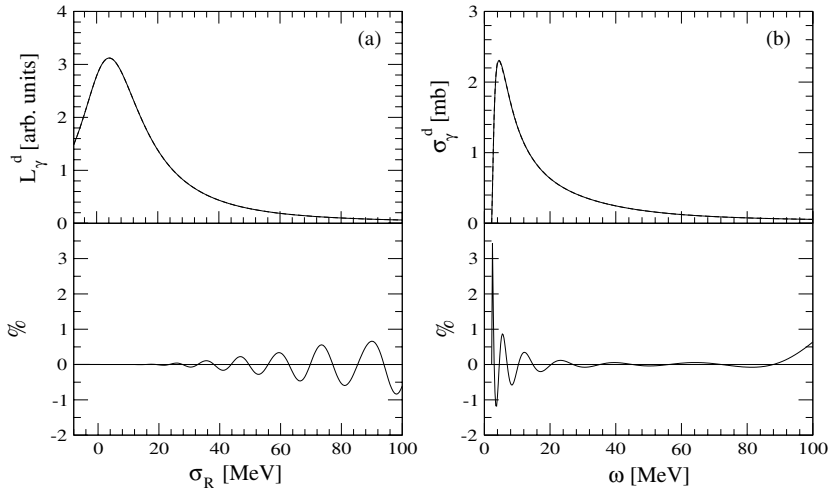

Figure 4. Deuteron photoabsorption, LIT L_γ^d of (7.1) with $\sigma_I = 10$ MeV (a) and corresponding cross section (b). Upper panels: absolute results with $N_{\rm HO} = 150$ (dashed) and $N_{\rm HO} = 2400$ (solid). Lower panels: relative difference of results with $N_{\rm HO} = 150$ and $N_{\rm HO} = 2400$ in %.

7.2. Lanczos response versus inverted LIT response

In this section we discuss the comparison between a response obtained with the LIT method and the corresponding LCZR calculated as described in section 4.4. To this end we reconsider the deuteron total photoabsorption cross section (see section 7.1). However, this time we use the non-local JISP6 potential [74]. This potential is parametrized in a harmonic oscillator (HO) basis and hence we also expand $\phi_{L=1,jl}$ of (7.1) over the same HO basis, up to a maximal value of the HO quantum number $N_{\rm HO}$ and solve for L_γ^d with the Lanczos method, as explained in section 3.7. (Results for such a calculation with the JISP6 potential are already published in [75].) Here we discuss this case because it allows us to demonstrate in a clear way the difference between a LIT inversion result and the LCZR of section 4.4.

In figure 4, we show L_γ^d and the cross section with the JISP6 potential using expansions of $\phi_{L=1,jl}$, with $N_{\rm HO} = 150$ and 2400. In both cases the maximal number of possible Lanczos steps, i.e. $N_{\rm HO}$, has been carried out. One observes that the increase of $N_{\rm HO}$ has no visible effect on L_γ^d (relative differences are below 0.01% in the whole peak region). Thus it is not surprising that also the corresponding cross sections, are practically identical (inversions of L_γ^d are made in a similar way as discussed for the AV14 case in section 7.1).

It is interesting to compare the obtained cross section with that of a LCZR approach. The results are illustrated in figure 5, where for the LCZR a halfwidth σ_I of 1 MeV is taken. With $N_{\rm HO} = 150$ a very poor result is obtained, exhibiting very strong unphysical oscillations. With $N_{\rm HO} = 2400$ the oscillations are considerably reduced, but they are still rather pronounced beyond 10 MeV. In addition the cross section is not reproduced correctly neither in the peak region nor at higher energies. One also notes a further deficiency: the cross section is non vanishing below the break-up threshold. If one decreases the halfwidth of the LCZR further to 0.5 and 0.25 MeV one does not gain much of an improvement, as shown in figures 5(c) and (d) for the $N_{\rm HO} = 2400$ case. The oscillations become visible also at lower energies and their magnitude grows considerably. One would need to increase $N_{\rm HO}$ much further in order to have a realistic result with a smooth and correct low-energy cross section.

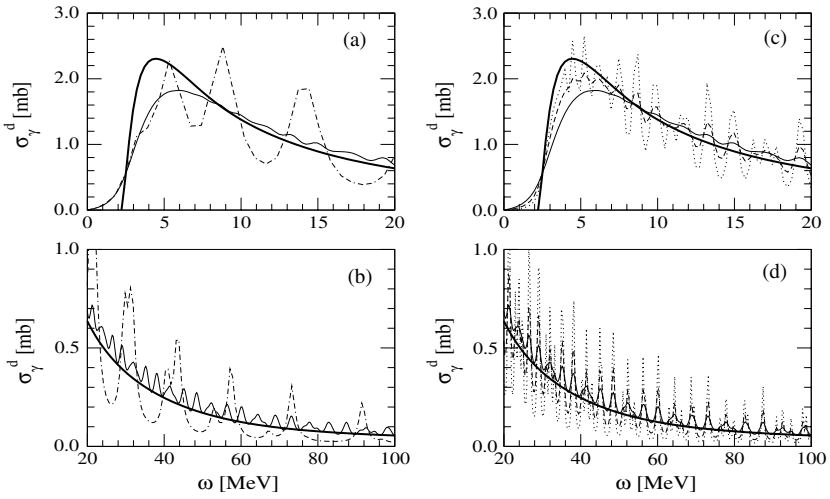

Figure 5. Deuteron total photoabsorption cross section, LIT result (thick solid) and various LCZR results: $\sigma_I = 1$ MeV with $N_{\rm HO} = 150$ (dash-dotted) and $N_{\rm HO} = 2400$ (thin solid) in (a) and (b); $N_{\rm HO} = 2400$ and $\sigma_I = 1$ MeV (thin solid), $\sigma_I = 0.5$ MeV (dashed) and $\sigma_I = 0.25$ MeV (dotted) in (c) and (d).

The oscillatory behaviour of the LCZR is due to the fact that only a tiny fraction of the Lanczos energy eigenvalues falls into the energy range of interest, while the vast majority of the about 10^4 eigenvalues (there are four different (j, l) combinations (see text after (7.1)) is located beyond 100 MeV. On the other hand we want to emphasize that $N_{\rm HO} = 150$ is fully sufficient to have a converged LIT for σ_I of 10 MeV, which after inversion leads to a practically identical cross section as the $N_{\rm HO} = 2400$ case (see figure 4). This shows that via the LIT approach the information is processed in a much better way than with the LCZR. On the other hand for many-body calculations one finds cases in the literature (see e.g. [52]), where one can work also successfully with the LCZR. In these cases one has a huge number of states and Hamiltonians (e.g. effective sd-shell interactions) that generate most of the Lanczos eigenvalues in the range of physical interest.

7.3. A test of the LIT method on the α-particle

In this section we illustrate a test of 'internal' consistency for the LIT method, when applied both to inclusive and exclusive cross sections. To this aim we calculate the total photoabsorption cross section of ^{4}He in unretarded dipole approximation in two different ways, namely in the direct way as an inclusive reaction (section 2.1) leading to $\sigma_\gamma^{\rm incl}$ and in an indirect way by summing the total cross sections of the $^4{\rm He}(\gamma, p)^3{\rm H}$ and $^4{\rm He}(\gamma, n)^3{\rm He}$ channels leading to $\sigma_\gamma^{\rm TB}$. The latter are determined by using the LIT formalism for exclusive reactions (see sections 2.2.1 and 2.2.2). Both approaches should yield identical results below the three-body break-up threshold, whereas beyond it one has $\sigma_\gamma^{\rm incl} \geqslant \sigma_\gamma^{\rm TB}$, since also other reaction channels are open. Such a comparison between $\sigma_\gamma^{\rm incl}$ and $\sigma_\gamma^{\rm TB}$ has already been made [76] for a LIT calculation taking the MT-I/III potential [77] as NN interaction. A rather good agreement between $\sigma_\gamma^{\rm incl}$ and $\sigma_\gamma^{\rm TB}$ has been obtained, but at very low energies non-negligible differences have been found. Since the low-energy region is particularly interesting, e.g. for reactions of astrophysical relevance, it is important to re-investigate this case. To this end we

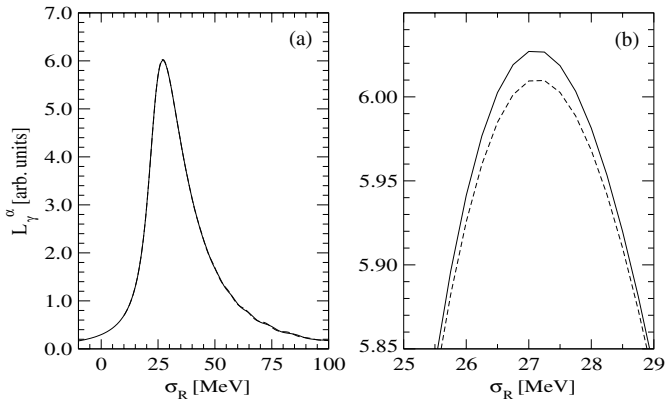

Figure 6. ^{4}He photoabsorption: LIT L_γ^α ($\sigma_I = 5$ MeV) up to 100 MeV (a) and a zoom on the peak region (b) for $K_0 = 8$, $K_{\rm LIT} = 9$ (dashed) and for $K_0 = 14$, $K_{\rm LIT} = 15$ (solid).

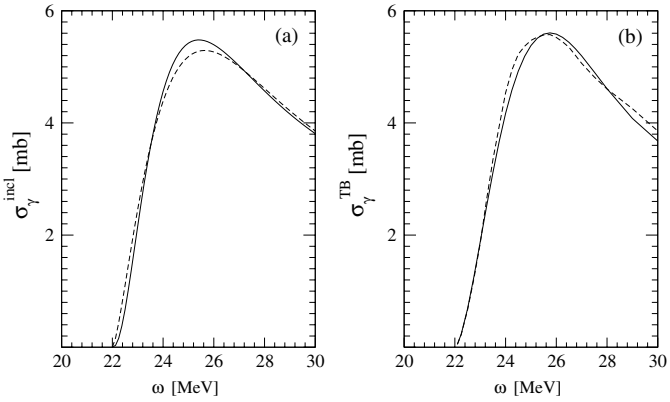

Figure 7. ^{4}He photoabsorption, convergence of HH expansion for $\sigma_\gamma^{\rm incl}$ (a) and $\sigma_\gamma^{\rm TB}$ (b): $K_0 = 8$, $K_{\rm LIT} = 9$ (dashed) and $K_0 = 14$, $K_{\rm LIT} = 15$ (solid).

choose a very simple NN potential, namely the Volkov model [78], which is a soft-core central interaction. In addition we neglect the Coulomb force, thus one has $\sigma_\gamma^{\rm TB} = 2\sigma(^4{\rm He}(\gamma, p)^3{\rm H})$. The LIT calculation is carried out using HH expansions via the EIHH method (see appendix B). In figure 6, we show the LIT of the total cross section with $\sigma_I = 5$ MeV, where we take the following maximal grand-angular momentum quantum numbers K: (i) $K_0 = 8$ (ground state), $K_{\rm LIT} = 9$ (LIT function) and (ii) $K_0 = 14$, $K_{\rm LIT} = 15$. It is evident that the difference between the two LITs is very small (about 0.5% in the peak region). Nonetheless one encounters important consequences for the inversion. For the case with $K_{\rm LIT} = 9$ one obtains unstable inversions already for $N_{\rm max} > 7$, while the stability range extends to $N_{\rm max} = 15$ for the $K_{\rm LIT} = 15$ case. Similar results are found for the various inversions which are necessary to determine $\sigma_\gamma^{\rm TB}$.

In figure 7, we show results for the cross sections $\sigma_\gamma^{\rm incl}$ and $\sigma_\gamma^{\rm TB}$ with the two different sets of K values. One observes that for $\sigma_\gamma^{\rm incl}(K_0 = 8, K_{\rm LIT} = 9)$ there is a steeper low-energy rise and a lower peak cross section than for $\sigma_\gamma^{\rm incl}(K_0 = 14, K_{\rm LIT} = 15)$. In contrast for $\sigma_\gamma^{\rm TB}$, one

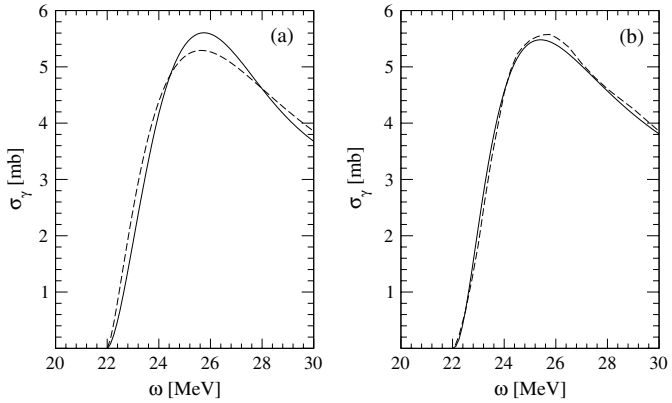

Figure 8. ^{4}He photoabsorption, comparison of $\sigma_\gamma^{\rm incl}$ (dashed) and $\sigma_\gamma^{\rm TB}$ (solid): $K_0 = 8$, $K_{\rm LIT} = 9$ (a) and $K_0 = 14$, $K_{\rm LIT} = 15$ (b).

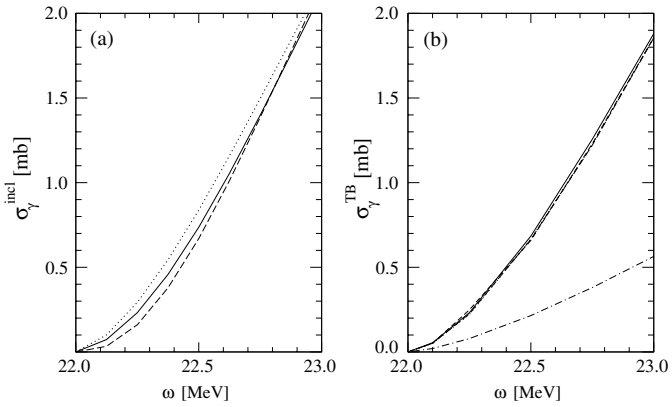

Figure 9. Low-energy ^{4}He total photoabsorption, $\sigma_\gamma^{\rm incl}$ (a) and $\sigma_\gamma^{\rm TB}$ (b) with $K_0 = 14$, $K_{\rm LIT} = 15$. Inversion results with set (3.12) for $\sigma_I = 5$ MeV (solid), $\sigma_I = 10$ MeV (dotted) and from set (3.15) with $\sigma_I = 5$ MeV (dashed). In (b) also shown the Born result (dash-dotted).

finds a good agreement up to about 1 MeV, but somewhat different peak shapes. In figure 8, we compare $\sigma_\gamma^{\rm incl}$ and $\sigma_\gamma^{\rm TB}$ for the same K value sets. It is evident that with the lower number of retained HH one does not have consistent results below the three-body break-up threshold of about 28 MeV, but with a higher number of them there is a much better picture. In order to judge the quality of the agreement of the results we have also investigated the uncertainty in the inversions using set (3.13) with two different σ_I values ($\sigma_I = 5$ and 10 MeV) and using the inversion set (3.16) with $\sigma_I = 5$ MeV. For $\sigma_\gamma^{\rm incl}$ with $\omega \leqslant 28$ MeV we find a rather energy independent error of about 0.08 mb. In contrast, the error on $\sigma_\gamma^{\rm TB}$ depends on ω. It is close to zero below 23 MeV, while in the peak region it amounts up to about 0.08 mb. In figure 9, we illustrate the situation below $\omega = 23$ MeV. It is evident that one has very stable threshold results for $\sigma_\gamma^{\rm TB}$, although the final-state interaction (FSI) contribution is rather large as the comparison with the Born result shows. On the other hand, $\sigma_\gamma^{\rm incl}$ exhibits a rather large relative error. The origin of this rather different behaviour for $\sigma_\gamma^{\rm incl}$ and $\sigma_\gamma^{\rm TB}$ is due to the

rather different LIT methods for inclusive and exclusive reactions. The main difference lies in the necessity to evaluate the principle value integral in (2.31) for the exclusive calculation. If the pole at $E = E'$ is sufficiently far from the cross section peak, i.e. for the energies of figure 9, then small differences in the peak shape do not matter much in the integral. In contrast, in case of the inclusive calculation one obtains one inversion result valid in the whole considered energy range and small differences in the peak shape propagate to the threshold region and can lead to rather large relative errors there. Of course, in the present case one could also try to increase the precision of the calculation by further increasing K_0 and $K_{\rm LIT}$, which then could lead to similarly precise results as for the deuteron case of figure 3.

As mentioned above, the low-energy region is of particular interest. Therefore it is an important finding that $\sigma_\gamma^{\rm TB}$ leads to very stable low-energy results: the convergence in K is rather good (see figure 7) and the inversion error is quite small (see figure 9).

7.4. Eigenvalue versus Lanczos methods

In the upper panel of figure 10, we compare the inclusive LIT for the photodisintegration of ^{4}He (see section 6.1.3) obtained with the eigenvalue method and with the Lanczos algorithm. The results have been obtained expanding the ^{4}He ground state $|\Psi_0\rangle$ and the LIT functions $|\tilde{\Psi}\rangle$ using the HH basis and applying the EIHH method, described in appendix B, to accelerate the convergence. For simplicity we have used the semirealistic central MT-I/III NN potential [77]. The ground state has been expanded on the set of four-body (anti)symmetrized hyperspherical harmonics (SYMHH) [58] characterized by angular momentum $L = 0$, spin $S = 0$, isospin $T = 0$ and $T_z = 0$, up to grandangular momentum quantum number $K_{\rm max} = 8$. Since the dipole operator has $j = 1$ and no spin degrees of freedom, the LIT function has been expanded on the set of four-body SYMHH associated with the quantum numbers $L = 1$, $S = 0$, $T = 1$ and $T_z = 0$. The dipole operator only allows transition by one unit of K, therefore it has been sufficient to consider HH states with $K \leqslant K_{\rm max} = 9$. The LIT obtained with these values of $K_{\rm max}$ have shown a sufficient convergence. The number of hyperradial basis functions has been 21 and the parameter σ_I has been set equal to 20 MeV. Since one difficulty in the Lanczos method is retaining the orthogonality of the basis vectors, we have checked this point and found that the overlap between the *pivot* and the 1000 th vector is smaller than 10^{-7}.

In figure 10, one sees that there is an excellent agreement between the results obtained in the two ways. In fact, up to 250 MeV, the maximal difference is lower than 5×10^{-7} (see lower panel). This picture deteriorates a bit when we decrease σ_I, but even for $\sigma_I = 10$ MeV the difference between the methods is better than 3×10^{-3} for the same σ_R range. Thus we can conclude that the two methods are essentially equivalent.

In the following we discuss the main advantages of the Lanczos technique, which are (i) its applicability to huge sparse matrices and (ii) a considerable reduction in the CPU time.

(i) It seldom happens that one has to deal with a Hamiltonian matrix which is either sparse or written as an outer product. For such matrices the calculation of the product $\hat{H}|\phi\rangle$ goes much faster than $O(n^2)$ (n is the dimension of the matrix), and there is a great incentive to use algorithms, like the Lanczos algorithm, that exploits this feature. In fact, the real power of the Lanczos formulation lies here: it opens up the way to work with a huge number of basis functions, which direct inversion methods or full diagonalization methods fail to address. (ii) The reduction in CPU time results from the fast convergence of the lowest (and highest) eigenvalues, so that it is not necessary to perform all the Lanczos steps. In fact, checking the convergence of $L(\sigma_R, \sigma_I)$ with respect to the number of Lanczos coefficients used in the continued fraction one finds the following: for $\sigma_R \to \infty$ only the first Lanczos

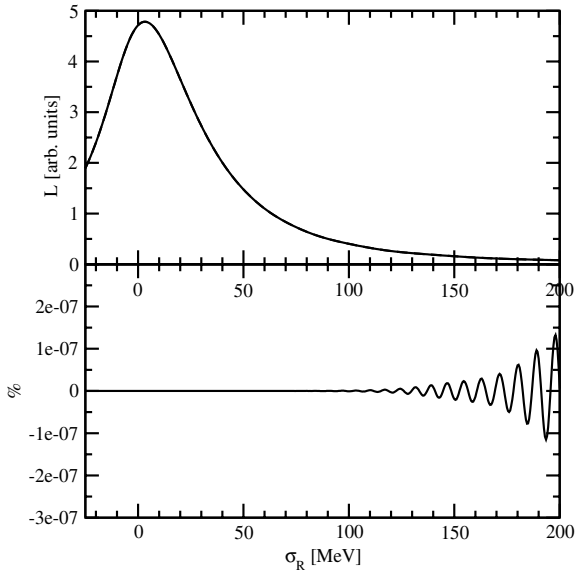

Figure 10. Upper panel: ^{4}He photoabsorption inclusive LITs calculated with the Hamiltonian inversion and with the Lanczos algorithm (150 Lanczos coefficients). The two curves are indistinguishable on this scale. In the lower panel the relative difference between them is plotted.

step is necessary, because the entire continued fraction is dominated just by σ_R. Also in the low σ_R region, as expected, the continued fraction converges rapidly, since for $\sigma_R \to 0$ the dominating contribution to the term $1/(z - \hat{H})$ is given by the lowest eigenvalue of $\hat{H}$, which is well approximated using only the first few Lanczos coefficients. It turns out that also in the intermediate σ_R region a rather small number of Lanczos coefficients are sufficient.

As an example in figures 11 and 12, we show the convergence patterns with respect to the number of Lanczos steps for the LIT of the inclusive photodisintegration of ^{4}He described above. This time, the calculation has been carried out with all the SYMHH states up to $K_{\max} = 15$ and with 21 hyperradial states, i.e. a total of about 18, 000 basis functions. If written in a matrix form the Hamiltonian would consume about 2.5 Gb of computer memory, and full diagonalization would be a long task. It can be seen that even for a sizable basis set the transforms converge very rapidly with only few hundreds Lanczos steps. As expected the convergence of the LIT is very good near threshold, then the number of Lanczos steps needed to achieve convergence grows with σ_R to a maximum value at about $\sigma_R \approx 100$ MeV and then, for higher values of σ_R convergence improves again.

To understand the effect of σ_I on the convergence pattern it is instructive to compare figures 11 ($\sigma_I = 10$ MeV) and 12 ($\sigma_I = 20$ MeV). Roughly speaking, the convergence of the LIT improves by almost one order of magnitude when σ_I is increased from 10 to 20 MeV. This follows from the reduction in the sensitivity of the LIT to the exact position of the eigenvalues of $\hat{H}$ (see (3.21)), when σ_I is large. In general for full tridiagonalization the Lanczos algorithm exhibits an $O(n^3)$ time complexity. However, since the continued fractions converge already with a number of Lanczos coefficients much smaller than n, the overall time needed to get the Lorentz integral transform is proportional to n^2. In practice we have found that about 1000 Lanczos steps are enough, even for very large bases.

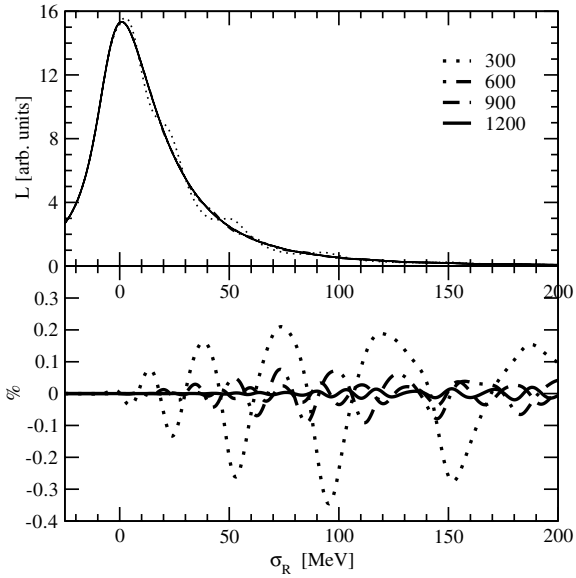

Figure 11. Upper panel: convergence of the ^{4}He photoabsorption inclusive LITs for $\sigma_I = 10$ MeV and for different numbers N of Lanczos coefficients. Lower panel: relative errors with respect to the converged Lanczos result ($N = 1500$).

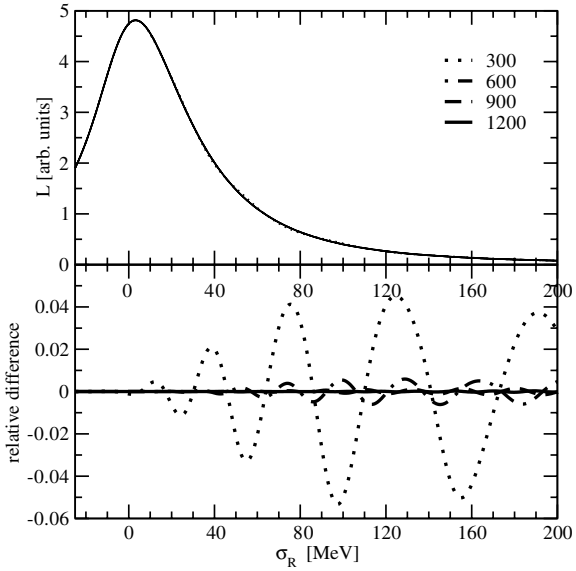

Figure 12. Same as figure 11, but for $\sigma_I = 20$.

In summary, reformulating the LIT method with the Lanczos algorithm represents an extremely powerful way to perform actual LIT calculations. All checks have shown that it is as accurate as any other method and it is much more efficient from the computational point of view.

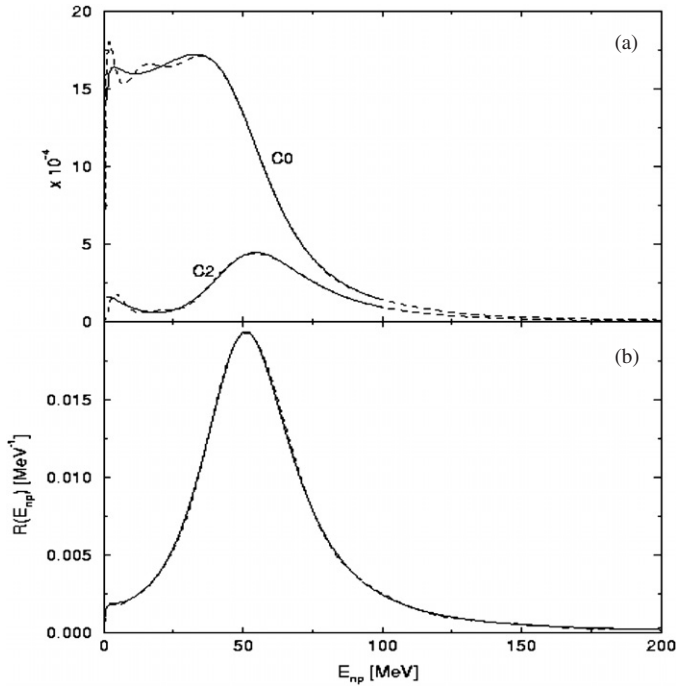

Figure 13. Longitudinal form factor $R_L(q, E_{np})$ of the $d(e, e'p)n$ reaction at $q = 440$ MeV/c for Paris potential [81] from LIT calculation (dashed curves) and from calculation with explicit np final-state wavefunctions (full curves): contribution of C0 and C2 multipoles (a) and total results (b).

8. Results

In this section we present the results of various LIT applications, to few-body systems of increasing number of nucleons. Those obtained in the two-body system mainly represent important tests of the LIT method. The others are results obtained within different potential models, ranging from semirealistic NN potentials (MT-I/III [77], TN [9], AV4' and AV8' [79] (solid), MN [80]) to realistic ones (Paris [81], AV14 [73], AV18 [82], BonnRA [83]). Also various versions of the 3N forces have been employed, namely the Urbana potentials UVIII [84] and UIX [85] and the Tucson–Melbourne (TM) [86].

8.1. Reactions with the two-body system

We start the discussion reviewing the very first LIT application, i.e. the calculation of the deuteron longitudinal form factor $R_L(q, \omega)$ at $q = 440$ MeV/c. In [3], where the LIT has been originally proposed, it served as a test case for the applicability of the LIT approach. There, in order to have reliable inversion results it has been necessary to separate contributions from the Coulomb monopole (C0) and quadrupole (C2) transitions from the other multipole transitions (see also section 3.5). The former lead to a shoulder of R_L close to threshold, while the latter exhibit a peak in the quasi-elastic region. In figure 13, we show the results of this important LIT test (note: E_{np} is the kinetic energy of the outgoing np-pair in the centre of mass system). In the upper panel of the figure one sees that the C0 and C2 multipoles exhibit a steep rise at the very threshold, leading to somewhat oscillating inversion results. In figure 13(b), we present the comparison on the total R_L, where also the other Coulomb

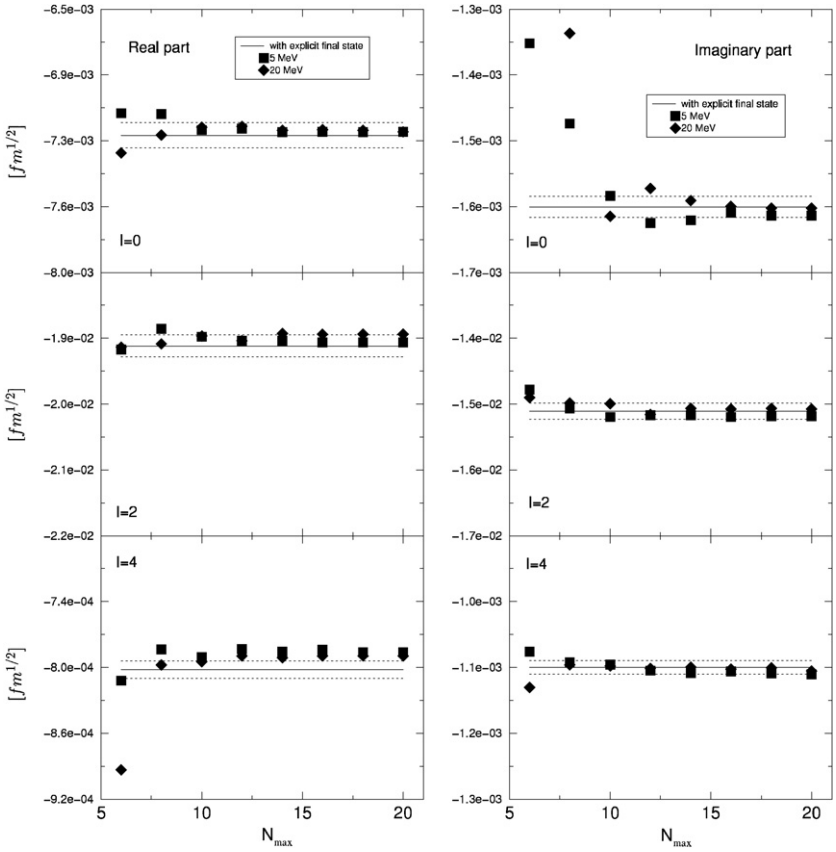

Figure 14. Deuteron electrodisintegration $d(e, e'p)n$. Real (left) and imaginary (right) parts of Coulomb transitions matrix elements of multipole order l (Born contribution subtracted) for a LIT calculation at $q = 440$ MeV/c and $E_{np} = 120$ MeV with TN potential as a functions of the number of inversion basis functions $N_{\max}$: diamonds ($\sigma_I = 5$ MeV), squares ($\sigma_I = 20$ MeV); also shown results for calculation with explicit np final-state wavefunction (full curves) and deviations of $\pm 1\%$ from these results (dotted curves).

multipoles are taken into account. It is evident that there is a very good agreement between the LIT result and the result of a calculation with explicit np continuum state wavefunctions.

In [21], a similar test study has been carried out for exclusive reactions. To this end the longitudinal part of the $d(e, e'N)N$ cross section has been investigated. In figure 14, we show results for a few selected Coulomb transition matrix elements. In order to make the comparison more significant the Born contribution (see section 2.2) is subtracted. One sees that (i) the calculation is essentially independent on the used σ_I-value and that (ii) there is a very good convergence in $N_{\max}$ in the inversion. Also shown are the results of a conventional calculation. Like for the inclusive test case of figure 13 they agree very well with the LIT results.

Among the two-body reactions considered within the LIT approach there exist also two interesting test cases concerning pion photoproduction. In [27], the Kroll–Ruderman term has been considered and it has been shown that the results are the same as in a conventional calculation with explicit scattering states. A further study has been carried out in [89], where the proper implementation of Δ degrees freedom in pion photoproduction has been successfully investigated for a LIT calculation.

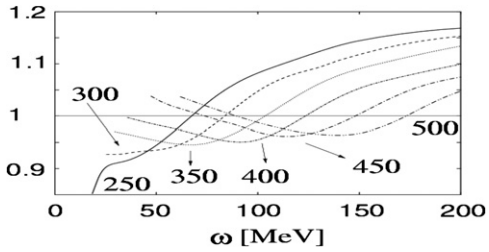

Figure 15. Ratios R_L(with 3N force)/R_L(without 3N force) for triton at various momentum transfers; q values indicated in the figure in units of MeV/c.

8.2. Reactions with three-body systems

8.2.1. Electrons. For the three-nucleon systems first LIT calculations of $R_L(q, \omega)$ ($q = 250, 300$ MeV/c) have been made using the Faddeev formalism and taking realistic NN potential models [30]. Like the deuteron cases of the previous section they have merely served as tests for the applicability of the LIT method. In fact an excellent agreement of the LIT results with those of a previous conventional Faddeev calculation has been obtained. Later a more systematic study of the effects of various theoretical ingredients on R_L has been carried out with the LIT approach for a wider momentum transfer range using the CHH expansion technique [25, 90]. The dependence on the following theoretical ingredients have been investigated: NN potential models, 3N potential models, relativistic corrections to the non-relativistic charge operator (spin–orbit and Darwin–Foldy terms), reference frame dependence. Here we give a short summary of the results of [90]. In general a rather small NN potential model dependence has been found, but in some cases there are also larger effects. These include the height of the quasi-elastic peak at lower q and the threshold behaviour. In figure 15, we illustrate the effect of the three-nucleon force (3NF). It is typically between 5% and 10%, but reaches up to 15% for the low-energy responses, far beyond the quasi-elastic peak. The dependence on the 3NF model is very small. Relativistic corrections are unimportant at lower q, but cannot be neglected for $q > 400$ MeV/c. For momenta up to $q = 500$ MeV/c, the comparison of the theoretical results with experimental data is generally rather satisfying. The experimental data, however, are in most cases not precise enough to draw conclusions about the 3NF effect. A nice exception is the ^{3}He low-energy response, where a 3NF proves to be necessary to obtain agreement with experiment (see upper panel of figure 16). At higher q and low-energy one finds a considerably higher R_L response in theory than in experiment (see lower panel of figure 16). In figure 16, for energies below the three-body break-up threshold, we also show results from a calculation with explicit three-nucleon final-state wavefunctions [88], where the same theoretical ingredients as in our LIT calculation are taken. One sees that there are rather good agreements between the results of the two different calculations.

A study of the R_L reference frame dependence has been already initiated in [90], but in [25] has been worked out in more detail and with consideration of higher momentum transfers. To this end the $R_L^{\rm fr}(\omega_{\rm fr}, q_{\rm fr})$ of different reference frames has been calculated and then transformed in a relativistically correct way to the laboratory system according to

$$R_L(\omega, q) = \frac{q^2}{q_{\rm fr}^2} \frac{E_T^{\rm fr}}{M_T} R_L^{\rm fr}(\omega_{\rm fr}, q_{\rm fr}), \tag{8.1}$$

(note the definition $R_L(\omega, q) \equiv R_L^{\rm lab}(\omega_{\rm lab}, q_{\rm lab})$) where $E_T^{\rm fr}$ and M_T are energy and mass of the target nucleus. In figure 17, we show results for four different frames [25], which are defined via

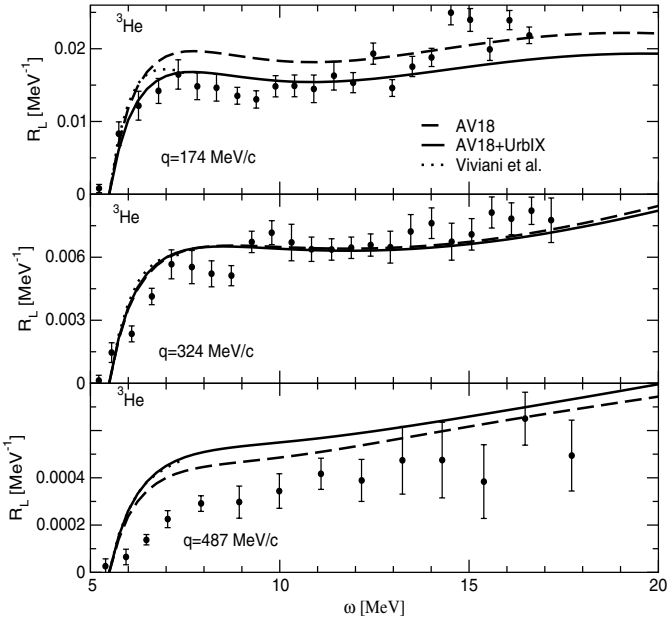

Figure 16. Comparison of theoretical and experimental R_L of ^{3}He: AV18+UIX potentials (solid) and AV18 potential (dashed), experimental data from [87]. Also shown theoretical results from [88] with AV18+UIX potentials (dotted) up to three-body break-up threshold.

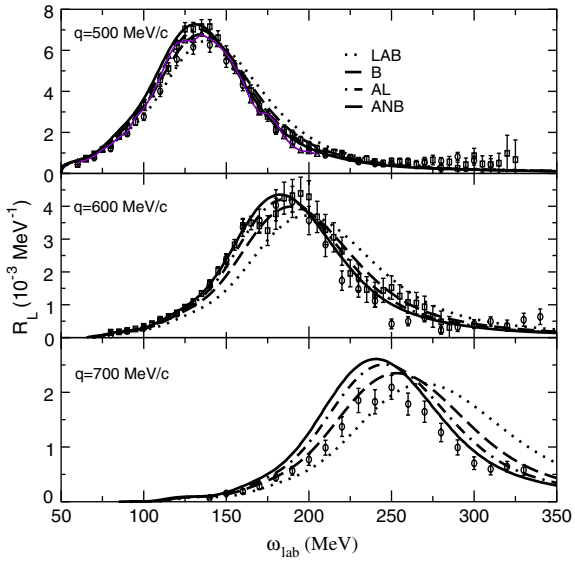

Figure 17. Frame dependence of R_L of ^{3}He: LAB (dotted), B (dashed), AL (dash-dotted), ANB (solid); experimental data from [91] (squares), [92] (triangles), [45] (circles).

the target nucleus initial momentum $\mathbf{P}_T^{\rm fr}$: $\mathbf{P}_T^{\rm lab} = 0$, $\mathbf{P}_T^{\rm B} = -\mathbf{q}/2$, $\mathbf{P}_T^{\rm AL} = -\mathbf{q}$, $\mathbf{P}_T^{\rm ANB} = -3\mathbf{q}/2$. It is readily seen that one obtains more and more frame-dependent results with growing q. As

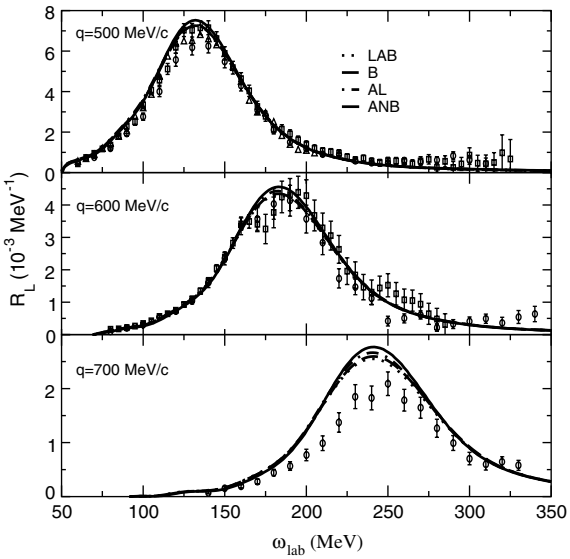

Figure 18. As in figure 17, but considering two-body relativistic kinematics for the final-state energy.

shown in [25] the frame dependence can be drastically reduced if one imposes quasi-elastic kinematics and takes the relativistic relative momentum between knocked-out nucleon and residual two-body system as input in the calculation. As seen in figure 18, in this way one finds almost frame independent results, which show a very good agreement with experimental data at q equal to 500 and 600 MeV/c, while at 700 MeV/c the experimental peak height is considerably lower than the theoretical one. We would like to point out that the ANB result of figure 17 lies within the band of almost frame independent results of figure 18. Thus one has to consider the ANB frame as the optimal frame for a non-relativistic calculation. In fact it leads to a proper description of the quasi-elastic peak region, with no need to assume quasi-elastic kinematics and thus its validity is not restricted to the peak region (further explanations why the ANB system is preferable are given in [25]).

8.2.2. Photons. Now we turn to the total three-nucleon photoabsorption cross sections. They have been studied with semirealistic NN potential models [94] first, and subsequently also with realistic nuclear forces (realistic NN potential + 3NF) [95]. In both cases CHH expansions have been used. In figure 19, we report the results of the first calculation of the total photoabsorption cross section with realistic forces [95]. The cross section is rather independent from a complete nuclear force model with NN and 3N forces. The role of 3NF is not negligible, they lead to a reduction of the low-energy peak by about 7% and to similarly strong increases at higher energies. One finds a rather good agreement of the theoretical results with experimental data. The experimental error bars, however, are quite large. In [29], the AV18+UIX LIT results, which are very similar to the AV14+UVIII and BonnRA+TM results of figure 19, have been successfully benchmarked with the Faddeev results of the Bochum–Cracow collaboration. In [29], also a check of the validity of the unretarded dipole approximation has been made. It has been found that retardation and higher multipole contributions are quite small up to moderate photon energies (below 2% for $\omega \leqslant 50$ MeV).

A high-precision comparison of CHH- and EIHH-LIT results with the AV18+UIX nuclear force model has been made in [96]. Finally we would like to mention that various

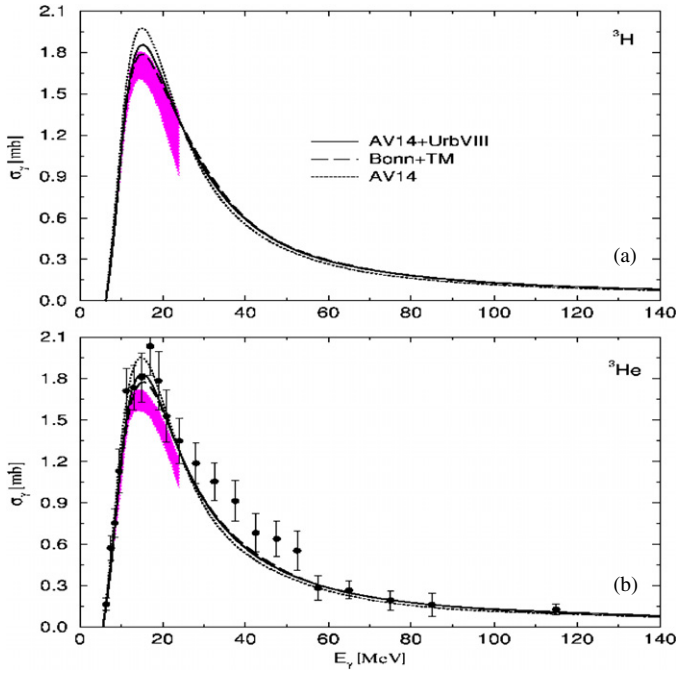

Figure 19. Total photoabsorption cross section of ^{3}H (upper panel) and ^{3}He (lower panel) with AV14 (dotted), AV14+UVIII (solid) and BonnRA+TM (dashed) potentials; the shaded area represents the data from [60] while the black dots are the data from [93].

photonuclear sum rules (polarizability, bremsstrahlungs, and TRK sum rules) have been studied in [94, 95].

8.2.3. Neutrinos. Next we consider weak reactions with three-body nuclei. The calculation of the cross section for neutral current neutrino scattering of ^{3}H and ^{3}He in the supernova scenario with realistic nuclear Hamiltonian and MEC currents has been presented in [97]. In the supernova scenario it is customary to assume that the neutrinos are in thermal equilibrium. Consequently, their spectra can be approximated by the Fermi–Dirac distribution with a characteristic temperature T_ν and with zero chemical potential

$$f(T_\nu, k) = \frac{N}{{T_\nu}^3} \frac{k^2}{\mathrm{e}^{k/T_\nu} + 1}, \tag{8.2}$$

where k is the neutrino momentum and $N^{-1} = 2\sum_{n=1}^{\infty}(-1)^{n+1}/n^3$ is a normalization factor. In order to estimate the mean neutrino interaction with the nuclear soap the calculated cross sections must be averaged over incident energy and angle. The quantities of interest are the temperature-averaged cross sections and energy transfer cross sections:

$$\langle\sigma\rangle_{T_\nu} = \int_{\omega_{\mathrm{th}}}^{\infty} \mathrm{d}\omega \int \mathrm{d}k_i \; f(T_\nu, k_i) \frac{\mathrm{d}\sigma}{\mathrm{d}k_f}, \tag{8.3}$$

$$\langle\omega\sigma\rangle_{T_\nu} = \int_{\omega_{\mathrm{th}}}^{\infty} \mathrm{d}\omega \int \mathrm{d}k_i \; f(T_\nu, k_i) \, \omega \frac{\mathrm{d}\sigma}{\mathrm{d}k_f}, \tag{8.4}$$

where $k_{i,f}$ are the initial and final neutrino energy, $\omega = k_i - k_f$ is the energy transfer, and ω_{th} denotes the threshold energy of the break-up reaction. In table 1, we present the results of [97]

Table 1. Averaged neutrino- and antineutrino-^{3}H and ^{3}He neutral-current inclusive inelastic cross sections per nucleon ($A = 3$): $\langle\sigma\rangle_{T_\nu} = \frac{1}{2A}\langle\sigma_\nu + \sigma_{\overline{\nu}}\rangle_{T_\nu}$ (left columns), and energy transfer cross sections, $\langle\omega\sigma\rangle_{T_\nu} = \frac{1}{2A}\langle\omega\sigma_\nu + \omega\sigma_{\overline{\nu}}\rangle_{T_\nu}$ (right columns), as a function of the neutrino temperature T_ν, in units of 10^{-42}cm^2 and 10^{-42}MeVcm^2 respectively.

T_ν [MeV]	^{3}H		^{3}He	
1	1.97×10^{-6}	1.68×10^{-5}	3.49×10^{-6}	2.76×10^{-5}
2	4.62×10^{-4}	4.73×10^{-3}	6.15×10^{-4}	5.94×10^{-3}
3	5.53×10^{-3}	6.38×10^{-2}	6.77×10^{-3}	7.41×10^{-2}
4	2.68×10^{-2}	3.37×10^{-1}	3.14×10^{-2}	3.77×10^{-1}
5	8.48×10^{-2}	1.14	9.70×10^{-2}	1.25
6	2.09×10^{-1}	2.99	2.35×10^{-1}	3.21
7	4.38×10^{-1}	6.61	4.87×10^{-1}	7.03
8	8.20×10^{-1}	13.0	9.03×10^{-1}	13.7
9	1.41	23.4	1.54	24.6
10	2.27	39.3	2.47	41.2

for the averaged neutrino and anti-neutrino neutral-current inclusive inelastic cross sections and energy transfer cross sections as a function of the neutrino temperature. The difference between the ^{3}H and the ^{3}He cross sections reflects the difference in thresholds between the two nuclei. The mirror symmetry between both nuclei is restored with higher neutrino energy. The leading contributions to the cross section are the axial E_1^A, M_1^A and E_2^A multipoles. The relative importance of these multipoles varies as a function of the momentum transfer, and thus as a function of the neutrino temperature. In comparison to inelastic excitations of ^{4}He studied in [98], the cross sections (the mean values of ^{3}H and ^{3}He) are about a factor 20 and 10 times larger at temperatures of 4 MeV and 6 MeV, respectively and the energy transfer cross sections are 8 and 2 times larger.

At low momentum transfer, the Gamow–Teller operator dominates for the cross section, consequently the MEC have a large effect of about 16% at a temperature of 1 MeV. At higher momentum transfer, higher order multipoles start to play an important role. Due to spatial symmetry, the MEC contribution to these multipoles is small and the overall effect of MEC decreases rapidly to less than 2% for temperatures above 4 MeV. While not directly important here, the asymmetry between the scattering of neutrinos and anti-neutrinos increases with temperature: the difference in the energy transfer cross sections grows gradually from 3% for a neutrino temperature of 3 MeV to more than 50% for a temperature of 10 MeV. Finally, the cutoff dependence of these observables is less than 2% for 1 MeV and less than 1% for higher temperatures. The estimated precision of these predicted cross sections is a few percent, which also includes estimates of the numerical accuracy.

8.3. Reactions with the four-body system

8.3.1. Electrons. The longitudinal form factor $R_L(q, \omega)$ of ^{4}He has been calculated in [101] at 300 MeV/$c \leqslant q \leqslant$ 500 MeV/c with the semirealistic TN potential via the LIT approach and using the CHH expansion technique. Already before, calculations with a realistic nuclear force had been carried out using the Green function Monte Carlo approach for the Laplace transform of the response [44]. However, the inversion of this integral transform is problematic (see discussion in section 4.1). In [101], a rather good agreement of the LIT results with experimental data has been found, as can be seen in figure 20. The figure also contains LIT results from [23], where R_L has been determined calculating the spectral function $S(E, k)$

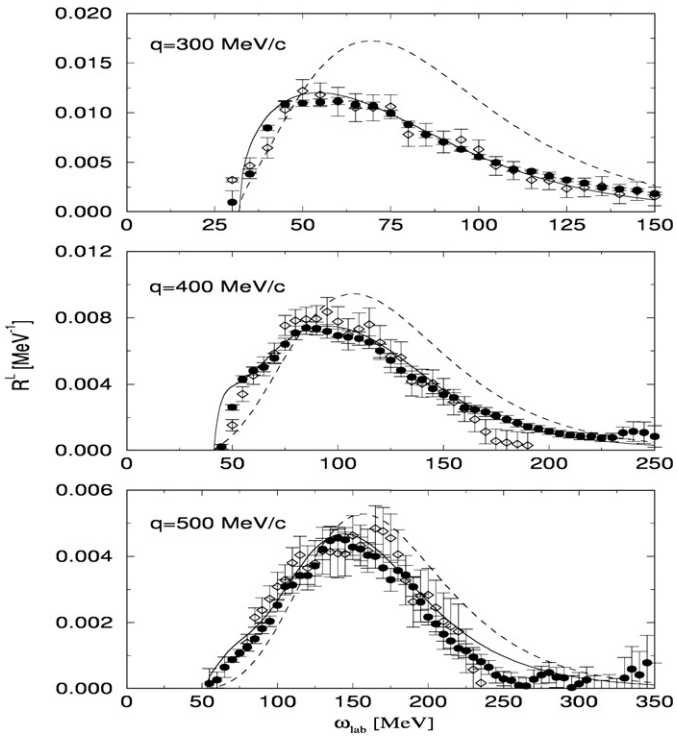

Figure 20. R_L of ^{4}He with the TN potential: plane wave impulse approximation result via use of spectral function (dashed curves) and full results (solid curves); experimental data from [99] (diamonds) and [100] (circles).

(see section 2.3) of the residual three-nucleon system in the $^4\mathrm{He}(e, e'p)X$ reaction. In the calculation with a spectral function the FSI of the outgoing proton with the residual three-nucleon system is not taken into account. The figure illustrates that the proton FSI is quite important. It leads to shifts of the quasi-elastic peak positions by about 15 MeV towards lower energy and reduces the peak heights quite considerably (30%, 20% and 10% at $q = 300$, 400, and 500 MeV/c respectively). Rather strong FSI effects are also found close to the break-up threshold.

Very recently also $R_T(q, \omega)$ has been studied [26] with the MT-I/III potential, using EIHH expansions. Besides the non-relativistic one-body currents (IA), a consistent meson exchange current (MEC) is taken into account explicitly, (with an approximation which, however, is shown to be very good at lower momentum transfer). In figure 21, we illustrate R_T for different momentum transfers in comparison to the available experimental data. The spin current strongly dominates the response function at higher momentum transfer (here not shown for $q = 300$ MeV/c, for more details see [26]), while at $q = 100$ MeV/c the convection current gives a large contribution. One also notes quite an important MEC contribution: at energies of about 100 MeV MEC lead to an enhancement by a factor of four with respect to the IA. With increasing q the enhancing effect of the MEC with respect to the IA is reduced dramatically. Unfortunately, there are no experimental data for the lower two q-values. At $q = 300$ MeV/c one finds a fair agreement with the data at lower and higher energies, but the quasi-elastic peak height is somewhat underestimated.

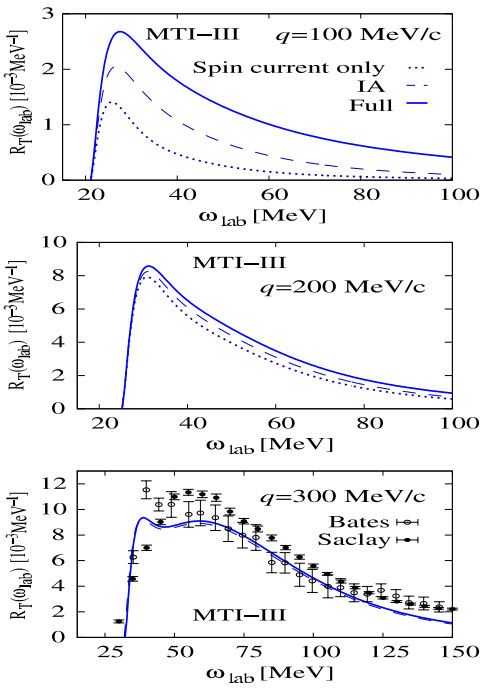

Figure 21. R_T of ^{4}He with the MT-I/III potential: spin current only (dotted), IA with spin and convection currents (dashed), full calculation with the inclusion of a consistent two-body current (solid); experimental data from [99] (open circles) and [100] (solid circles).

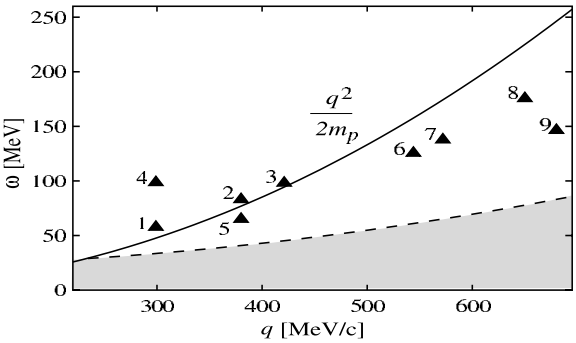

Figure 22. ^{4}He$(e, e'p)^3$H reaction: position of the various kinematics of figure 23 with respect to the $\omega = q^2/(2m_p)$ ridge. Shaded area represents the region below the break-up threshold.

For the four-body system two electron induced exclusive reactions have been considered with the LIT method (CHH expansion technique) and using semirealistic NN potentials: the longitudinal parts of the cross sections of ^{4}He$(e, e'p)^3$H, close to quasi-elastic kinematics [103], and of ^{4}He$(e, e'd)^2$H, at rather low ω and 250 MeV/$c \leqslant q \leqslant$ 450 MeV/c [104]. For ^{4}He$(e, e'p)^3$H results on the FSI effects and a comparison with experimental data are shown in figures 22 and 23. In figure 22 the considered kinematics, labelled with numbers from 1 to 9, are illustrated in the q-ω plane. In figure 23, the effects of the FSI for the nine cases are

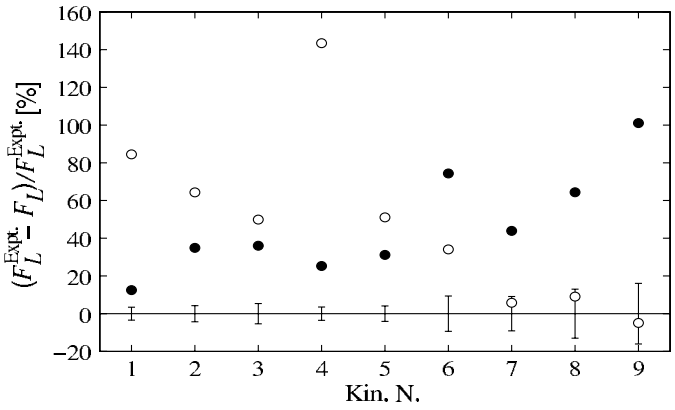

Figure 23. ^{4}He$(e, e'p)^3$H reaction: percentage deviation of theoretical differential cross section from the experimental values of [102]: without FSI (open circles) with inclusion of full FSI (solid circles).

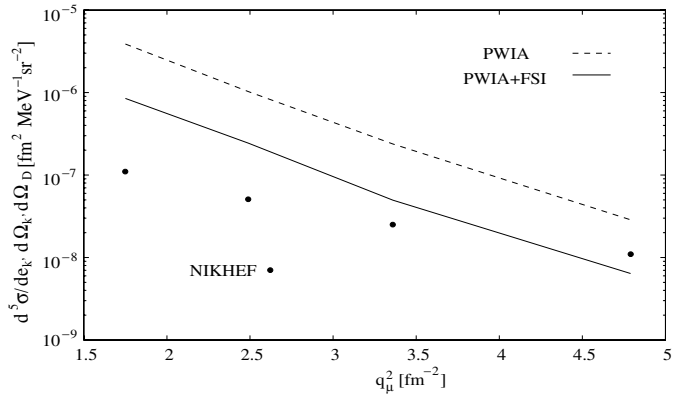

Figure 24. ^{4}He$(e, e'd)d$ reaction, differential cross section at a kinetic energy of the outgoing dd-pair of 35 MeV and averaged over a missing momentum range between 100 and 150 MeV as a function of q_μ^2 (four-momentum transfer squared): without FSI (dashed), with FSI (solid). Experimental data from [105].

shown. One sees that FSI reduces/increases the cross section below/above $q = 500$ MeV/c leading to an improved agreement with experiment only for q below 500 MeV/c. Presumably for higher q an inclusion of relativistic effects might be important and possibly lead to a better agreement with experiment.

For the $(e, e'd)$ reaction of figure 24, one finds an enormous reduction of the cross section due to FSI, which, however, is not sufficient to describe the rather small experimental cross section at lower q. As discussed in [104], a consideration of the tensor force could be particularly important for the FSI and possibly lead to an improved agreement with experiment.

8.3.2. Photons. The ^{4}He photodisintegration has a rather long history and many different experiments have been carried out over the years (see e.g. [76]). Unfortunately, the results of

the various experiments on the total photoabsorption cross section differ quite substantially in the size of the giant resonance peak. About ten years ago theory [111] and experiment [109, 110] seemed to converge to a rather low peak cross section. However, in the LIT calculation of [113] a much more pronounced giant resonance peak was found. The calculation had been carried out in the unretarded dipole approximation with semirealistic NN potentials models (TN and MT-I/III potentials) using CHH expansions. We would like to point out that the unretarded dipole approximation should work even for higher energies than for the total photoabsorption cross sections of two- and three-body nuclei, since the ^{4}He root mean square radius is smaller than the radii of ^{2}H, ^{3}H and ^{3}He. An improved LIT calculation has been later pursued using EIHH expansions [114]. Somewhat modified results have been found, but the pronounced giant dipole peak cross section has been confirmed. The relative importance of the considered reaction and the contradiction of theoretical and experimental results have led to a renewed interest in the low-energy ^{4}He photodisintegration. New experimental data [108, 112] as well as LIT calculations for the exclusive $^4\mathrm{He}(\gamma, p)^3\mathrm{H}$ and $^4\mathrm{He}(\gamma, n)^3\mathrm{He}$ reactions (CHH expansions) [76] and a first calculation for the total ^{4}He photoabsorption cross section with a realistic nuclear force (EIHH expansions) [119] has become available thanks to the LIT method. The present situation for the total cross section is summarized in figure 25. One observes a rather good agreement of the theoretical calculation with the data of [108], while there is a large discrepancy with the data of [112]. One further notes that the effect of the three-nucleon force is quite large, it reduces the giant dipole peak height by about 10% and increases the high-energy cross section quite considerably (35% at pion threshold). The comparison of the full theoretical result with the data of [106] is quite satisfying, although the data show an even higher peak cross section.

Very recently a LIT calculation using chiral nuclear forces (NN+3N) [120] has been carried out. The total ^{4}He cross section results are very similar to the AV18+UIX results of figure 25. Calculations with non-local nuclear force models, where a 3NF is eliminated by construction (JISP6 and UCOM [121] NN potentials) have also been performed with the LIT method [75, 122]. They confirm the pronounced giant dipole cross section, but with peak positions at somewhat higher energies.

In [123], the integrated ^{4}He total photoabsorption strength has been considered. In particular the polarization, bremsstrahlung and TRK sum rules with the AV18+UIX nuclear force have been investigated. With their help proton–proton and neutron–neutron distances have been determined and a small deviation from the tetrahedral symmetry of the spatial configuration of ^{4}He has been found.

The exclusive reactions $^4\mathrm{He}(\gamma, N)^3\mathrm{X}$ have been calculated with the semirealistic MT-I/III potentials. The sum of the two channel cross sections can be compared with the total ^{4}He photoabsorption cross section. Below the three-body break-up threshold both results should be identical, since other channels are not open ($^4\mathrm{He}(\gamma, d)d$ cross section is zero in unretarded dipole approximation). On the other hand at higher energies the difference between the total $^4\mathrm{He}(\gamma)$ and the $^4\mathrm{He}(\gamma, p)^3\mathrm{H}$ plus $^4\mathrm{He}(\gamma, n)^3\mathrm{He}$ cross sections leads to an estimate for the more-body break-up cross section. The following results have been found in [76]. Below the three-body break-up threshold the agreement between the cross sections of the two kinds of calculations is rather good, but not yet completely satisfying. Therefore in section 7.3 we have reconsidered a similar consistency check of the LIT calculation. There it is shown that the HH expansion has to be carried out to a somewhat higher value of the grand angular HH quantum number K than has been done in [76] in order to find a satisfying agreement between both calculations. Concerning the more-body break-up cross section, in figure 26 we show the sum of three- and four-body channel cross sections obtained as described above. One sees that there is a fair agreement between experimental and theoretical results.

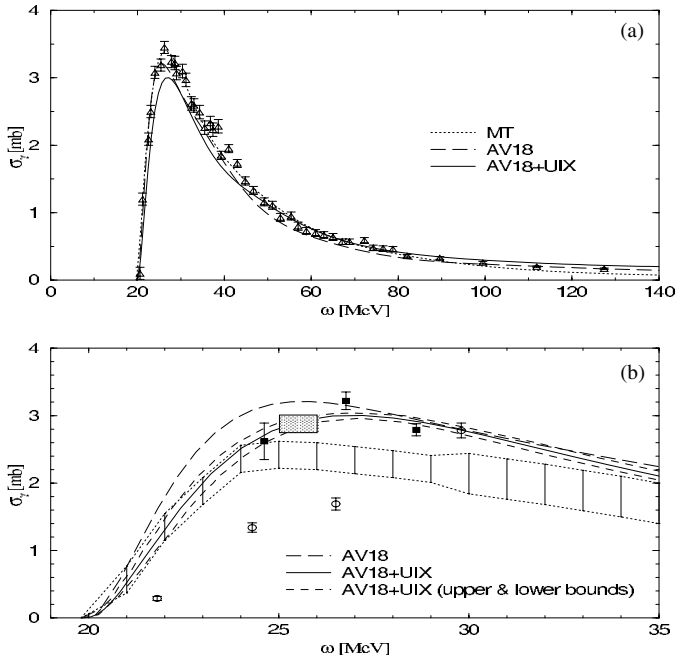

Figure 25. Total ^{4}He photoabsorption cross section: (a) MT-I/III (dotted), AV18 (dashed), AV18+UIX (solid). Experimental data from [106]. (b) as (a) but with upper/lower bounds included (estimate of theoretical error of EIHH convergence); experimental cross sections: dotted box [107], squares [108], open circles [112]. The area between dotted lines has been obtained combining data from [109] and [110].

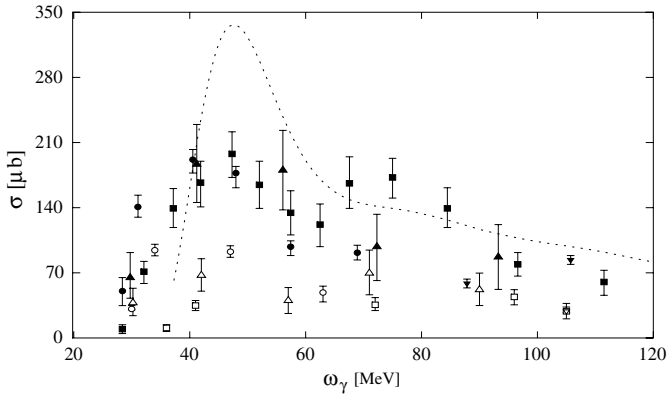

Figure 26. More-body break-up cross section in ^{4}He photodisintegration: total theoretical result of three- and four-body break-up (dotted); experimental results for ^{4}He$(\gamma, pn)d$ (full symbols) and ^{4}He$(\gamma, 2p2n)$ (open symbols), [115] (upward triangles), [116] (squares), [117] (circles), [118] (downward triangles).

8.3.3. Neutrinos. The inelastic neutral current neutrino scattering from ^{4}He has been calculated in [124] in the impulse approximation using the AV8' NN potential. Later in

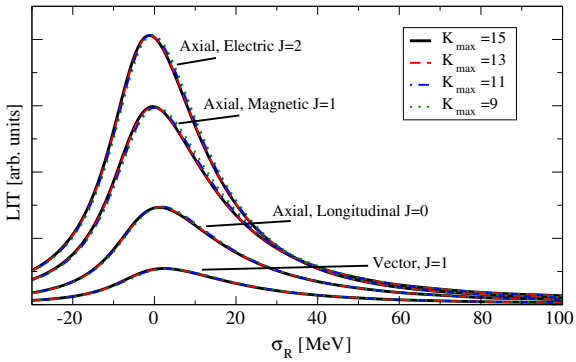

Figure 27. LIT convergence in $K_{\max}$ for the leading multipoles.

Table 2. Temperature averaged neutral current inclusive inelastic cross section per nucleon (in 10^{-42} cm^2) as a function of neutrino temperature (in MeV).

	$\langle\sigma_x^0\rangle_T = \frac{1}{2}\frac{1}{A}\langle\sigma_{\nu_x}^0 + \sigma_{\bar{\nu}_x}^0\rangle_T$ [10^{-42} cm^2]			
T_ν (MeV)	AV8' [124]	AV18	AV18+UIX	AV18+UIX+MEC
4	2.09 (−3)	2.31 (−3)	1.63 (−3)	1.66 (−3)
6	3.84 (−2)	4.30 (−2)	3.17 (−2)	3.20 (−2)
8	2.25 (−1)	2.52 (−1)	1.91 (−1)	1.92 (−1)
10	7.85 (−1)	8.81 (−1)	6.77 (−1)	6.82 (−1)
12	2.05	2.29	1.79	1.80
14	4.45	4.53	3.91	3.93

[98] the full nuclear Hamiltonian with the AV18+UIX potential has been used and MEC have been included.

In the supernova scenario one has to consider neutrinos with up to about 60 MeV. Usually, the leading contributions in weak nuclear processes are the Gamow–Teller and the Fermi operators. Due to the total angular momentum and spin structure of the ^{4}He nucleus, they are both strongly suppressed. In fact, the Gamow–Teller operator contributes only due to the small P- and D-wave components of the ground-state wavefunction. In addition, ^{4}He is an almost pure zero-isospin state [125, 126], hence the Fermi operator vanishes. Therefore, the leading contributions to the inelastic cross section are due to the axial vector operators E_2^A, M_1^A, L_0^A, L_2^A and the vector operators C_1^V, E_1^V, L_1^V (the latter are all proportional to each other due to the Siegert theorem). For the neutrino energies considered here it is sufficient to retain contributions up to $O(q^2)$ in the multipole expansion [124]. In figure 27 we present the convergence in $K_{\max}$ for these multipoles. It can be seen that the EIHH method results in a rapid convergence of the LIT calculation to a sub-percentage accuracy level.

In table 2, we present the temperature averaged total neutral current inelastic cross section as a function of the neutrino temperature for the AV8', AV18, and the AV18+UIX nuclear Hamiltonians and for the AV18+UIX Hamiltonian adding a MEC derived from a chiral EFT Lagrangian [127]. From the table it can be seen that the low-energy cross section is rather sensitive to details of the nuclear force model (the effect of 3NF is about 30%). This sensitivity gradually decreases with growing energy. In contrast the effect of MEC is rather small. Similar behaviour has also been observed for the *hep* process [128]. The small contribution of the MEC can be understood in the following way. The symmetry of the vertices in this

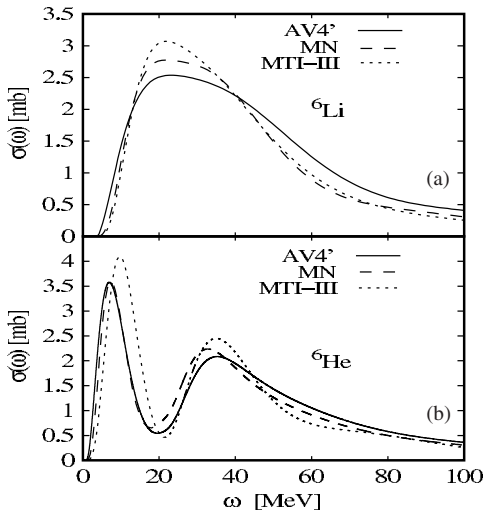

Figure 28. Total photoabsorption cross section of the six-body nuclei for various semirealistic NN potentials: AV4' (solid), MN (dashed), MT-I/III (dotted): (a) ^{6}Li and (b) ^{6}He.

low-energy approximation dictate a symmetry between the two nucleons interacting via the meson exchange. The leading one-body multipoles have negative parity, as a result the MEC contributions to them is small. In comparison the MEC correction to the Gamow–Teller is of the same magnitude as the one-body current, however both terms become marginal with increasing momentum transfer. Although presented for the neutral current, these arguments hold true also for the charged currents since the response functions are related by isospin rotation. These results are the first fully microscopic study of $\nu - \alpha$ reactions, using a state of the art nuclear Hamiltonian and including MEC. The overall accuracy of the calculation is estimated to be of the order of 5%. This is mainly due to the strong sensitivity of the cross section to the nuclear model. The numerical accuracy of the calculations is of the order of 1%, and the cutoff dependence of the MEC is of the same order.

8.4. Reactions with systems with $A > 4$

Different from the lightest nuclear systems the photodisintegrations of nuclei with $A > 4$ have not yet been studied in microscopic calculations with realistic nuclear forces, but LIT calculations with semirealistic NN interactions have been carried out [129–131]. with the MT-I/III, MN, and AV4' NN potentials. Different from the two former potential models the AV4' interaction includes a nonzero force also for the relative P-waves and also other odd waves. For the three- and four-nucleon systems such simple interactions lead to rather realistic total photoabsorption cross sections [95, 119], thus also for $A > 4$ cases one can expect that they lead to similarly good results.

In figure 28, we show the ^{6}He and ^{6}Li photoabsorption cross sections calculated with the above-mentioned semirealistic potential models. Particularly interesting is the ^{6}He case, which exhibits two separate cross section peaks. In a cluster model picture the low-energy peak can be explained by excitations of the surface neutrons (soft mode or 'pigmy resonance') leading to a final state with an α-particle and two neutrons, while the second peak corresponds to the classical electric dipole resonance (relative motion of neutrons against protons) with a break-up of the α-core. A similar double-peak picture is not found for ^{6}Li, even though a

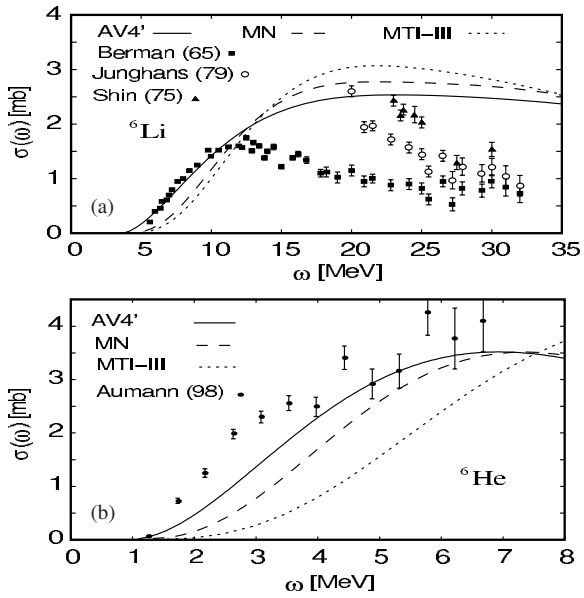

Figure 29. As in figure 28 but experimental data are also shown: (a) ^{6}Li(γ, n) data from [132] (solid squares) and ^{6}Li(γ,^{3}H)^{3}He data from [133] (open circles) and [134] (solid triangles) added to the (γ, n) data, (b) ^{6}He data from [135] (solid circles) (theoretical results convoluted with instrumental response function).

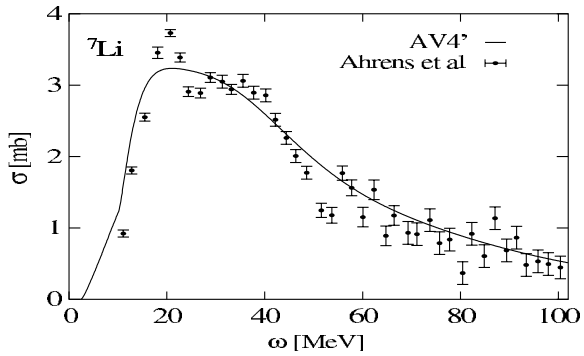

Figure 30. Total photoabsorption cross section of ^{7}Li: theoretical result with AV4' potential (solid) and experimental data from [136] (circles).

disintegration to a final state with an α-particle and a $^1S_0\,np$ pair is possible. However, such a transition is not energetically as well separated as the NN+α channel and the α break-up channel in ^{6}He. Note that a similar two-body break-up in case of ^{6}He into the ^{3}H–^{3}H channel is not induced by the electric dipole operator. In figure 29, we show the comparison with experimental data. Compared with the other two interaction models the AV4' potential leads to a better agreement with experiment at lower energy both for ^{6}He and ^{6}Li. In fact for ^{6}Li one finds a rather good description of the data up to 10 MeV, while at higher energies more precise data are needed in order to draw more definite conclusions. The agreement of theoretical and experimental low-energy results is less satisfying for ^{6}He. On the other hand one has to take

into account that the ^{6}He photodisintegration cross section has not been determined from a direct measurement, but extracted from the Coulomb excitation in the field of a heavy nucleus.

Now we turn to the ^{7}Li photodisintegration. In figure 30, we show the cross section calculated with the AV4' potential in comparison with experimental data. One finds quite a good agreement in the whole considered energy range. The data exhibit a few fluctuations, but one would need more precise data in order to decide whether such structures in the cross section really exist. We would like to point out that the experimental ^{7}Li total photoabsorption cross section had been determined via flux attenuation measurements in forward direction and not by summing up the cross sections of the various break-up channels. In the near future similar measurements for ^{4}He and ^{6,7}Li are planned at MAXLab (Lund) and will hopefully also be performed at the HIγS facility (Duke).

9. Summary

We have reviewed the theory, tests and applications of the Lorentz integral transform method for perturbation-induced reactions into the many-body continuum. The method is a novel approach, which allows the microscopic calculation of inclusive and exclusive cross sections without using complicated many-body continuum wavefunctions. Since its proposal in 1994 the method has been applied to quite a number of electroweak processes with few-body nuclei, among them are the first calculations with a realistic nuclear interaction (NN and 3N forces) for the total ^{3}H, ^{3}He and ^{4}He photoabsorption cross sections [95, 119] and the inelastic neutral current neutrino scattering off ^{4}He [98]. Even reactions into the six- and seven-body continuum have been considered [129–131] treating the many-body continuum interaction in a rigourous way. We would like to point out that at present there are no alternative approaches allowing similar *ab initio* calculations for $A \geqslant 4$.

Acknowledgments

WL and GO thanks the Department of Physics of the George Washington University for the warm hospitality. The work of NB was supported by the Israel Science Foundation (grant no. 361/05). VDE acknowledges support from the RFBR, grant no. 07-02-01222a, and the Russian Ministry of Education and Science, grant no. NS-8756.2006.2. The authors are grateful to M Schwamb for carefully reading the manuscript.

Appendix A. The correlated HH method (CHH)

In this appendix the CHH method is described. Not only the general idea of the method is summarized, but we also describe the details of its application, which has led to the results presented in section 8.

The basis functions we use are antisymmetric with respect to particle permutations. Such a basis is combined in a simple way from hyperspherical harmonics $\mathcal{Y}$ belonging to a given type of permutational symmetry and from spin–isospin functions θ belonging to a conjugated type of permutational symmetry. The set of $\mathcal{Y}$ differs from the unsymmetrized set (5.7) and we denote them $\mathcal{Y}^{[f]\mu}_{KLM_L,\alpha}$. They are components μ of a given irreducible representation [f] of the permutation group and they have a given grandangular momentum K, orbital momentum L with projection M_L. The label α enumerates the various HH with the same $K, L, M_L, [f]$ and μ. The $\mathcal{Y}^{[f]\mu}_{KLM_L,\alpha}$ may be constructed applying the Young operators to the simple $\mathcal{Y}_{[K]}(\hat{\Omega})$ of (5.7). This gives them in the form of linear combinations of the $\mathcal{Y}_{[K]}(P\hat{\Omega})$, where P are

particle permutations. These HH must be combined with spin–isospin functions $\theta^{[\bar{f}]\bar{\mu}}_{SM_S TM_T}$ as follows:

$$\sum_{\mu} \left\{ \mathcal{Y}^{[f]\mu}_{KL,\alpha} \otimes \theta^{[\bar{f}]\bar{\mu}}_{STM_T} \right\}_{JM}. \tag{A.1}$$

The spin–isospin functions have given spin S, M_S and isospin T, M_T quantum numbers and belong to the conjugated representation $[\bar{f}]$ of the permutation group. The spin–isospin function with a $\bar{\mu}$ value is conjugated to the spatial function with given μ so that the functions (A.1) are antisymmetric with respect to particle permutations. They possess a given total momentum J and its projection M. When solving the dynamic equations, products of the functions (A.1) and hyperradial functions $R_\beta(\rho)$ can be taken as spatial basis functions χ to expand $|\tilde{\Psi}\rangle$ in coordinate representation. For brevity we shall write the total basis functions as

$$\phi_i = \sum_{\gamma} \chi_{i,\gamma} \theta_\gamma, \tag{A.2}$$

where θ_γ are the spin–isospin functions of the above-mentioned form, and $\chi_{i\gamma}$ are the conjugated spatial functions.

The short range repulsion at small distances, present in the central components of conventional NN interactions, slows down the convergence of the HH expansion (A.2) considerably. To speed up the convergence one may include correlation factors in the basis functions. In [13], it has been shown that, in the case of central NN potentials, the inclusion of a Jastrow correlation factor $\omega = \prod_{i<j} f(r_{ij})$ in the HH expansion accelerates the convergence drastically. To compensate for the strong short range repulsion potential that is present in the A-body dynamic equation the pair correlation function $f(r_{ij})$ should approximately be a solution of the two-body equation with this potential. When the mentioned simple Jastrow correlation factor is employed this may be fulfilled only for s-states of the NN pair and only when the triplet and singlet potentials $\hat{V}_{31}(r_{ij})$ and $\hat{V}_{13}(r_{ij})$ are close to each other in the region of short-distance repulsion. To go beyond these frames a more general ansatz has been proposed [95, 137]:

$$|\Psi\rangle = \hat{\omega} \sum_i c_i \phi_i, \tag{A.3}$$

where ϕ_i are the HH-spin–isospin-hyperradial basis functions (A.2) and $\hat{\omega}$ is the correlation operator of the form

$$\hat{\omega} = \mathcal{S} \prod_{i<j} \sum_{S,T} f_{ST}(r_{ij}) \hat{P}_{ST}(ij). \tag{A.4}$$

Here $\hat{P}_{ST}(ij)$ are the projection operators onto nucleon pair (ij) states of spin S and isospin T and $\mathcal{S}$ is the particle symmetrization operator. The inclusion of $\mathcal{S}$ is necessary since $\hat{P}_{ST}(ij)$ for different pairs (ij) do not commute with each other. Operators of a similar type have been used in direct variational calculations of light nuclei, e.g. in [84]. In (A.3) $|\Psi\rangle$ stands for the initial state $|\Psi_0\rangle$, or for the LIT function $|\tilde{\Psi}\rangle$.

This form of the correlation operator is easily incorporated into the calculations by first constructing the set of coefficients $\langle\theta_{\gamma'}|\hat{\omega}|\theta_\gamma\rangle$ and then writing

$$|\Psi\rangle = \sum_i c_i \tilde{\phi}_i, \tag{A.5}$$

where

$$\tilde{\phi}_i = \sum_{\gamma'} \tilde{\chi}_{i,\gamma'} \theta_{\gamma'}, \qquad \tilde{\chi}_{i,\gamma'} = \sum_{\gamma} \langle\theta_{\gamma'}|\hat{\omega}|\theta_\gamma\rangle \chi_{i,\gamma}. \tag{A.6}$$

The pair correlation functions entering (A.4) are constructed as follows. At $r \leqslant r_0$ ($r \equiv r_{ij}$) they are solutions of the two-body equation

$$-\frac{\hbar^2}{M}\left[\frac{\mathrm{d}^2 f}{\mathrm{d}r^2} + \frac{2}{r}\frac{\mathrm{d}f}{\mathrm{d}r} - \frac{l(l+1)}{r^2} f\right] + \left[\hat{V}^c_{ST}(r) + \hat{V}^m_{ST}(r)\right] f = 0, \tag{A.7}$$

where $f = f_{ST}$. Here $l = 0$ for even states and $l = 1$ for odd states of a nucleon pair. The potential $\hat{V}^c_{ST}$ is the central component of the NN interaction. The potential $\hat{V}^m_{ST}$ takes approximately into account the other components of the NN interaction and also the interaction produced by other nucleons. (In the case $S = T = 1$ the corresponding p-wave NN interaction is j dependent which is disregarded in (A.7).) The potentials in (A.7) should ensure that $f'(r_0) = 0$ at some point r_0. Equation (A.7) is solved in the range $0 \leqslant r \leqslant r_0$ and at $r > r_0$ one sets $f(r) = f(r_0) = 1$.

In the $A = 3$ calculations with realistic NN+3N forces presented in this review the procedure described above has been applied. For even NN states the potential $\hat{V}^m_{ST}$ was disregarded in (A.7). In the $A = 4$ calculations with central NN forces the simple Jastrow correlation factor has been used with an average potential equal to $1/2[\hat{V}_{31}(r) + \hat{V}_{13}(r)]$.

In order to diminish the number of basis states in the correlated HH calculations one may optimize the potentials $\hat{V}^m_{ST}$ in (A.7). In addition, one may apply different correlation operators (A.4) to different parts of $|\tilde{\Psi}\rangle$ or $|\Psi_0\rangle$. The correlation functions may also be obtained from equations of (A.7) form for finite energies. These energies may be fixed from the condition that f''_{ST} is continuous, i.e. $f''_{ST}(r_0) = 0$ [13], or in another way. In the ground-state case the parameters determining $f_{ST}(r)$ may be optimized from the minimum energy requirement or from the condition

$$\min\{\langle(\hat{H} - E_0)\Psi_0|(\hat{H} - E_0)\Psi_0\rangle\}. \tag{A.8}$$

In the integral transform case these parameters may be chosen from the condition

$$\min\{\langle(\hat{H} - \tilde{E})\tilde{\Psi} - Q|(\hat{H} - \tilde{E})\tilde{\Psi} - Q\rangle\} \tag{A.9}$$

for some typical $\tilde{E}$ values, where $|Q\rangle$ indicates the source terms in the inhomogeneous equations (see section 2.1). In general, conditions of (A.8) and (A.9) form may be used to fix nonlinear parameters in variational few-body calculations that are not based on the minimum energy principle. In particular in variational methods for calculating reactions the condition

$$\langle(\hat{H} - E)\Psi^{\pm}|(\hat{H} - E)\Psi^{\pm}\rangle = \min \tag{A.10}$$

may be used for this purpose.

Besides correlations caused by the strong short distance repulsion in NN potentials long range tensor correlations also require to reach high K values in the HH expansion. In the $A = 4$ CHH calculations presented here, as well as in some of the $A = 3$ ones a selection of correlated HH has been used. In general only HH that have small l_n and K_{n-1} values before applying the Young symmetrization operators are to be retained [54, 138]. This prescription is justified for non-correlated HH and in the case of the ground state, but seems to work in our case as well. A more detailed selection within these frames has been done (see also [126].) For example, in the case of $A = 3$ bound state it has been found that for high K values only those HH are to be retained that in the notation of section 5.1 had quantum numbers $l_2 = 2$ and $l_1 = 0$ before applying the Young symmetrization operators.

Convergent results have been obtained in the calculations with the CHH method (for judging the accuracy reached see [96] in $A = 3$ calculations). Also in [139, 140] accurate results have been obtained in the $A = 4$ case with realistic nuclear forces in a CHH basis for the ground-state and low-energy scattering. There, different Jastrow-type correlation factors for different parts of wavefunctions have been applied. It is interesting to note that, due

to flexibility of the basis, accurate results e.g. for the α-particle ground state with realistic NN+3N interactions, have been obtained retaining only low K values (up to $K = 8$).

A final comment regards the practical way to calculate matrix elements of the Hamiltonian between CHH states. In the $A = 3$ case, an analytic integration over the Euler angles that determine the orientation of the system as a whole has been performed [141]. The remaining three-dimensional integration has been carried out with regular quadratures. In the $A > 3$ case, the Monte Carlo integration has been applied.

Appendix B. The effective interaction HH method (EIHH)

In the effective interaction approach [142–146] the lowest eigenvalues of an A-body Hamiltonian

$$\hat{H}^{[A]} = \hat{H}_0 + \hat{V} \tag{B.1}$$

is treated in the following way. The Hilbert space of $\hat{H}^{[A]}$ is divided into a model space and a residual space, through the use of the eigenprojectors $\hat{P}$ and $\hat{Q}$ of $\hat{H}_0$, which satisfy the relations

$$[\hat{H}_0, \hat{P}] = [\hat{H}_0, \hat{Q}] = 0; \qquad \hat{Q}\hat{H}_0\hat{P} = \hat{P}\hat{H}_0 Q = 0; \qquad \hat{P} + \hat{Q} = 1. \tag{B.2}$$

The Hamiltonian $\hat{H}^{[A]}$ is then replaced by the effective model space Hamiltonian

$$\hat{H}^{[A]\mathrm{eff}} = \hat{P}\hat{H}_0\hat{P} + \hat{P}\hat{V}^{[A]\mathrm{eff}}\hat{P} \tag{B.3}$$

that by construction has the same energy levels as the low-lying states of $\hat{H}^{[A]}$. In general the effective interaction appearing in (B.3) is an A-body interaction, and its construction is usually as difficult as finding the full-space solutions of the A-body problem. Therefore, one has to approximate $\hat{V}^{[A]\mathrm{eff}}$. However, one must build the approximate effective potential in such a way that it coincides with the bare one for $P \to 1$, so that an enlargement of the model space leads to a convergence of the eigenenergies to the *true* values. The EIHH method is developed along these lines.

In the HH formalism the internal A-body Hamiltonian $\hat{H}^{[A]}$ is written as

$$\hat{H}^{[A]} = \hat{T}_\rho + \hat{T}_K(\rho) + \hat{V}^{[A]}(\rho, \hat{\Omega}), \tag{B.4}$$

where

$$\hat{V}^{[A]}(\rho, \hat{\Omega}) \equiv \sum_{i<j}^{A} v_{ij} \tag{B.5}$$

denotes the bare two-body potential and

$$\hat{T}_\rho = -\frac{1}{2m}\Delta_\rho, \qquad \hat{T}_K(\rho) = \frac{1}{2m}\frac{\hat{K}^2_{A-1}}{\rho^2} \tag{B.6}$$

are the hyperradial and hypercentrifugal kinetic energies, respectively. In the previous equation Δ_ρ is the Laplace operator with respect to the hyperradial coordinate ρ, while $\hat{K}_{A-1}$ is the hyperspherical grand angular momentum (see equations (5.5) and (5.6)). The hyperradial kinetic energy $\hat{T}_\rho$ and the residual Hamiltonian

$$\hat{\mathcal{H}}^{[A]}(\rho) \equiv \hat{T}_K(\rho) + \hat{V}^{[A]}(\rho, \hat{\Omega}) \tag{B.7}$$

are often considered separately. The Hamiltonian $\hat{\mathcal{H}}^{[A]}(\rho)$, often used as a starting point in atomic and molecular calculations, is called adiabatic [147] as the hyperradial coordinate ρ is a *slow* coordinate with respect to the hyperangles. In the EIHH method [145, 146] the effective interaction is calculated starting with this adiabatic Hamiltonian. The unperturbed Hamiltonian

$\hat{H}_0$ is chosen to be $\hat{T}_K(\rho)$ with the hyperspherical harmonics $\mathcal{Y}_{[K_{A-1}]}$ as eigenfunctions. The model space P is defined as the complete set of HH basis functions with generalized angular momentum quantum number $K \leqslant K_P$, and the Q-space as the complete set of HH basis functions with $K > K_P$. The states are denoted by $\{|p\rangle;\ p = 1, 2, \ldots, n_P\}$ for the P-space and $\{|q\rangle; q = n_{p+1}, n_{p+2}, \ldots, n_Q\}$ for the Q-space. Of course, in principle one has $n_Q \to \infty$. In actual calculations one considers finite Q-spaces. However, n_Q must be sufficiently large.

For each value of the hyperradius ρ an effective adiabatic Hamiltonian is constructed

$$\hat{\mathcal{H}}^{[A]\text{eff}}(\rho, \hat{\Omega}) = \hat{P}\hat{T}_K(\rho)\hat{P} + \hat{P}\hat{V}^{[A]\text{eff}}(\rho, \hat{\Omega})\hat{P}. \tag{B.8}$$

However, as already pointed out, the effective potential would be a complicated A-body interaction, therefore $\hat{V}^{[A]\text{eff}}$ is approximated by a sum of *quasi-two-body* terms

$$\hat{V}^{[A]\text{eff}} \simeq \sum_{i<j}^{A} \hat{v}_{i,j}^{[2]\text{eff}}. \tag{B.9}$$

Due to the use of antisymmetric wavefunctions one only needs to calculate the effective interaction operator relative to one pair, since

$$\langle \hat{V}^{[A]\text{eff}} \rangle \simeq \left\langle \sum_{i<j}^{A} \hat{v}_{i,j}^{[2]\text{eff}} \right\rangle = \frac{A(A-1)}{2} \langle \hat{v}_{A,(A-1)}^{[2]\text{eff}} \rangle. \tag{B.10}$$

The *quasi-two-body* effective potential $\hat{v}_{A,(A-1)}^{[2]\text{eff}}$ is determined as follows. First for each value ρ of the hyperradial coordinate one defines a *quasi-two-body* adiabatic Hamiltonian containing the hypercentrifugal kinetic energy and the bare potential between the last two particles (the prefix *quasi* is justified, because this Hamiltonian depends on the A-body coordinate ρ)

$$\hat{\mathcal{H}}^{[2]}(\rho; \theta_{A-1}, \hat{\eta}_{A-1}) = \hat{T}_K(\rho) + \hat{v}_{A,(A-1)}(\sqrt{2}\rho \sin\theta_{A-1} \cdot \hat{\eta}_{A-1}). \tag{B.11}$$

The Hamiltonian of equation (B.11) is then diagonalized on the A-body HH basis. Such a diagonalization is easily performed since ρ is only a parameter in $\hat{\mathcal{H}}^{[2]}$, (there are no derivatives with respect to ρ) and for each value of ρ the Hamiltonian $\hat{\mathcal{H}}^{[2]}(\rho; \theta_{A-1}, \hat{\eta}_{A-1})$ depends only on three variables. This is just due to our choice of the A-$(A-1)$ pair in (B.10). The obtained eigenstates are denoted by $|j(\rho)\rangle$ as they are continuous functions of ρ.

One proceeds applying the Lee–Suzuki [148–150] similarity transformation to $\hat{\mathcal{H}}^{[2]}(\rho; \theta_{A-1}, \hat{\eta}_{A-1})$ in order to get the corresponding Hermitian effective Hamiltonian

$$\hat{\mathcal{H}}^{[2]\text{eff}}(\rho; \theta_{A-1}, \hat{\eta}_{A-1}) = \hat{U}^{\dagger}(\rho)\hat{\mathcal{H}}^{[2]}(\rho; \theta_{A-1}, \hat{\eta}_{A-1})\hat{U}(\rho), \tag{B.12}$$

where

$$\hat{U}(\rho) = (\hat{P} + \hat{\omega}(\rho))\frac{1}{\sqrt{\hat{P}(1 + \hat{\omega}(\rho)^{\dagger}\hat{\omega}(\rho))\hat{P}}}. \tag{B.13}$$

The operator $\hat{\omega}(\rho)$ is obtained using the following property [148]

$$\hat{\omega}(\rho) = \hat{Q}\hat{\omega}(\rho)\hat{P}. \tag{B.14}$$

The matrix $\hat{\omega}(\rho)$ is calculated for each value of ρ taking the n_P states $|j(\rho)\rangle$ with the lowest eigenvalues. Each of these states leads to the following system of $(n_Q - n_P)$ equations:

$$\langle q|j(\rho)\rangle = \sum_{p} \langle q|\hat{\omega}(\rho)|p\rangle\langle p|j(\rho)\rangle. \tag{B.15}$$

The $n_P(n_Q - n_P)$ matrix elements $\langle q|\hat{\omega}(\rho)|p\rangle$ are obtained by solving the equation system (B.15). Once the effective *quasi-two-body* Hamiltonian $\hat{\mathcal{H}}^{[2]\text{eff}}$ is constructed, the effective

potential is obtained by a subtraction of the hypercentrifugal kinetic energy

$$\hat{v}^{[2]\mathrm{eff}}_{A,(A-1)} = \hat{\mathcal{H}}^{[2]\mathrm{eff}}(\rho) - \hat{T}_K(\rho). \tag{B.16}$$

Using this ρ-dependent effective potential and taking into account (B.8)–(B.10) one solves the A-body problem with the effective Hamiltonian

$$\hat{H}^{[A]\mathrm{eff}} = \hat{T}_\rho + \hat{\mathcal{H}}^{[A]\mathrm{eff}} = \hat{T}_\rho + \hat{T}_K + \sum_{i<j} \hat{v}^{[2]\mathrm{eff}}_{ij} \tag{B.17}$$

in the P-space. One repeats the procedure enlarging the P-space up to a convergence of the low-lying energies of the A-body system.

We would like to emphasize the following points:

(i) it is evident that $\hat{U}(\rho) \to 1$ for $P \to 1$ and thus $\hat{v}^{[2]\mathrm{eff}}$ converges to the bare $\hat{v}_{A,(A-1)}$; therefore the energy spectrum converges to the exact one;
(ii) in such a construction of an effective interaction the hyperradius is a parameter rather than a coordinate, and $\hat{v}^{[2]\mathrm{eff}}_{ij}$ is determined for various fixed ρ values; therefore, while being a two-body interaction, it depends on the whole A-body system via this collective coordinate;
(iii) there is an additional dependence of $\hat{v}^{[2]\mathrm{eff}}$ on the quantum number K_{A-2} of the residual system (see equations (19) and (20) of [145]);
(iv) via the operator $\hat{U}(\rho)$ the effective potential $\hat{v}^{[2]\mathrm{eff}}$ contains information about a large part of the PQ-space interaction, hence the convergence to the exact eigenvalues of $\hat{H}^{[A]}$ is accelerated with respect to the normal HH expansion;
(v) application of the transformation operator $\hat{U}(\rho)$ to the hyperradial kinetic energy operator yields corrections to $\hat{T}_\rho$ that go beyond the adiabatic effective interaction [151];
(vi) the convergence of the EIHH method can be further improved through the use of a three-body effective interaction [151].

The effectiveness of the EIHH method can be best demonstrated comparing the convergence rate of a normal HH expansion with that of an EIHH one for some typical observable. As an example in figure B1 such a comparison is shown for the binding energy and root mean square matter radius of a four-particle system interacting through the MTV NN potential. From the figure it can be seen that, whereas the EIHH method gives almost converged results for $K_{\max} = 4$, the HH calculation with the bare interaction misses about 1.5 MeV for $K_{\max} = 20$.

Appendix C. The multipole expansions of the response functions

If the Hamiltonian is rotationally invariant it is useful to expand the states Q and Q' in (2.1) over states possessing given values J and M of the total angular momentum and its projection. Then the whole calculation may be done in separate subspaces of states belonging to given J and M. Furthermore, the calculations are M independent. Here we shall present the required relationships for the case of longitudinal and transverse electrodisintegration response functions of a nucleus.

We start from (6.13) and (6.14), omitting the indices 'α' and 'β':

$$r^L(q,\omega) = \frac{1}{2J_0+1} \sum_{M_0,J,M} \sum\!\!\!\!\!\!\int \mathrm{d}f \langle \Psi_0(J_0,M_0)|\hat{\rho}^\dagger(\mathbf{q})|\Psi_f(J,M)\rangle$$
$$\times \langle \Psi_f(J,M)|\hat{\rho}(\mathbf{q})|\Psi_0(J_0,M_0)\rangle \delta\left(E_f(J) - E_0 + \frac{q^2}{2M_T} - \omega\right), \tag{C.1}$$

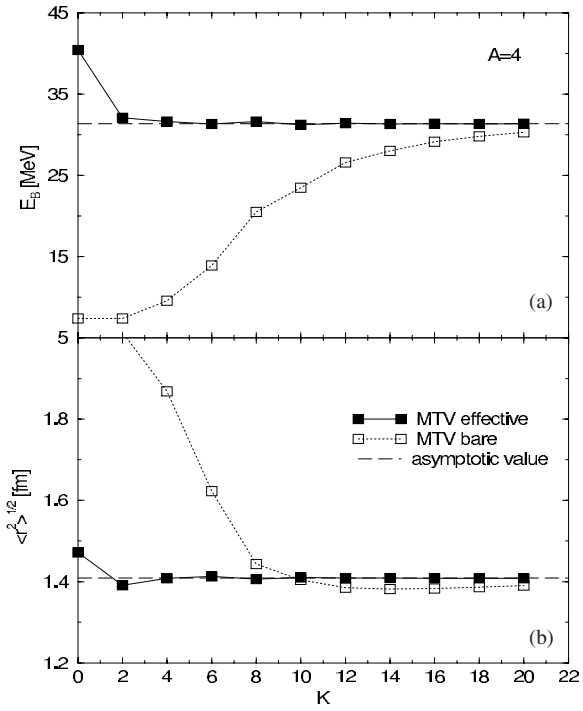

Figure B1. Binding energy (a) and root mean square radius (b) of ^{4}He for the MTV potential, as a function of the maximal hyperangular momentum $K_{\max}$. The asymptotic value has been indicated by a dashed line.

$$r^T(q,\omega) = \frac{1}{2J_0+1}\sum_{M_0,J,M}\sum\!\!\!\!\!\!\int \mathrm{d}f\,\langle\Psi_0(J_0,M_0)|\hat{\mathbf{j}}^{T\dagger}(\mathbf{q})|\Psi_f(J,M)\rangle$$
$$\times\langle\Psi_f(J,M)|\hat{\mathbf{j}}^{T}(\mathbf{q})|\Psi_0(J_0,M_0)\rangle\delta\left(E_f(J)-E_0+\frac{q^2}{2M_T}-\omega\right), \tag{C.2}$$

where the rotational quantum numbers J and M have been put in evidence. One then substitutes the expansions

$$\hat{\rho}(\boldsymbol{q}) = 4\pi\sum_{jm}\mathrm{i}^j\hat{\rho}_{jm}(q)Y^*_{jm}(\hat{\mathbf{q}}), \tag{C.3}$$

$$\hat{\mathbf{j}}_T(\boldsymbol{q}) = 4\pi\sum_{\lambda=\mathrm{el,mag}}\sum_{jm}\mathrm{i}^{j-\epsilon}\hat{T}^{\lambda}_{jm}(q)\mathbf{Y}^{\lambda *}_{jm}(\hat{\mathbf{q}}) \tag{C.4}$$

into (C.1), (C.2) and apply the operation $(4\pi)^{-1}\int \mathrm{d}\hat{\mathbf{q}}$ to both sides of the arising expressions. This operation does not affect the responses while in their right-hand sides it leads to a simplification due to the orthonormality property of spherical harmonics or vector spherical harmonics. This gives

$$r^L(q,\omega) = \frac{4\pi}{2J_0+1}\sum_{M_0,J,M,j,m}\sum\!\!\!\!\!\!\int \mathrm{d}f\,\langle\Psi_0(J_0,M_0)|\hat{\rho}^{\dagger}_{jm}|\Psi_f(J,M)\rangle$$
$$\times\langle\Psi_f(J,M)|\hat{\rho}_{jm}|\Psi_0(J_0,M_0)\rangle\delta\left(E_f-E_0+\frac{q^2}{2M_T}-\omega\right), \tag{C.5}$$

$$r^T(q,\omega) = \frac{4\pi}{2J_0+1}\sum_{\lambda}\sum_{M_0,J,M,j,m}\sum\!\!\!\!\!\!\int \mathrm{d}f \langle\Psi_0(J_0,M_0)|\hat{T}^{\lambda\dagger}_{jm}|\Psi_f(J,M)\rangle$$
$$\times\langle\Psi_f(J,M)|\hat{T}^{\lambda}_{jm}|\Psi_0(J_0,M_0)\rangle\delta\left(E_f - E_0 + \frac{q^2}{2M_T} - \omega\right). \tag{C.6}$$

Now we express these formulae in terms of the quantities

$$Q^j_{JM} = (\hat{\rho}_j \otimes \Psi_0(J_0))_{JM}, \qquad Q^{j\lambda}_{JM} = \left(\hat{T}^{\lambda}_j \otimes \Psi_0(J_0)\right)_{JM}. \tag{C.7}$$

These play the role of source terms in the LIT calculation. The notation of (C.7) type means the Clebsch–Gordan coupling of the tensors of ranks j and J_0 to the tensor of rank J. Using the orthogonality property of this transformation, we finally obtain

$$r^L(q,\omega) = \frac{4\pi}{2J_0+1}\sum_{Jj}(2J+1)(r^L)^j_J, \tag{C.8}$$

$$r^T(q,\omega) = \frac{4\pi}{2J_0+1}\sum_{\lambda=\mathrm{el,mag}}\sum_{Jj}(2J+1)(r^T)^{j\lambda}_J, \tag{C.9}$$

where

$$(r^L)^j_J = \sum\!\!\!\!\!\!\int \mathrm{d}f \langle Q^j_{JM}|\Psi_f(J,M)\rangle\langle\Psi_f(J,M)|Q^j_{JM}\rangle\delta\left(E_f - E_i + \frac{q^2}{2M_T} - \omega\right), \tag{C.10}$$

$$(r^T)^{j\lambda}_J = \sum\!\!\!\!\!\!\int \mathrm{d}f \langle Q^{j\lambda}_{JM}|\Psi_f(J,M)\rangle\langle\Psi_f(J,M)|Q^{j\lambda}_{JM}\rangle\delta\left(E_f - E_i + \frac{q^2}{2M_T} - \omega\right). \tag{C.11}$$

The quantities on the right-hand sides of (C.10) and (C.11) do not depend on M. In fact one may note that

$$\langle\Psi_f(J,M)|Q^j_{JM}\rangle = (2J+1)^{-1/2}(\Psi_f(J)\|\hat{\rho}_j\|\Psi_0(J_0)), \tag{C.12}$$

$$\langle\Psi_f(J,M)|Q^{j\lambda}_{JM}\rangle = (2J+1)^{-1/2}(\Psi_f(J)\|\hat{T}^{\lambda}_j\|\Psi_0(J_0)), \tag{C.13}$$

where the right-hand sides include the conventional reduced matrix elements.

Similar to (3.1) we consider the partial transforms $(L^L)^j_J$ and $(L^T)^{j\lambda}_J$ of the contributions (C.10) and (C.11). Taking into account the completeness of the set $\Psi_f(J,M)$ in the subspace of states with given J and M one calculates these partial transforms as

$$(L^L)^j_J = \langle(\hat{H} - E_0 - \sigma_R + \mathrm{i}\sigma_I)^{-1}Q^j_{JM}|(\hat{H} - E_0 - \sigma_R + \mathrm{i}\sigma_I)^{-1}Q'^j_{JM}\rangle, \tag{C.14}$$

$$(L^T)^{j\lambda}_J = \langle(\hat{H} - E_0 - \sigma_R + \mathrm{i}\sigma_I)^{-1}Q^{j\lambda}_{JM}|(\hat{H} - E_0 - \sigma_R + \mathrm{i}\sigma_I)^{-1}Q'^{j\lambda}_{JM}\rangle. \tag{C.15}$$

Similar to (C.12) and (C.13) the quantities (C.14) and (C.15) are M-independent. The total transforms of the responses (C.8) and (C.9) are

$$L^L(q,\sigma_R) = \frac{4\pi}{2J_0+1}\sum_{Jj}(2J+1)(L^L)^j_J(q,\sigma_R), \tag{C.16}$$

$$L^T(q,\sigma_R) = \frac{4\pi}{2J_0+1}\sum_{\lambda=\mathrm{el,mag}}\sum_{Jj}(2J+1)(L^T)^{j\lambda}_J(q,\sigma_R). \tag{C.17}$$

To obtain the responses (C.8) and (C.9) from these transforms the integral equations of the form (3.1) are to be solved. Alternatively, one may invert the single terms separately and then sum up the corresponding partial contributions to the responses (C.8) and (C.9).

The source terms (C.7) possess definite parities. If $\hat{\mathcal{P}}$ is the parity operator then

$$\hat{\mathcal{P}}\hat{\rho}_{jm}\hat{\mathcal{P}} = (-1)^j \hat{\rho}_{jm}, \tag{C.18}$$

$$\hat{\mathcal{P}}\hat{T}^{\mathrm{el}}_{jm}\hat{\mathcal{P}} = (-1)^j \hat{T}^{\mathrm{el}}_{jm}, \tag{C.19}$$

$$\hat{\mathcal{P}}\hat{T}^{\mathrm{mag}}_{jm}\hat{\mathcal{P}} = (-1)^{j+1} \hat{T}^{\mathrm{mag}}_{jm}. \tag{C.20}$$

Therefore dynamic calculations proceed in subspaces of states with given J, M and given parities $P = P(j)P_0$ where P_0 is the parity of the ground state and $P(j)$ is $(-1)^j$ or $(-1)^{j+1}$.

References

[1] Faddeev L D 1961 *Sov. Phys.—JETP* **12** 1014
[2] Yakubowsky O 1967 *Yad. Fiz.* **5** 1312 (in Russian)
Yakubowsky O 1967 *Sov. J. Nucl. Phys.* **5** 937 (in English)
[3] Efros V D, Leidemann W and Orlandini G 1994 *Phys. Lett.* B **338** 130
[4] Efros V D 1985 *Yad. Fiz.* **41** 1498 (in Russian)
Efros V D 1985 *Sov. J. Nucl. Phys.* **41** 949 (in English)
[5] Tikhonov A N and Arsenin V Y 1977 *Solutions of Ill-Posed Problems* (Washington, DC: V H Winston and Sons)
[6] Efros V D, Leidemann W and Orlandini G 1993 *Few-Body Syst.* **14** 151
[7] Acton F S 1970 *Numerical Methods that Work* (New York: Harper and Row)
[8] Jaines E T 1978 *The Maximum Entropy Formalism* ed R D Levune and M Tribus (Cambridge: MIT Press) p 15
[9] Efros V D, Leidemann W and Orlandini G 1999 *Few-Body Syst.* **26** 251
[10] Efros V D, Leidemann W and Orlandini G 2001 *Yad. Fiz.* **64** 536 (in Russian)
Efros V D, Leidemann W and Orlandini G 2001 *Phys. At. Nucl.* **64** 482 (in English)
[11] Leidemann W 2002 *Proc. Int. Conf. on Few-Body Problems in Physics '02 (Bled, Slovenia) Few-Body Syst. Suppl.* **14** 313
[12] Leidemann W 2006 *Proc. IUPAP Conf. on Few-Body Problems in Physics (Santos, Brazil) Nucl. Phys.* A **790** 24c
[13] Fenin Y I and Efros V D 1972 *Yad. Fiz.* **15** 887 (in Russian)
Fenin Y I and Efros V D 1972 *Sov. J. Nucl. Phys.* **15** 497 (in English)
[14] Ballot J L and Fabre de la Ripelle M 1980 *Ann. Phys., NY* **127** 62
[15] Rosati S, Kievsky A and Viviani M 1992 *Few-Body Syst. Suppl.* **6** 563
[16] Barnea N, Leidemann W and Orlandini G 1999 *Nucl. Phys.* A **650** 427
[17] Krivec R and Mandelzweig V B 1990 *Phys. Rev.* A **42** 3779
[18] Krivec R 1998 *Few-Body Syst.* **25** 199
[19] Goldberger M L and Watson K W 1964 *Collision Theory* (New York: Wiley)
[20] Efros V D 1999 *Yad. Fiz.* **62** 1975 (in Russian)
Efros V D 1999 *Phys. At. Nucl.* **62** 1833 (in English)
[21] La Piana A and Leidemann W 2000 *Nucl. Phys.* A **677** 423
[22] Frullani S and Mougey J 1984 *Adv. Nucl. Phys.* **14** 1
[23] Efros V D, Leidemann W and Orlandini G 1998 *Phys. Rev.* C **58** 582
[24] Glauber R J 1955 *Phys. Rev.* **100** 242
[25] Efros V D, Leidemann W, Orlandini G and Tomusiak E L 2005 *Phys. Rev.* C **72** 011002(R)
[26] Bacca S, Arenhövel H, Barnea N, Leidemann W and Orlandini G 2007 *Phys. Rev.* C **76** 014003
[27] Reiss C, Leidemann W, Orlandini G and Tomusiak E L 2003 *Eur. Phys. J.* A **17** 589
[28] Andreasi D, Leidemann W, Reiss C and Schwamb M 2005 *Eur. Phys. J.* A **24** 361
[29] Golak J *et al* 2002 *Nucl. Phys.* A **707** 365
[30] Martinelli S, Kamada H, Orlandini G and Glöckle W 1995 *Phys. Rev.* C **52** 1778
[31] Lanczos C 1950 *J. Res. Natl. Bur. Stand.* **45** 255
[32] Golub G H and Van Loan C F 1983 *Matrix Computations* (Baltimore, MD: John Hopkins University Press)

[33] Marchisio M A, Barnea N, Leidemann W and Orlandini G 2003 *Few-Body Syst.* **33** 259
[34] Dagotto E 1994 *Rev. Mod. Phys.* **66** 763
[35] Hallberg K A 1995 *Phys. Rev.* B **52** 9827
[36] Kühner T D and White S R 1995 Dynamical correlation functions using the density matrix renormalization group *Preprint* cond-mat/9812372
[37] Fulde P 1991 *Electron Correlations in Molecules and Solids (Springer Series in Solid State Physics* vol 100*)* (Berlin: Springer)
[38] Efros V D 1980 *Ukr. Fiz. Zh.* **25** 907 (in Russian)
Efros V D 1980 *Ukr. Phys. J.* **25** 907 (in English)
[39] Thirumalai D and Berne B J 1983 *J. Chem. Phys.* **79** 5029
[40] Carlson J and Schiavilla R 1998 *Rev. Mod. Phys.* **70** 743
[41] Baym G and Mermin N D 1961 *J. Math. Phys.* **2** 232
[42] Silver R N, Sivia D S and Gubernatis J E 1990 *Phys. Rev.* B **41** 2380
[43] Gubernatis J E, Jarrel M, Silver R N, Sivia D S and Gubernatis J E 1991 *Phys. Rev.* B **44** 6011
[44] Carlson J and Schiavilla R 1992 *Phys. Rev. Lett.* **68** 3682
[45] Carlson J, Jourdan J, Schiavilla R and Sick I 2002 *Phys. Rev.* C **65** 024002
[46] Langhoff P W 1980 *Theory of Applications of Moment Methods in Many-Fermion Systems* ed B J Dalton (New York: Plenum) p 191
[47] Reinhardt W P *et al* 1980 *Theory of Applications of Moment Methods in Many-Fermion Systems* ed B J Dalton *et al* (New York: Plenum) p 129
[48] Rosenfelder R 1980 *Ann. Phys.* **128** 188
[49] Ishikawa S, Kamada H, Glöckle W, Golak J and Witala H 1994 *Phys. Lett.* B **339** 293
[50] Kamada H, Koike Y and Glöckle W 2003 *Prog. Theor. Phys.* **109** 869L
[51] Uzu E, Kamada H and Koike Y 2003 *Phys. Rev.* C **68** 061001 and references therein
[52] Haxton W C, Nollett K M and Zurek K M 2005 *Phys. Rev.* C **72** 065501
[53] Stetcu I *et al* 2007 *Nucl. Phys.* A **785** 307
[54] Efros V D 1972 *Yad. Fiz.* **15** 226 (in Russian)
Efros V D 1972 *Sov. J. Nucl. Phys.* **15** 128 (in English)
[55] Fabre de la Ripelle M 1983 *Ann. Phys., NY* **147** 281
[56] Abramowitz M and Stegun I 1964 *Handbook of Mathematical Functions* (New York: Dover)
[57] Novoselsky A and Katriel J 1994 *Phys. Rev.* A **49** 833
[58] Barnea N and Novoselsky A 1997 *Ann. Phys., NY* **256** 192
[59] Barnea N and Novoselsky A 1998 *Phys. Rev.* A **57** 48
[60] Faul D D, Berman B L, Meyer P and Olson D L 1981 *Phys. Rev.* C **24** 849
[61] de Forest T Jr and Walecka J D 1966 *Adv. Phys.* **15** 1
[62] de Forest T 1984 *Nucl. Phys.* A **414** 347
[63] Friar J M 1973 *Ann. Phys., NY* **81** 332
[64] Buchmann A, Leidemann W and Arenhövel 1985 *Nucl. Phys.* A **443** 726
[65] Riska D O 1985 *Phys. Scr.* **31** 471
[66] Arenhövel H and Schwamb M 2001 *Eur. Phys. J.* A **12** 207
[67] Varshalovich D A, Moskalev A N and Khersonskii V K 1988 *Quantum Theory of Angular Momentum* (Singapore: World Scientific)
[68] Arenhövel H and Sanzone M 1991 *Few-Body Syst. Suppl.* **3** 1
[69] Woosley S E, Pinto P A and Ensman L 1988 *Astrophys. J.* **324** 466
[70] Woosley S E, Hartmann D H, Hoffman D R and Haxton W C 1990 *Astrophys. J.* **356** 272
[71] Donnelly T W and Walecka J D 1976 *Nucl. Phys.* A **274** 368
[72] Park T S *et al* 2003 *Phys. Rev.* C **67** 055206
[73] Wiringa R B, Smith R A and Ainsworth T L 1984 *Phys. Rev.* C **29** 1207
[74] Shirokov A M, Vary J P, Mazur A I, Zaytsev S A and Weber T A 2005 *Phys. Lett.* B **621** 96
[75] Barnea N, Leidemann W and Orlandini G 2006 *Phys. Rev.* C **74** 034003
[76] Quaglioni S, Leidemann W, Orlandini G, Barnea N and Efros V 2004 *Phys. Rev.* C **69** 044002
[77] Malfliet R A and Tjon J A 1969 *Nucl. Phys.* A **127** 161
[78] Volkov A B 1965 *Nucl. Phys.* **74** 33
[79] Wiringa R B and Pieper S C 2002 *Phys. Rev. Lett.* **89** 182501
[80] Thomson D R, LeMere M and Tang Y C 1977 *Nucl. Phys.* A **286** 53
Reichstein I and Tang Y C 1970 *Nucl. Phys.* **158** 529
[81] Lacombe M, Loiseau B, Richard J M, Vinh Mau R, Côté J, Pirès P and de Tourreil R 1980 *Phys. Rev.* C **21** 861
[82] Wiringa R B, Stoks V G J and Schiavilla R 1995 *Phys. Rev.* C **51** 38

[83] Machleidt R 1989 *Adv. Nucl. Phys.* **19** 189
[84] Wiringa R B 1991 *Phys. Rev.* C **43** 1585
[85] Pudliner B S, Pandharipande V R, Carlson J, Pieper S C and Wiringa R B 1997 *Phys. Rev.* C **56** 1720
[86] Coon S A, Scadron M D, McNamee P C, Barrett B R, Blatt D W E and McKellar B H J 1979 *Nucl. Phys.* A **317** 242
Coon S A and Glöckle W 1981 *Phys. Rev.* C **23** 1790
Coon S A 1999 Private communication giving the parameters as $a' = -1.35\mu^{-1}, b' = -2.86\mu^{-3}, d = -0.64\mu^{-3}$
[87] Retzlaff G A *et al* 1994 *Phys. Rev.* C **49** 1263
[88] Viviani M, Kievsky A, Marcucci L E, Rosati S and Schiavilla R 2000 *Phys. Rev.* C **61** 064001
[89] Reiss C, Arenhövel H and Schwamb M 2005 *Eur. Phys. J.* A **25** 171
[90] Efros V D, Leidemann , Orlandini G and Tomusiak E L 2004 *Phys. Rev.* C **69** 044001
[91] Marchand C *et al* 1985 *Phys. Lett.* B **153** 29
[92] Dow K *et al* 1988 *Phys. Rev. Lett.* **61** 1706
[93] Fetisov V N, Gorbunov A N and Varfolomeev A T 1965 *Nucl. Phys.* A **71** 305
[94] Efros V D, Leidemann W and Orlandini G 1997 *Phys. Lett.* B **408** 1
[95] Efros V D, Leidemann W, Orlandini G and Tomusiak E L 2000 *Phys. Lett.* B **484** 223
[96] Barnea N, Leidemann W, Orlandini G, Efros V D and Tomusiak E L 2006 *Few-Body Syst.* **39** 1
[97] O'Connor E, Gazit D, Horowitz C J, Schwenk A and Barnea N 2007 *Phys. Rev.* C **75** 055803
[98] Gazit D and Barnea N 2007 *Phys. Rev. Lett.* **98** 192501
[99] Dytman S A *et al* 1988 *Phys. Rev.* C **38** 800
[100] Zghiche A *et al* 1994 *Nucl. Phys.* A **572** 513
[101] Efros V D, Leidemann W and Orlandini G 1997 *Phys. Rev. Lett.* **78** 432
[102] Ducret J E *et al* 1993 *Nucl. Phys.* A **556** 373
[103] Quaglioni S, Efros V D, Leidemann W and Orlandini G 2005 *Phys. Rev.* C **72** 064002
[104] Andreasi D, Quaglioni S, Efros V D, Leidemann W and Orlandini G 2006 *Eur. Phys. J.* A **27** 47
[105] Ent R, Blok H, van den Brand J F J, Bulten H J, Jans E, Lapikas L and Morita H 1991 *Phys. Rev. Lett.* **67** 18
[106] Arkatov Yu M *et al* 1979 *Yad Konst.* **4** 55
[107] Wells D P *et al* 1992 *Phys. Rev.* C **46** 449
[108] Nilsson B *et al* 2005 *Phys. Lett.* B **626** 65
[109] Berman B L, Faul D D, Meyer P and Olson D L 1980 *Phys. Rev.* C **22** 2273
[110] Feldman G *et al* 1990 *Phys. Rev.* C **22** R1167
[111] Ellerkmann G, Sandhas W, Sofianos S A and Fiedelday H 1996 *Phys. Rev.* C **53** 2638
[112] Shima T *et al* 2005 *Phys. Rev.* C **72** 044004
[113] Efros V D, Leidemann W and Orlandini G 1997 *Phys. Rev. Lett.* **78** 4015
[114] Barnea N, Efros V D, Leidemann W and Orlandini G 2001 *Phys. Rev.* C **63** 057002
[115] Gorbunov A N and Spiridonov V M 1958 *Zh. Eksp. Teor. Fiz.* **34** 866 (in Russian)
Gorbunov A N and Spiridonov V M 1958 *Sov. Phys.—JETP* **34** 600 (in English)
Gorbunov A N 1969 *Yad. Fiz.* **10** 469 (in Russian)
Gorbunov A N 1969 *Sov. J. Nucl. Phys.* **10** 268 (in English)
[116] Arkatov Yu M, Bazaeva A V, Vatset P I, Voloshchuk P I, Klyucharev A P and Khodyachikh A F 1969 *Yad. Fiz.* **10** 1123 (in Russian)
Arkatov Yu M, Bazaeva A V, Vatset P I, Voloshchuk P I, Klyucharev A P and Khodyachikh A F 1970 *Sov. J. Nucl. Phys.* **10** 639 (in English)
[117] Balestra F, Busso L, Garfagnini R, Piragino G and Zanini A 1979 *Nuovo Cimento* A **49** 575
[118] Doran S M *et al* 1993 *Nucl. Phys.* A **559** 347
[119] Gazit D, Bacca S, Barnea N, Leidemann W and Orlandini G 2006 *Phys. Rev. Lett.* **96** 112301
[120] Quaglioni S and Navrátil P 2007 *Preprint* nucl-th/0704.1336
[121] Roth R, Neff T, Hergert H and Feldmeier H 2004 *Nucl. Phys.* A **745** 3
[122] Bacca S 2007 *Phys. Rev.* C **75** 044001
[123] Gazit D, Bacca S, Barnea N, Leidemann W and Orlandini G 2006 *Phys. Rev.* C **74** 061001(R)
[124] Gazit D and Barnea N 2004 *Phys. Rev.* C **70** 048801
[125] Nogga A, Kamada H, Glöckle W and Barrett B R 2002 *Phys. Rev.* C **65** 054003
[126] Viviani M, Kievsky A and Rosati S 2005 *Phys. Rev.* C **71** 024006
[127] Ananyan S M, Serot B D and Walecka J D 2002 *Phys. Rev.* C **66** 055502
[128] Marcucci L E, Schiavilla R, Viviani M, Kievsky A, Rosati S and Beacom J F 2000 *Phys. Rev.* C **63** 015801
[129] Bacca S, Marchisio M A, Barnea N, Leidemann W and Orlandini G 2002 *Phys. Rev. Lett.* **89** 052502
[130] Bacca S, Barnea N, Leidemann W and Orlandini G 2004 *Phys. Rev.* C **69** 057001

[131] Bacca S, Arenhövel H, Barnea N, Leidemann W and Orlandini G 2004 *Phys. Lett.* B **603** 159
[132] Berman B L, Bramblett R L, Caldwell J T, Harvey R R and Fultz S C 1965 *Phys. Rev. Lett.* **15** 727
[133] Junghans G, Bangert K, Berg U E P, Stock R and Wienhard K 1979 *Z. Phys.* A **291** 353
[134] Shin Y M, Skopik D M and Murphy J J 1975 *Phys. Lett.* B **55** 297
[135] Aumann T, Aleksandrov D, Axelsson L and Baumann T 1999 *Phys. Rev.* C **59** 1952
[136] Ahrens J *et al* 1975 *Nucl. Phys.* A **251** 479
[137] Leidemann W, Efros V D, Orlandini G and Tomusiak E L 1999 *Fizika* **8** 135
[138] Efros V D 1978 *Yad. Fiz.* **27** 845 (in Russian)
Efros V D 1978 *Sov. J. Nucl. Phys.* **27** 448 (in English)
[139] Viviani M, Kievsky A and Rosati S 1995 *Few-Body Syst.* **18** 1580
[140] Viviani M, Kievsky A and Rosati S 1998 *Phys. Rev. Lett.* **81** 1580
[141] Efros V D 2002 *Few-Body Syst.* **32** 169
[142] Zheng D C, Vary J P and Barrett B R 1994 *Phys. Rev.* C **50** 2841
[143] Navrátil P, Vary J P and Barrett B R 2000 *Phys. Rev. Lett.* **84** 5728
[144] Ellis P J, Engeland T, Hjorth-Jensen M, Holt A and Osnes E 1994 *Nucl. Phys.* A **573** 216
[145] Barnea N, Leidemann W and Orlandini G 2000 *Phys. Rev.* C **61** 054001
[146] Barnea N, Leidemann W and Orlandini G 2001 *Nucl. Phys.* A **693** 565
[147] Macek J 1968 *J. Phys. B: At. Mol. Phys.* **1** 831
[148] Suzuki K and Lee S J 1980 *Prog. Theor. Phys.* A **64** 2091
[149] Suzuki K 1982 *Prog. Theor. Phys.* A **68** 246
[150] Suzuki K and Okamoto R 1983 *Prog. Theor. Phys.* A **70** 439
[151] Barnea N, Leidemann W and Orlandini G 2000 *Phys. Rev.* C **67** 054003